NATIONAL ADVISORY COMMITTEE FOR AERONAUTICS

TECHNICAL NOTE

No. 1302

THE EFFECT OF MODIFICATIONS TO THE HORIZONTAL-TAIL PROFILE ON THE HIGH-SPEED LONGITUDINAL CONTROL OF A PURSUIT AIRPLANE

By Charles F. Hall

Ames Aeronautical Laboratory
Moffett Field, Calif.

Washington

August 1947

NATIONAL ADVISORY COMMITTEE FOR AERONAUTICS

TECHNICAL NOTE NO. 1302

THE EFFECT OF MODIFICATIONS TO THE HORIZONTAL-TAIL PROFILE ON THE HIGH-SPEED LONGITUDINAL CONTROL OF A PURSUIT AIRPLANE

By Charles F. Hall

SUMMARY

This report presents the results of high-speed wind-tunnel research on the effects of modifications to the horizontal-tail profile on the static longitudinal stability and control of a pursuit airplane at high speeds. Two symmetrical stabilizers (a modified NACA four-digit and an NACA 65-series airfoil), two flat-sided elevators, and three elevators with bulged profiles were investigated. The tests covered Mach numbers from approximately 0.30 to 0.80. The pitching-moment and elevator hinge-moment characteristics for a model airplane with the various tails are shown. The distribution of pressure over the tails is presented.

The data indicate that the modifications to the horizontal-tail profile have almost no effect on the pitching-moment characteristics of the model, but have a powerful effect on the hinge-moment characteristics. The effect of bulging the elevator profile, with either stabilizer, is to improve the control characteristics by eliminating or reducing the severity of the reversal of stick force at high speeds and reducing the stick-force gradient.

INTRODUCTION

The attainment of supercritical speeds by airplanes in high-speed dives has made imperative the determination of the longitudinal stability and control of those airplanes in the speed range above the critical, since many pilots have reported large changes in these characteristics in this speed range. As part of a program to study stability and control characteristics at supercritical speeds, the wind-tunnel tests discussed in this report were undertaken.

The airplane used as the subject of these tests was chosen because it had exhibited no dangerous longitudinal characteristics during recoveries from high-speed dives. It was believed that a

knowledge of the factors producing the satisfactory dive-recovery characteristics of the airplane would be of value to designers.

In order to determine the effect of the bulged elevator profile of this airplane on the longitudinal-stability and -control characteristics, it was felt desirable to test a flat-sided elevator. It was also decided to test a stabilizer having a low-drag airfoil profile in conjunction with one flat-sided elevator and two elevators with bulged profiles to determine if the satisfactory stability and control characteristics could be maintained or improved at the same time that the drag of the airplane was decreased. The five different tails were therefore tested on the model at Mach numbers from approximately 0.30 to 0.80.

APPARATUS AND TESTS

The tests discussed in this report were made in the Ames 16-foot high-speed wind tunnel.

The model represented a U. S. Army pursuit airplane to one-third scale and was designed and built at the Ames Aeronautical Laboratory according to lines supplied by the designers of the airplane. Pertinent dimensions of the model, together with corresponding airplane dimensions, are given in the appendix. A three-view drawing of the model is shown in figure 1, and photographs are presented in figures 2 to 4.

Drawings and dimensions of the five tails tested on the model are shown in figures 5 to 9. For brevity, these tails will be referred to as the H, H_0, H_1, H_2, and H_3 tails. When not specified, the H (standard) tail is implied.

The plan forms of all tails were the same except that the H_1, H_2, and H_3 tails had a tip shape different from that on the H and H_0 tails and did not have the paddle balances on the elevators. The profiles of the various tails are summarized in the following table:

Tail	Stabilizer section	Elevator section
H (standard)	NACA 0011 (at root)	Bulge
H_o	NACA 0011 (at root)	Flat side
H_1	NACA 65_2-010	Flat side
H_2	NACA 65_2-010	Large bulge
H_3	NACA 65_2-010	Small bulge

The root chords of the H and H_o elevators were extended to make the actual root thickness of the tails 10.25 percent of the chord. The tip section of the H and H_o stabilizers was similar to the NACA 0009 section, although slightly thinner from the point of maximum thickness to the elevator hinge line. The actual thickness of the tip section was 9.75 percent of the chord.

The elevator of the H tail was constructed of solid dural. The elevators of the other tails were constructed of laminated wood screwed to steel cores. The hinge moments for all elevators were measured by electric resistance strain gages.

The investigations of the stability characteristics of the model with the H and Ho tails were made with the cooling duct removed. (See fig. 3.) This deviation from the standard model was necessary because the construction of a duct conforming to new lines developed during preceding tests of a full-scale prototype in the 16-foot wind tunnel had not been completed. A comparison of subsequent tests of the model with and without the cooling duct, however, indicated that the duct had a negligible effect on the pitching-moment coefficient. It is also believed that the cooling duct had little effect on the hinge-moment data for the two tails.

REDUCTION OF DATA

Coefficients and Symbols

The wind-tunnel data were reduced to standard NACA coefficients based upon the model dimensions. Pitching moments were computed with respect to the normal center-of-gravity location. (See appendix.) The coefficients and symbols used in this report are defined as follows:

C_L	lift coefficient (lift/qS)
C_m	pitching-moment coefficient (pitching moment/qSc)
C_{he}	elevator hinge-moment coefficient (elevator hinge moment/$qb_e\overline{c_e^2}$)
P	pressure coefficient $[(p_L - p_s)/q]$
P_{cr}	critical pressure coefficient (the pressure coefficient at which the speed of sound is reached locally)
M	Mach number (V/a)
M_{cr}	critical Mach number (the Mach number at which the speed of sound is reached locally)
α	angle of attack, degrees (The angle is measured relative to the fuselage reference line.)
δ_e	elevator angle, degrees (The angle is considered positive when the trailing edge is down.)
A_Z	indicated acceleration normal to flight path, expressed as a factor of the acceleration of gravity
g	acceleration due to gravity, (32.2 feet per second per second)
q	dynamic pressure, pounds per square foot
V	velocity of air stream corrected for constriction effects, feet per second
a	speed of sound in free stream, feet per second
p_s	free-stream static pressure, pounds per square foot
p_L	local static pressure, pounds per square foot
S	wing area, square feet
c	mean aerodynamic chord of wing, feet
b_e	elevator span, feet
$\overline{c_e^2}$	mean square of elevator chord behind hinge line, feet squared

Mach Number Calibration

After the tests discussed in this report were completed, refinements were made in the methods used to calibrate the wind tunnel. (See reference 1.) Since it is believed the calibration obtained by these improved methods is more accurate than that used during the original testing, the results in this report have been based on the later calibration.

Tunnel-Wall and Tare Corrections

The corrections applied to the data to account for the constricting effects of the tunnel wall are those discussed in reference 1. Corrections to account for the induced effects were calculated from reference 2. The tare corrections were evaluated by supporting the model at the wing tips (fig. 4) and determining the aerodynamic characteristics of the model with and without the normal support system in place.

RESULTS AND DISCUSSION

Longitudinal Characteristics of Model

Lift.- The lift coefficient of the model in relation to the angle of attack and Mach number is shown in figure 10. The slope of the lift curve increases from 0.086 to 0.104 between 0.30 and 0.70 Mach number. With further increase in Mach number to 0.80, the slope decreases to 0.056. The wind-tunnel data indicate no increase in the angle of attack for zero lift with Mach number, a characteristic in contrast to that of many wings at high speeds. This is a desirable characteristic from the standpoint of longitudinal stability, as will be discussed later. No well-defined relationship is indicated between the critical Mach number of the wing (fig. 11) and the Mach number at which the lift coefficient for constant angle of attack decreases. A comparison of figures 10(b) and 11 shows that up to an angle of attack of 4° this Mach number corresponds quite closely with the critical value at wing station 62.33, the station having the highest critical Mach number.

Pitching moment.- The pitching-moment coefficient of the model with the H tail but with the cooling duct removed is shown in figure 12. The data indicate that $-\partial C_m/\partial C_L$ decreases as the Mach number is increased from 0.30 to 0.70; with further increase in Mach number to 0.80, $-\partial C_m/\partial C_L$ shows a large increase. It will be noticed

that the Mach number of demarcation between decreasing and increasing $-\partial C_m/\partial C_L$ coincides with that between increasing and decreasing $\partial C_L/\partial \alpha$.

Figure 12 also shows the effect of Mach number on the pitching-moment coefficient for constant lift coefficient. The data indicate an abrupt decrease in pitching-moment coefficient with increasing Mach number above 0.675 at 0.80 lift coefficient and above 0.75 at zero lift. This abrupt decrease in pitching-moment coefficient causes the elevator-angle variation with speed to become unstable, which if not compensated by the elevator hinge-moment characteristics will produce large increases in the pull required on the stick for dive recoveries.

The data for the model with the empennage off (fig. 13) do not show an abrupt decrease of pitching-moment coefficient with increasing Mach number as do those for the complete model but, on the contrary, indicate an increase at the high Mach numbers. The difference between the pitching-moment characteristics with and without the tail must be attributed, therefore, to a decrease in download or an increase in upload on the tail. The change in the load on the tail is caused primarily by the increase in angle of attack of the tail due mainly to the increase of model angle of attack with Mach number necessary to maintain a constant lift coefficient, but also to a small extent due to changes in the angle of downwash from the wing caused by a small outboard shift of the lift on the wing at high Mach numbers. Since the major cause of the abrupt decrease in pitching-moment coefficient with increasing Mach number is the increase in the angle of attack of the model, it is obvious that this pitching-moment characteristic would be greatly aggravated by increases in the angle of attack for zero lift with Mach number. As previously stated, the wing of this model does not exhibit these unfavorable lift characteristics, a factor partly responsible for the good dive-recovery qualities of the airplane at high speeds.

To a smaller degree the change in load on the tail is caused by the variation of $\partial C_L/\partial \alpha$ of the tail with increasing Mach number. Data from tests of the model with different stabilizer angles indicate that $\partial C_L/\partial \alpha$ of the tail increases with Mach number up to 0.70, but decreases with further increase in Mach number. This characteristic will aggravate the abrupt decrease in pitching-moment coefficient when the tail load is downward, but will relieve it when the load is upward.

The pitching-moment data for the model with the other four tails

discussed in this report are shown in relation to elevator angle and lift coefficient at a constant Mach number in figures 15 to 18, as are those for the H tail in figure 14. Although the data for the four tails are rather meager with respect to Mach number variations, a comparison of these data with those for the H tail indicates trends almost identical with those previously discussed. It therefore can be said that the changes of elevator profile discussed in this report have no appreciable effect on the longitudinal-stability characteristics of the model.

Elevator Hinge-Moment Characteristics

The elevator hinge-moment coefficients and the pitching-moment coefficients are shown in figures 14 to 18 for the five tails tested on the model. The elevator angle and the hinge-moment coefficient for balance with zero tab angle can therefore be determined at each Mach number from these figures. In addition, some of the more important characteristics shown in figures 14 to 18 are summarized in table 1.

As indicated in figures 14 to 18 and in table 1, the value of $\partial C_{h_e}/\partial \delta_e$ at 0.30 Mach number is negative throughout the elevator-angle and lift-coefficient range of the tests for each tail and, in addition, is nearly constant. These data also show the effect of the bulged elevator profile at 0.30 Mach number. Comparison of the results for the flat-sided elevators with those for the H tail (standard) shows that the average values of $\partial C_{h_e}/\partial \delta_e$ for the H_0 and H_1 tails are approximately 62 and 52 percent more negative, respectively, than that for the H tail. For the H_2 and H_3 tails the values are approximately 4 and 21 percent more negative respectively. It should be noted that these average values of $\partial C_{h_e}/\partial \delta_e$ are somewhat different from those shown in the summary table since the latter correspond to zero lift and pitching moment. The values in the summary, however, also show the large beneficial effects of the bulged elevator profile.

The data indicate that increasing Mach number up to 0.80 produces little change in the variation of hinge-moment coefficient with elevator angle for the flat-sided elevators. The values of $\partial C_{h_e}/\partial \delta_e$ still are negative throughout the lift-coefficient and elevator-angle range of the tests, although somewhat less negative than the values for these elevators at 0.30 Mach number.

The effect of increasing Mach number on $\partial C_{h_e}/\partial \delta_e$ for the

elevators with bulged profiles, however, is pronounced. The data indicate that for the H tail the value of $\partial C_{h_e}/\partial \delta_e$ does not remain negative throughout the lift- and elevator-angle ranges at higher Mach numbers, but becomes positive at 0.60 Mach number, 0.60 lift coefficient, and -1° elevator angle. This overbalance with respect to elevator deflection increases with Mach number, extending over a range of 5° elevator angle at 0.80 Mach number. The H_2 tail shows even a larger variation of $\partial C_{h_e}/\partial \delta_e$ with Mach number than does the H tail. At 0.80 Mach number the quantity is positive over a 6° range of elevator deflection. For the Hs tail $\partial C_{h_e}/\partial \delta_e$ varies with Mach number to a lesser extent than for either the H or H_2 tail and no overbalance is indicated within the range of the tests. At 0.80 Mach number, however, the average value of $\partial C_{h_e}/\partial \delta_e$ is approximately 30 percent less negative than at 0.30 Mach number.

An insight into the causes of the variation of $\partial C_{h_e}/\partial \delta_e$ with increasing Mach number for the elevators with a bulged profile is shown by the pressure distribution over the elevator surfaces. These data are shown in figure 19 for the five tails tested at elevator angles from -4° to 4°. A comparison of the data for the H and H_0 tails shows that the bulge causes a large pressure peak to occur on both the upper and lower surfaces varying from approximately 60 to 80 percent of the tail-plane chord. At 0.30 Mach number the peaks on the upper and lower surfaces tend to oppose each other and, therefore, do not alter to a great extent the resultant load on the elevator. In general, a decrease in elevator angle increases the download along the entire elevator chord as indicated for the H_0 tail. With variation in elevator angle the load on the elevator does change more near the hinge line and less aft of the 80-percent-chord station for the H tail than for the H_0 tail. At 0.80 Mach number the effect of the bulge on the lower surface is similar to that at 0.30 Mach number, but there are large changes in the pressures on the upper surface. For example, for an elevator-angle movement from 4° to 0°, the pressure peak moves aft from 70 to 78 percent of the chord and the coefficient decreases from -0.64 to -0.77 at 0.80 Mach number; whereas, at 0.30 Mach number, the peak moves aft from 72 to 77 percent of the chord and the coefficient increases from -0.56 to -0.46. The result of the large changes in pressure distribution on the upper surface is to alter completely the load distribution on the H elevator from that on the H_0 elevator. Aft of the 75-percent-chord station the variation of load with elevator angle is opposite that for the H_0 tail, thereby causing the overbalance indicated by the H tail.

The data for the elevators of the low-drag tails (H_1, H_2, and Hs)

indicate phenomena somewhat different from that discussed for the H and H_0 tail. The pressure peaks on the elevators with the bulges occur at approximately 85 percent of the chord and neither elevator angle nor Mach number variation alters the location of the peak. The data also indicate that increases of Mach number affect the pressures over the bulge on both the upper and lower surfaces equally. Near the hinge line, the variation of load with elevator angle is similar for the three tails at all Mach numbers. Near the trailing edge, however, the bulges on the elevator profile cause a reversal in the variation of load with elevator angle, which becomes more pronounced with increasing Mach number. Since it occurs near the trailing edge, the reversal of load variation with elevator angle has a large effect on the hinge-moment coefficient. The data of figure 19 also indicate that the pressure coefficient for the H tail considerably exceeds the critical pressure coefficient at 0.80 Mach number. The bulges on the low-drag tails were designed to reduce the large pressure peaks on the elevator. The data indicate that the pressure coefficient for the H_2 tail slightly exceeds the critical at 0.80 Mach number and that for the Hs tail it remains subcritical throughout the range of the tests.

The data of figures 14 to 18 and table I also indicate the effect on $\partial C_{h_e}/\partial C_L$ of the bulge on the elevator profile. At 0.30 Mach number, the quantity is negative for both the flat-sided elevators throughout the lift-coefficient and elevator-angle range of the tests. With increasing Mach number the quantity tends toward zero and becomes slightly positive for both elevators at 0.80 Mach number over a portion of the elevator-angle range. For the H, H_2, and Hs elevators, $\partial C_{h_e}/\partial C_L$ is positive throughout nearly the entire range of the tests and varies almost directly with the algebraic value of $\partial C_{h_e}/\partial \delta_e$. Hence, the largest positive value of $\partial C_{h_e}/\partial C_L$ occurs at 0.80 Mach number for the H_2 tail, the tail having the greatest overbalance with respect to elevator deflection. This variation of hinge-moment coefficient with model lift coefficient counteracts the overbalance with respect to elevator deflection. It is sufficiently large to indicate that no overbalance will occur in the Mach number range of the tests. For the H tail, though, the decrease in $\partial C_{h_e}/\partial C_L$ and the increase in $\partial C_{h_e}/\partial \delta_e$ in the elevator-angle range required for balance at 0.80 Mach number indicate that overbalance may possibly occur at higher values of Mach number.

The effects on the hinge-moment characteristics of the bulge on the H and H_2 tails also indicate the possibility of an instantaneous reversal of stick force during rapid maneuvering.

If the attitude of the airplane is such that it is flying in a region for which both $\partial C_{h_e}/\partial \delta_e$ and $\partial C_{h_e}/\partial C_L$ are positive, a rapid stick movement might produce a stick force opposite to normal due to the positive value of $\partial C_{h_e}/\partial \delta_e$. After the airplane responds to the elevator movement, the stick force will become normal again because of the positive value of $\partial C_{h_e}/\partial C_L$. There have been no reports of such a reversal occurring in flight, however.

Figures 14 to 18 and table I also indicate the large effect of the bulged elevator profile on the elevator angle corresponding to zero hinge moment. For both of the flat-sided elevators, the elevator angle corresponding to zero hinge moment and zero lift decreases slightly more than 1° from 0.30 to 0.80 Mach number. For a similar variation of Mach number, the H, H_2, and H_3 tails undergo decreases of approximately 4½°, 8°, and 3°, respectively. This floating characteristic of the elevators with a bulge on the profile will tend to pull an airplane using such surfaces out of a dive as the Mach number is increased. It is probably largely responsible for the good dive-recovery characteristics of the pursuit airplane with the standard tail.

In general, it can be said that the effect of the bulge on the elevator profile is to cause both $\partial C_{h_e}/\partial \delta_e$ and $\partial C_{h_e}/\partial C_L$ to become less negative and even attain positive values over portions of the test range; that is, their values increase algebraically. Increasing $\partial C_{h_e}/\partial \delta_e$ algebraically tends to reduce the stick-force gradient, and increasing $\partial C_{h_e}/\partial C_L$ tends to increase it. However, since for this model the effect of $\partial C_{h_e}/\partial \delta_e$ on the stick-force gradient is between six and twelve times greater than that of $\partial C_{h_e}/\partial C_L$, the effect of the bulge on the elevator profile, in general, is to reduce the stick-force gradient.

Calculated Characteristics of Airplane

Stick force and elevator angle.— The over-all effect of the various parameters previously discussed can best be shown by calculating the stick force and elevator angle for the airplane in various attitudes of flight. Consequently, the calculated control characteristics of the airplane with the various horizontal tails are shown in figures 20 to 23. It must be remembered in viewing these results that these stick forces were computed from data obtained with solid model elevators. The stick-force characteristics of the full-scale airplane probably differ from those

discussed here due to distortion of the fabric or metal surfaces of the elevator. However, this fact should not influence the discussion of the relative merits of the various tails. In figure 20 the variation of stick force and elevator angle with true airspeed is shown for the airplane with the H tail (standard tail) at five different altitudes. The data indicate that the variation of elevator angle with airspeed is unstable above speeds ranging from 575 miles per hour at sea level (approximately 0.75 Mach number) to 470 miles per hour at 40,000 feet altitude (approximately 0.70 Mach number). The stick-force variation with airspeed for zero tab setting is stable, however, throughout the entire speed range of the tests up to 30,000 feet altitude. This is due to the floating characteristics of the elevator previously mentioned.

The airspeed above which the variation of the calculated elevator angle with speed is unstable (stick-fixed instability) is shown in figure 21. The curve was obtained by cross-plotting the data from figure 20. Figure 21 also shows the airspeed above which the airplane is indicated to be unstable with the stick free. Stick-free instability is defined as an unstable variation of stick force with airspeed at the trim speed. The data indicate that the airplane equipped with the H tail will be stable with the stick free for 20 to 40 miles per hour higher speed than with the stick fixed. This characteristic, although beneficial in the Mach number range of these tests, might prove undesirable at higher values. The pilot might be unaware that he was applying more up-elevator deflection because of the continuance of stick-free stability or of the possibly low stick forces when the airplane became unstable stick free. It is therefore possible he would allow the airplane to reach a Mach number at which the remaining stick travel would be insufficient to effect a recovery.

The variation of stick force and elevator angle with airspeed for the tests of the five tails are shown in figure 22. The data indicate that the changes in elevator profile made during these tests have no effect on the stick-fixed stability; stick-fixed instability occurs at approximately the same airspeed for all tails. The changes in the elevator profile do affect greatly the variation of stick force with airspeed. The data indicate that the stick-force variation with airspeed for the H_2 tail will remain stable to a speed above that for the H tail and above the range of the tests at zero tab angle. The push force with the H_2 tail also shows a greater increase with airspeed than that with the H tail. Although the push force with the H_3 tail increases more with airspeed than that with the H tail, the data show a reversal of stick force

at the high speeds. With the H_0 and H_1 tails a reversal in the variation of stick force with airspeed also occurs at approximately the same speed as that for the H_3 tail. The reversal with the H_0 and H_1 tails, however, is much more severe. Such a reversal in stick force is indicative that large pull forces would be required for dive recoveries. It occurs because the hinge-moment characteristics of the flat-sided elevators have not compensated for the stick-fixed instability as have those of the bulged elevators.

Stick-force gradient.- In order to simplify the computation of the stick forces for the airplane in accelerated flight, it was assumed that for normal accelerations greater than 1g the airplane was at the bottom of a pull-out and for normal accelerations of 1g or less the airplane flight path was straight.

The variation of stick force with normal acceleration for the airplane at several altitudes and speeds is shown in figure 23 for each of the five tails tested. The data indicate that the stick-force gradient with the H_2 tail (low-drag stabilizer, large bulge on elevator profile) is smaller than that with the other tails below 535 miles per hour at sea level and 500 miles per hour at 20,000 feet altitude (approximately 0.70 Mach number). At the higher speeds and low accelerations the H tail (standard) shows the smallest gradient. As previously mentioned, the very small value and the trend of the stick-force gradient with the H tail at the highest speed indicates that overbalance may occur at speeds above the maximum of the tests. At all speeds the H_0 tail (standard stabilizer, flat-sided elevator) shows the largest gradient. On the other hand the stick-force gradient with H_1 tail (low-drag stabilizer, flat-sided elevator) compares quite favorably with the gradients for the other low-drag tails at high speeds.

CONCLUSIONS

Wind-tunnel tests to determine the effect of modifications to the profile of the horizontal tail on the longitudinal static stability and control characteristics of a pursuit airplane indicate the following:

1. With the exception of small changes in the elevator angle for zero pitching moment, the profile changes have almost no effect on the pitching-moment characteristics of the model.

2. The effect of a bulge on the elevator profile with a

stabilizer having either a modified NACA four-digit or a 65-series airfoil profile is to change the quantities $\partial C_{h_e}/\partial \delta_e$ and $\partial C_{h_e}/\partial C_L$ from negative values to smaller negative or positive values and to cause the elevator angle corresponding to zero hinge moment to become more negative with increase in Mach number.

3. With either stabilizer, the flat-sided elevators produce a severe reversal in the variation of stick force with airspeed at high speeds. A small bulge on the elevator with the low-drag stabilizer reduces the severity of the reversal appreciably, but does not increase the speed at which it occurs. A large bulge on the elevator with either stabilizer eliminates the reversal throughout the wind-tunnel test range.

4. The effect of the bulged elevator profile is to reduce the stick-force gradient.

Ames Aeronautical Laboratory,
National Advisory Committee for Aeronautics,
Moffett Field, Calif., March 1947.

APPENDIX

AIRPLANE AND MODEL DIMENSIONS

	Model	Airplane
Wing area, square feet	25.91	233.19
Wing mean aerodynamic chord, feet	2.21	6.63
Wing span, feet	12.34	37.03
Aspect ratio of wing	5.89	5.89
Wing incidence at root, degrees	1.00	1.00
Elevator span (one elevator), feet	2.013	6.040
Mean square of elevator chord behind hinge line, feet squared	.133	1.196
Tail length (25 percent M.A.C. to elevator hinge line), feet	5.75	17.25
Stabilizer setting from fuselage reference line (all tails), degrees	2.00	2.00
Normal center-of-gravity location		
Percent mean aerodynamic chord	--	24.60
Distance below fuselage reference line, inches	--	10.60
Relation of stick force to elevator hinge moment, pounds per pound-foot	--	.602

REFERENCES

1. Nissen, James M., Gadeberg, Burnett L., and Hamilton, William T.: Correlation of the Drag Characteristics of a P-51B Airplane Obtained from High-Speed Wind-Tunnel and Flight Tests. NACA ACR No. 4K02, 1945.

2. Silverstein, Abe, and White, James Aubrey: Wind-Tunnel Interference with Particular Reference to Off-Center Positions of the Wing and to the Downwash at the Tail. NACA Rep. No. 547, 1935.

TABLE I.- SUMMARY OF ELEVATOR HINGE-MOMENT CHARACTERISTICS

TAIL	Elevator profile	Shape of C_{h_e}, δ_e curve for $C_L = 0$		[a] $\left(\frac{\partial C_{h_e}}{\partial \delta_e}\right)$		[a] $\left(\frac{\partial C_{h_e}}{\partial C_L}\right)$		δ_e for $C_{h_e} = 0$ at $C_L = 0$	
		Mach number							
		0.304	0.80	0.304	0.80	0.304	0.80	0.304	0.80
H	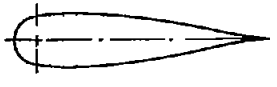	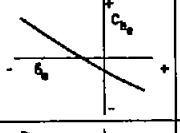	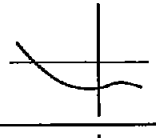	-.0041	-.0012	+.0072	+.0232	-2.07	-6.36
H_0	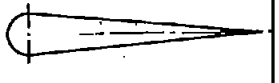	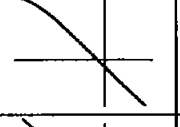	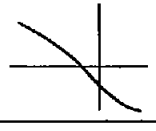	-.0094	-.0086	-.0142	-.0098	-0.65	-1.86
H_1	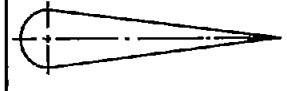	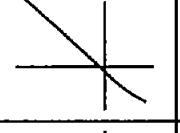	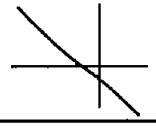	-.0082	-.0068	-.0103	+.0068	-0.45	-1.80
H_2	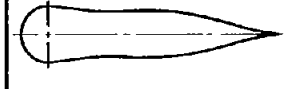	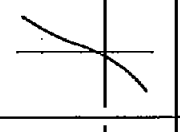	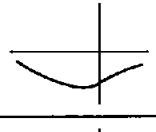	-.0059	+.0011	+.0038	+.1030	-1.00	[b]9.00
H_3	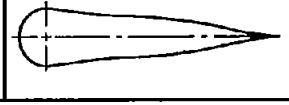	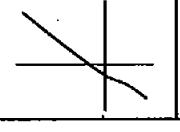	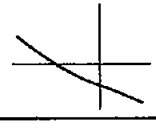	-.0057	-.0035	+.0036	+.0340	-1.37	-4.47

[a] Values measured at $C_L = 0$ and $C_m = 0$
[b] Value extrapolated

NATIONAL ADVISORY COMMITTEE FOR AERONAUTICS

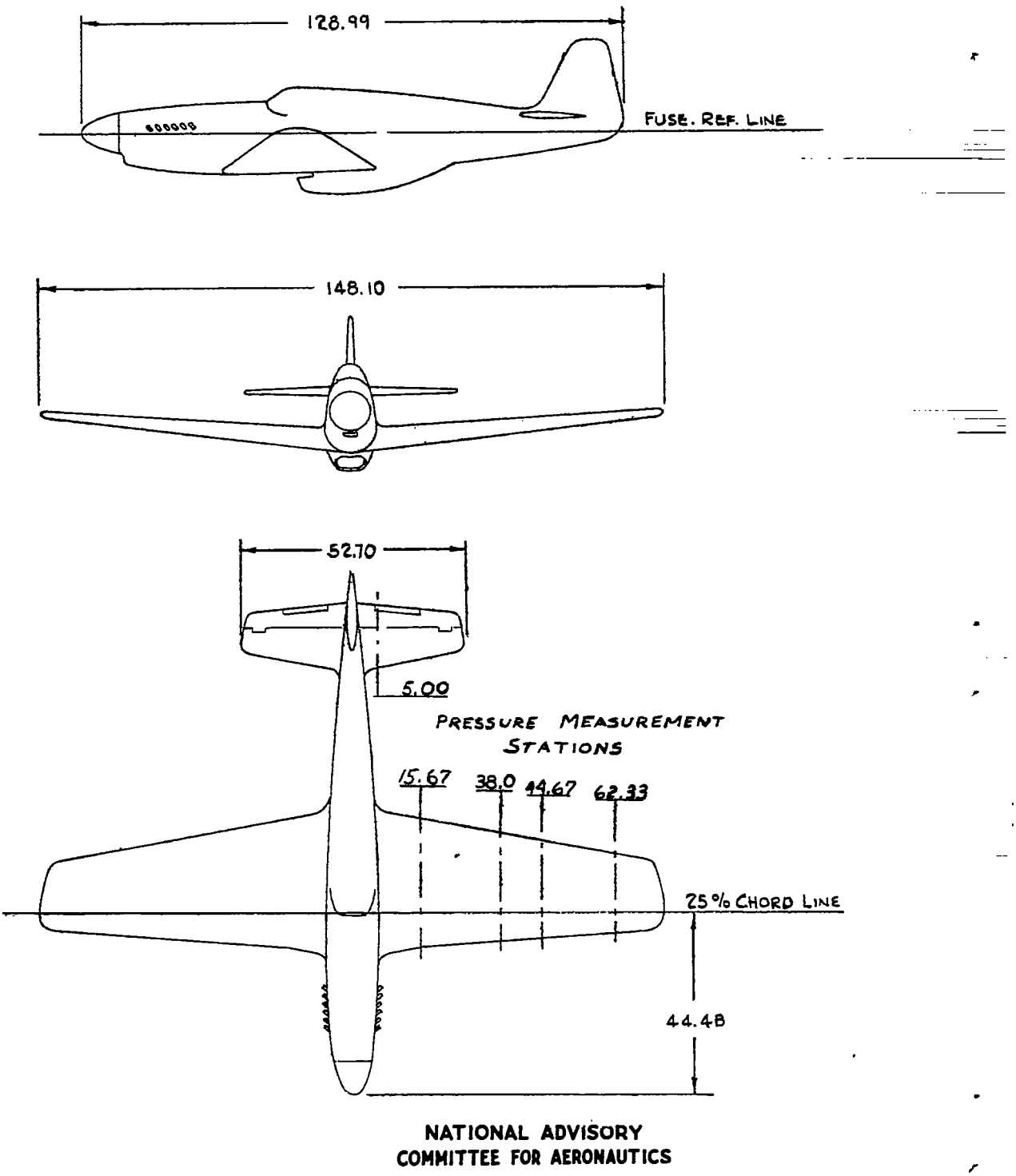

FIGURE 1.- THREE-VIEW DRAWING OF THE 1/3-SCALE MODEL OF THE PURSUIT AIRPLANE.

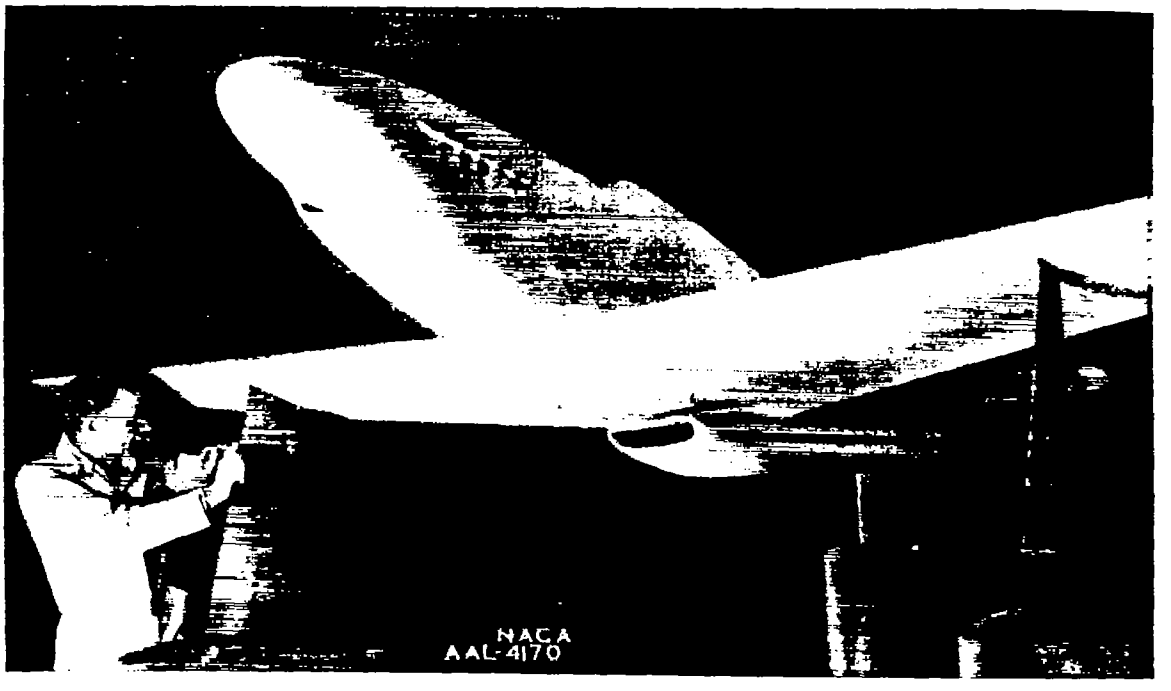

Figure 2.- The P-51B model in the 16-foot wind tunnel.

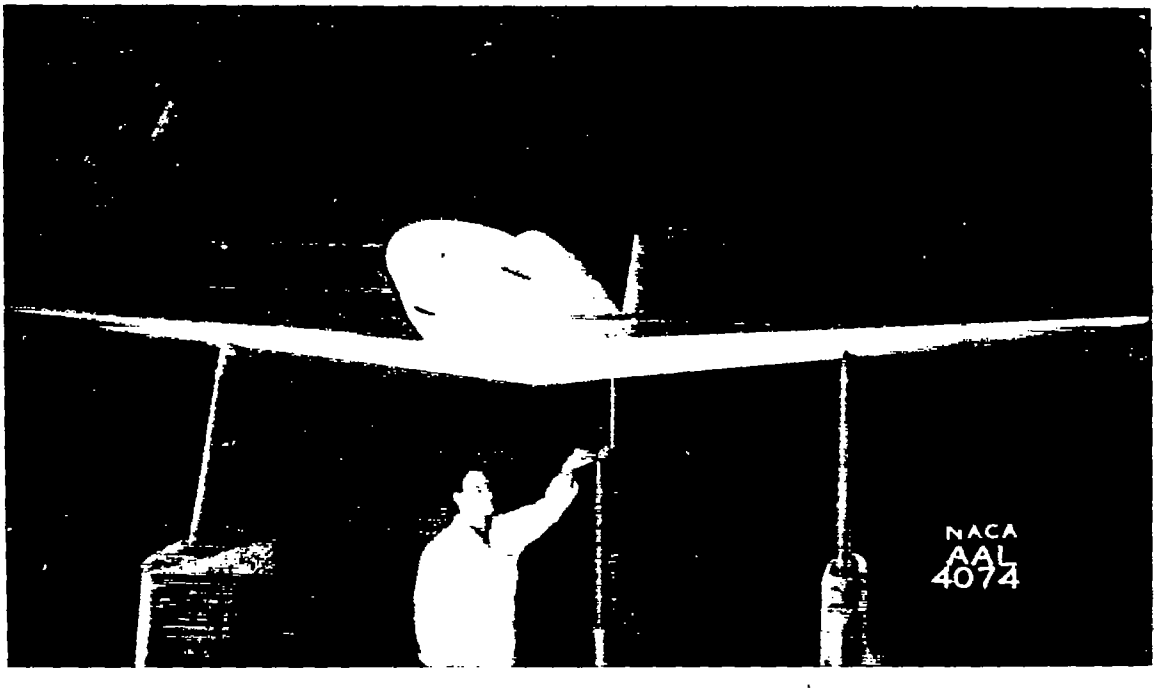

Figure 3.- The P-51B model with the cooling duct removed.

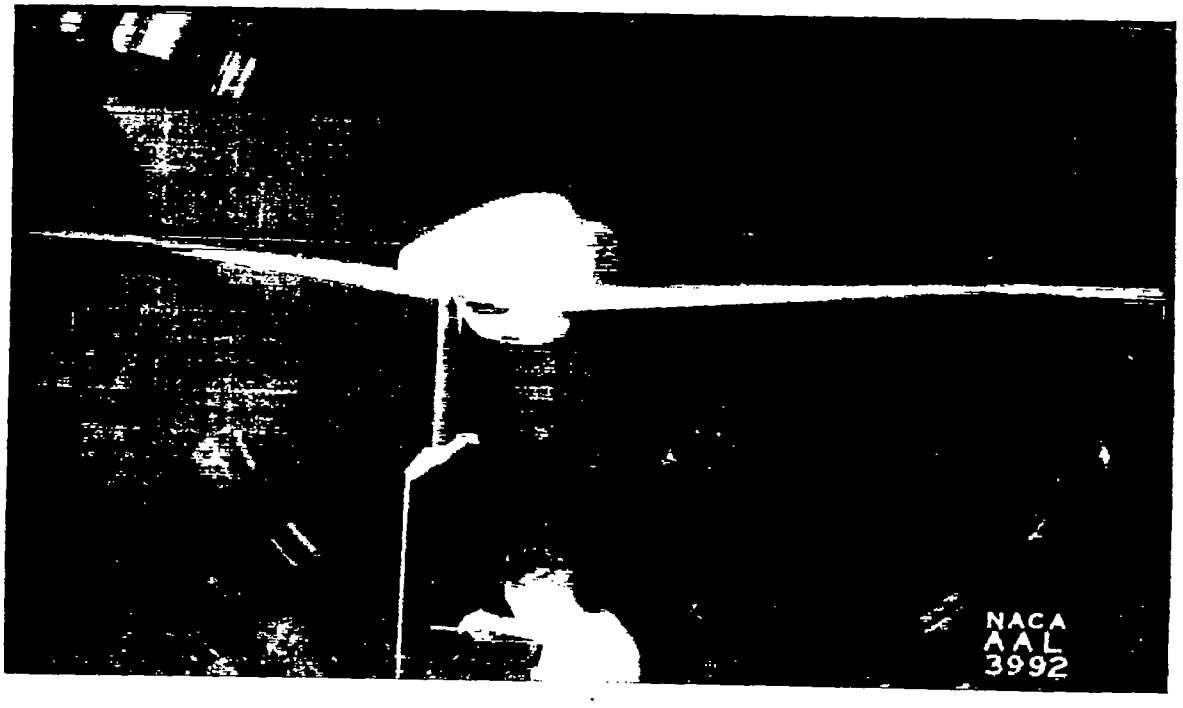

Figure 4.- The P-51B model supported at the wing tips and at the tail.

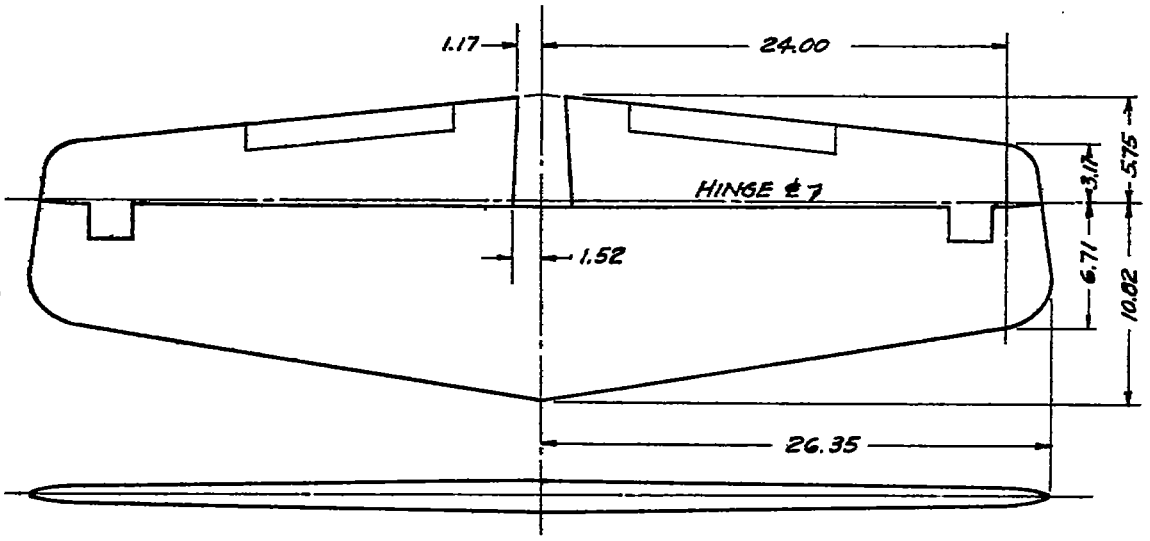

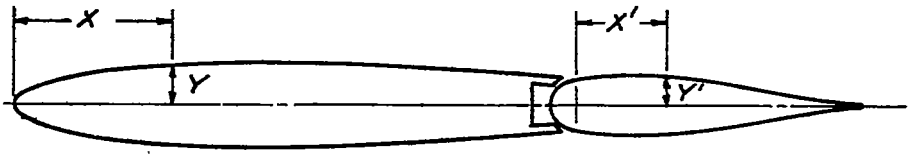

SECTION AT ℄ STABILIZER AND INB'D END OF ELEVATOR

TAIL SURFACE COORDINATES							
STABILIZER				ELEVATOR			
STA. 0		STA. 24		INB'D END		STA. 24	
X	Y	X	Y	X'	Y'	X'	Y'
0	0	0	0	L.E. RAD.	0.520	L.E. RAD	0.350
0.400	0.373	0.123	0.147	0	0.527	0	0.357
1.067	0.573	0.707	0.317	0.333	0.560	0.333	0.383
1.650	0.677	1.374	0.407	0.667	0.583	0.667	0.387
2.233	0.750	2.707	0.477	1.000	0.597	1.000	0.367
2.817	0.793	4.040	0.463	1.333	0.600	1.333	0.333
3.567	0.830	5.374	0.413	1.667	0.587	1.667	0.280
4.233	0.847	6.707	0.340	2.000	0.560	2.000	0.220
4.817	0.847	L.E. RAD.	0.097	2.667	0.480	2.333	0.157
5.484	0.840			3.333	0.377	2.667	0.093
6.817	0.797			4.000	0.263	3.000	0.037
8.150	0.723			4.500	0.180	3.170	0
9.484	0.627			5.167	0.077	T.E. RAD.	0.016
10.817	0.520			5.633	0		
L.E. RAD.	0.203			T.E. RAD.	0.016		

NATIONAL ADVISORY
COMMITTEE FOR AERONAUTICS

FIGURE 5. - DIMENSIONAL DATA FOR H TAIL.
(STANDARD TAIL)

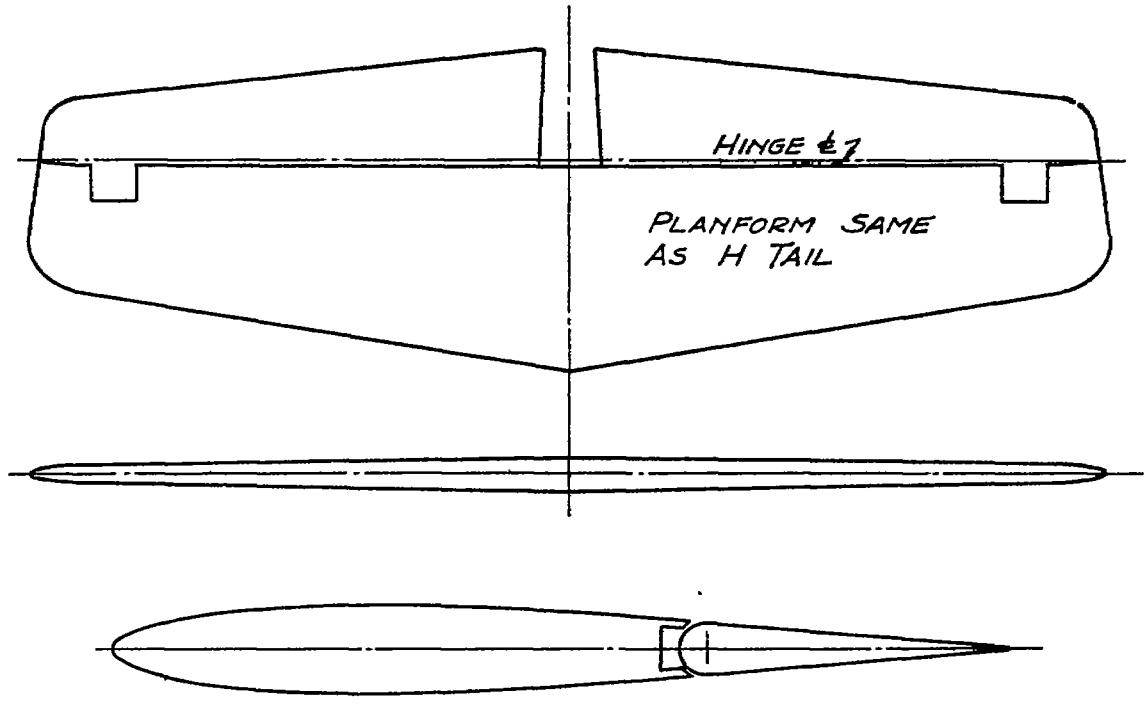

SECTION AT ℄ STABILIZER AND INB'D END OF ELEVATOR

TAIL SURFACE COORDINATES					
STABILIZER		ELEVATOR			
STA. 0	STA. 24	INB'D END		STA. 24	
SAME AS H TAIL	SAME AS H TAIL	L.E. RAD.	0.509	L.E. RAD.	0.340
		STRAIGHT LINE TANG. TO RADII		STRAIGHT LINE TANG. TO RADII	
		T.E. RAD.	0.016	T.E. RAD.	0.016

NATIONAL ADVISORY
COMMITTEE FOR AERONAUTICS

FIGURE 6.- DIMENSIONAL DATA FOR H_o TAIL
(STANDARD TAIL; FLAT-SIDED ELEVATOR)

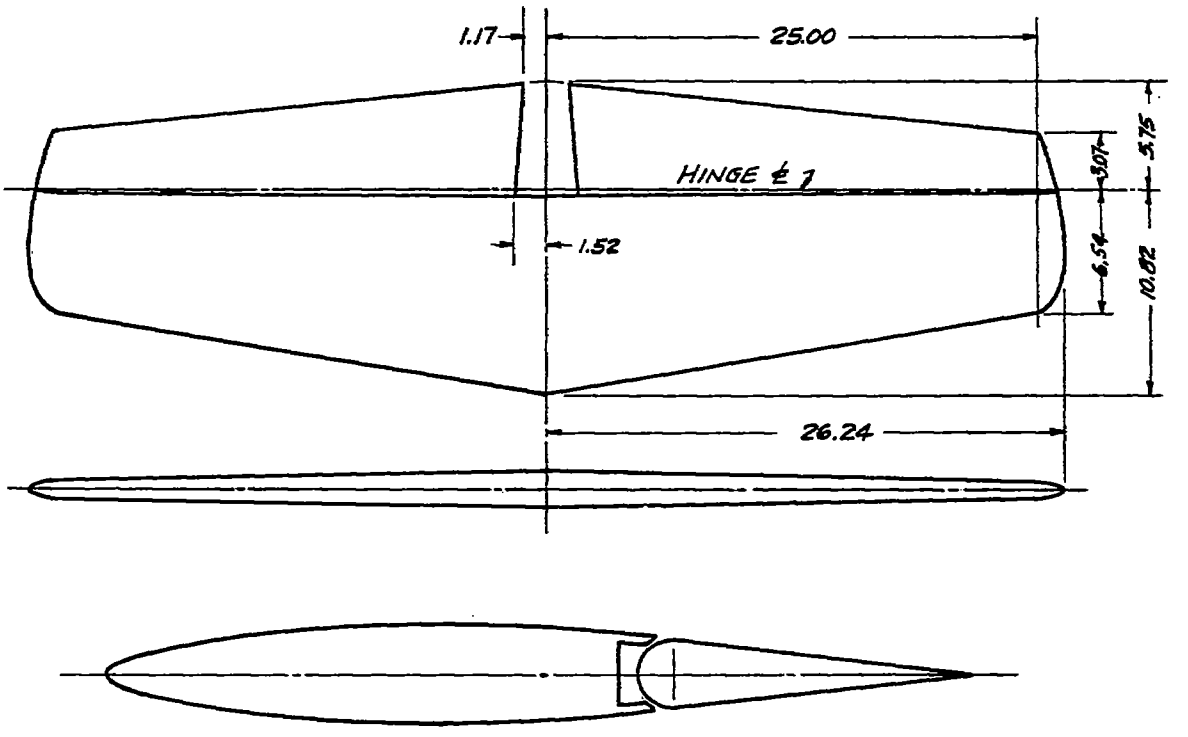

SECTION AT ℄ STABILIZER AND INB'D END OF ELEVATOR

TAIL SURFACE COORDINATES					
STABILIZER		ELEVATOR			
STA. 0	STA. 25	INB'D END		STA. 25	
NACA 65_2-012	NACA 65_2-010	L.E. RAD.	0.685 STRAIGHT LINE TANG. TO RADII	L.E. RAD.	0.314 STRAIGHT LINE TANG TO RADII
		T.E. RAD.	0.016	T.E. RAD.	0.016

NATIONAL ADVISORY COMMITTEE FOR AERONAUTICS

FIGURE 7. - DIMENSIONAL DATA FOR H, TAIL. (LOW-DRAG TAIL)

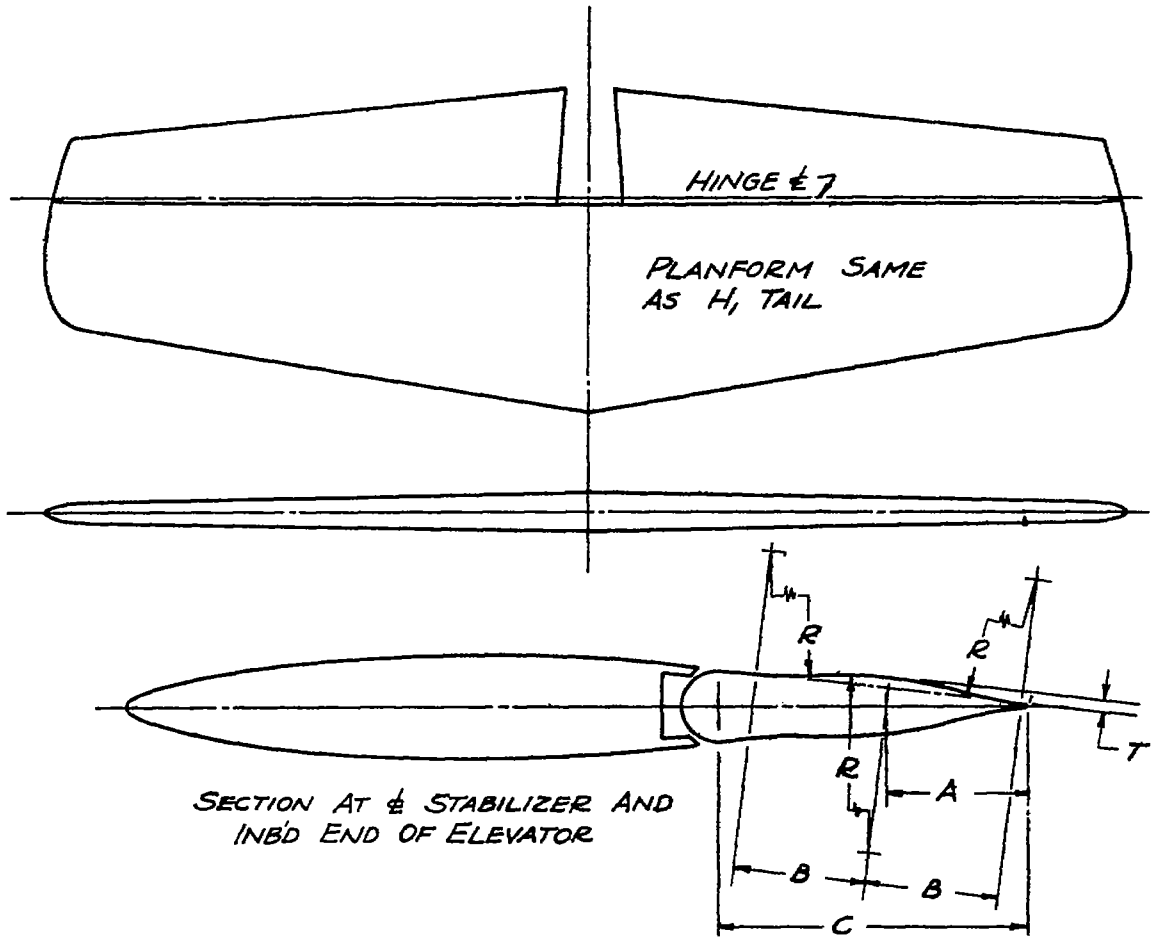

TAIL SURFACE COORDINATES					
STABILIZER		ELEVATOR			
STA. 0	STA. 25	INB'D END		STA. 25	
SAME AS H, TAIL	SAME AS H, TAIL	A	2.57	A	1.41
		B	2.44	B	1.33
		C	5.62	C	3.07
		R	7.67	R	4.19
		T	0.196	T	0.107
		BULGES DIMENSIONED ABOVE WERE ADDED TO ELEVATOR OF H, TAIL			

NATIONAL ADVISORY COMMITTEE FOR AERONAUTICS

FIGURE 8.- DIMENSIONAL DATA FOR H_2 TAIL. (LOW-DRAG TAIL; LARGE BULGE ON ELEVATOR)

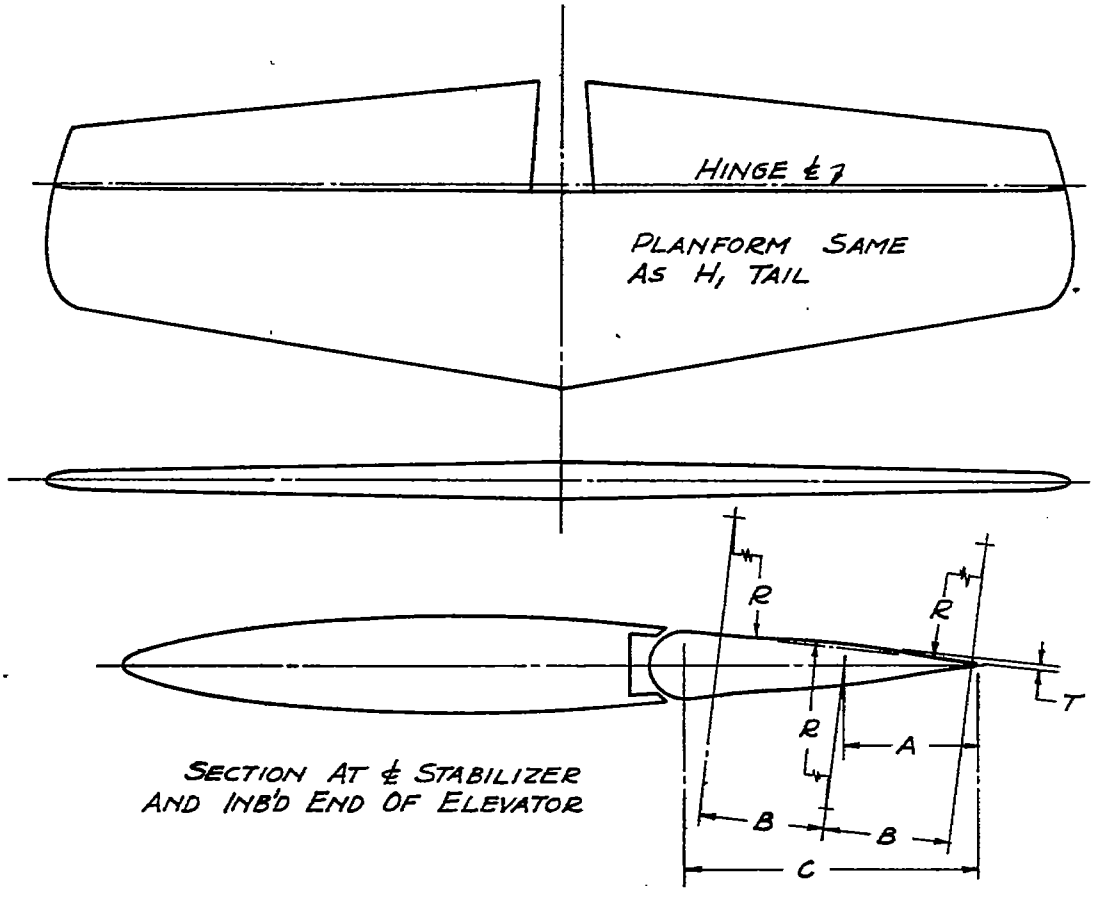

TAIL SURFACE COORDINATES					
STABILIZER		ELEVATOR			
STA. 0	STA. 25	INB'D END		STA. 25	
SAME AS H, TAIL	SAME AS H, TAIL	A	2.57	A	1.41
		B	2.44	B	1.33
		C	5.62	C	3.07
		R	15.30	R	8.37
		T	0.098	T	0.054
		BULGES DIMENSIONED ABOVE WERE ADDED TO ELEVATOR OF H, TAIL			

NATIONAL ADVISORY COMMITTEE FOR AERONAUTICS

FIGURE 9.- DIMENSIONAL DATA FOR H_3 TAIL. (LOW-DRAG TAIL; SMALL BULGE ON ELEVATOR)

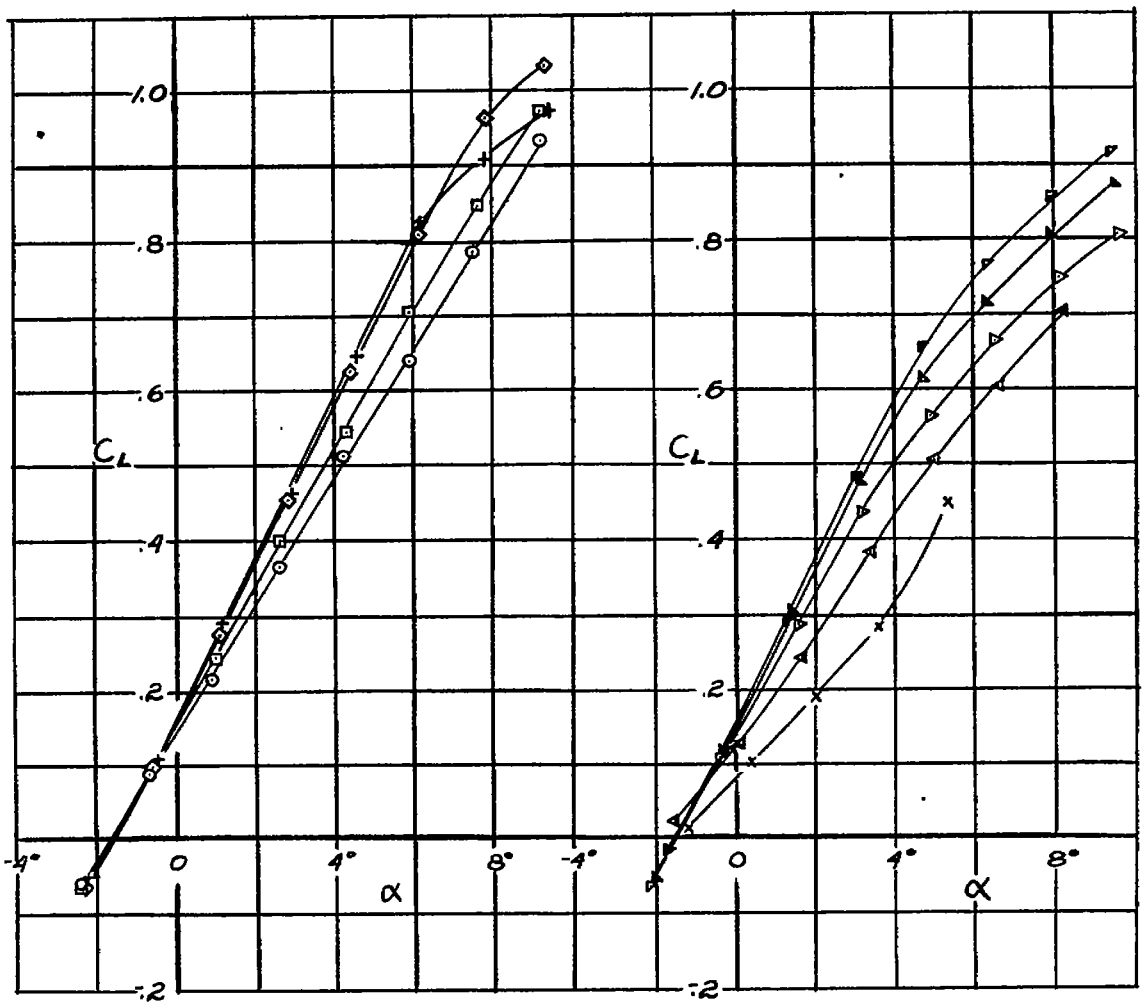

M		M	
○	0.304	▽	0.704
□	0.504	△	0.728
◇	0.654	▷	0.754
+	0.679	◁	0.779
		×	0.808

(a) In relation to angle of attack.

Figure 10.- The lift coefficient.

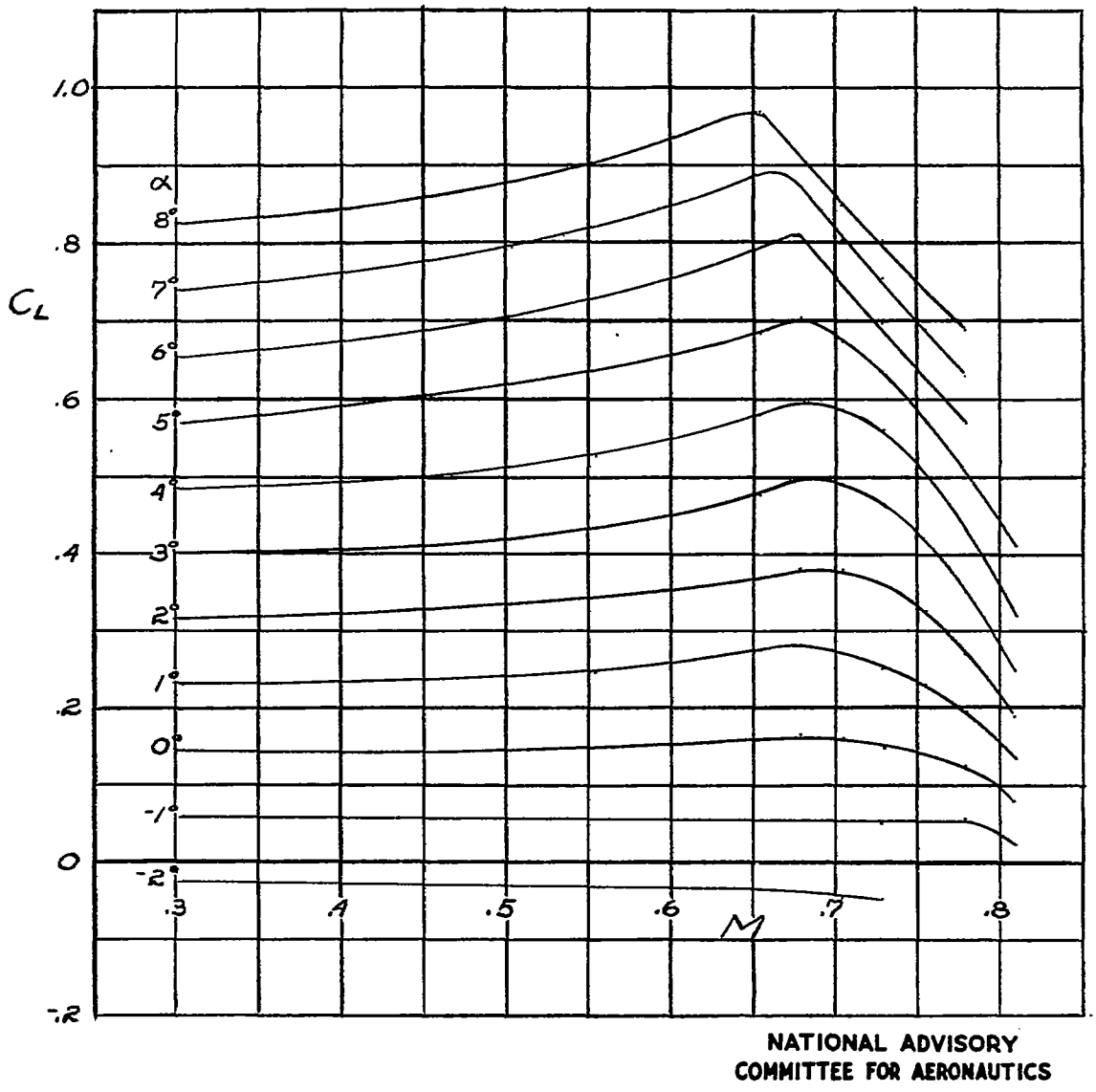

(b) In relation to Mach number.

Figure 10.- Concluded.

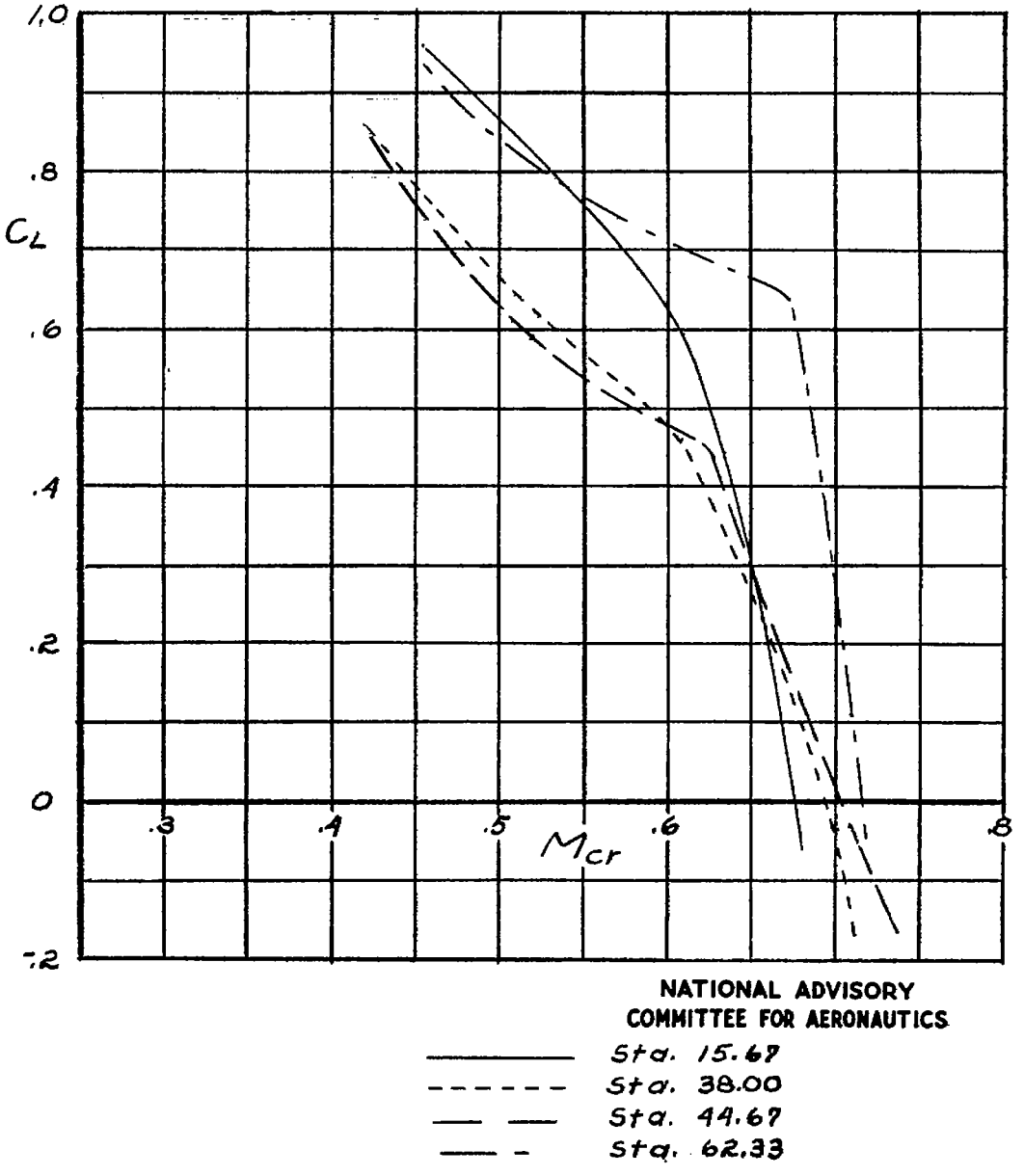

Figure 11.- The critical Mach number at four stations on the wing.

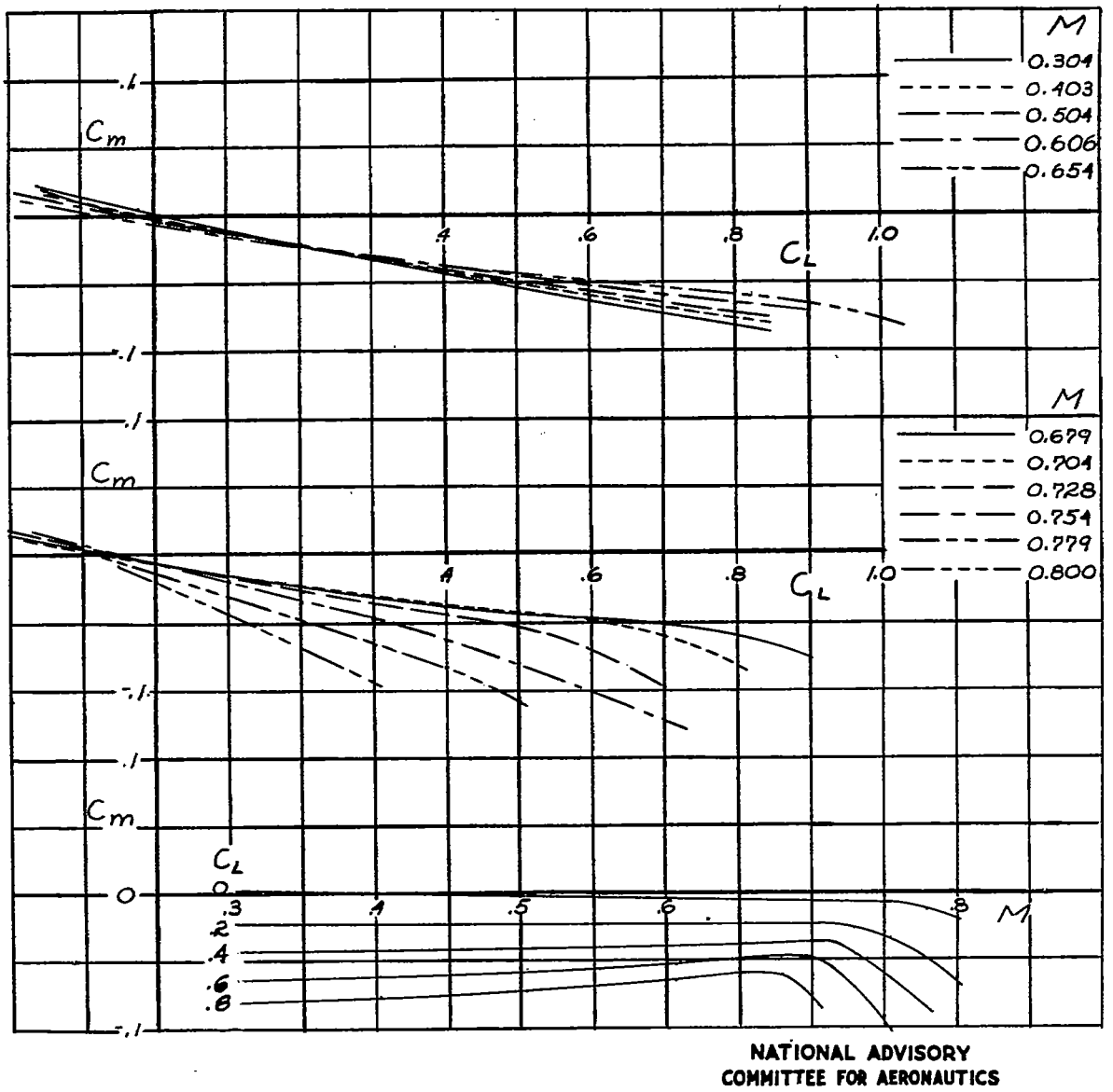

Figure 12.- The pitching-moment coefficient of the model with the cooling duct removed, H tail, 0° elevator angle.

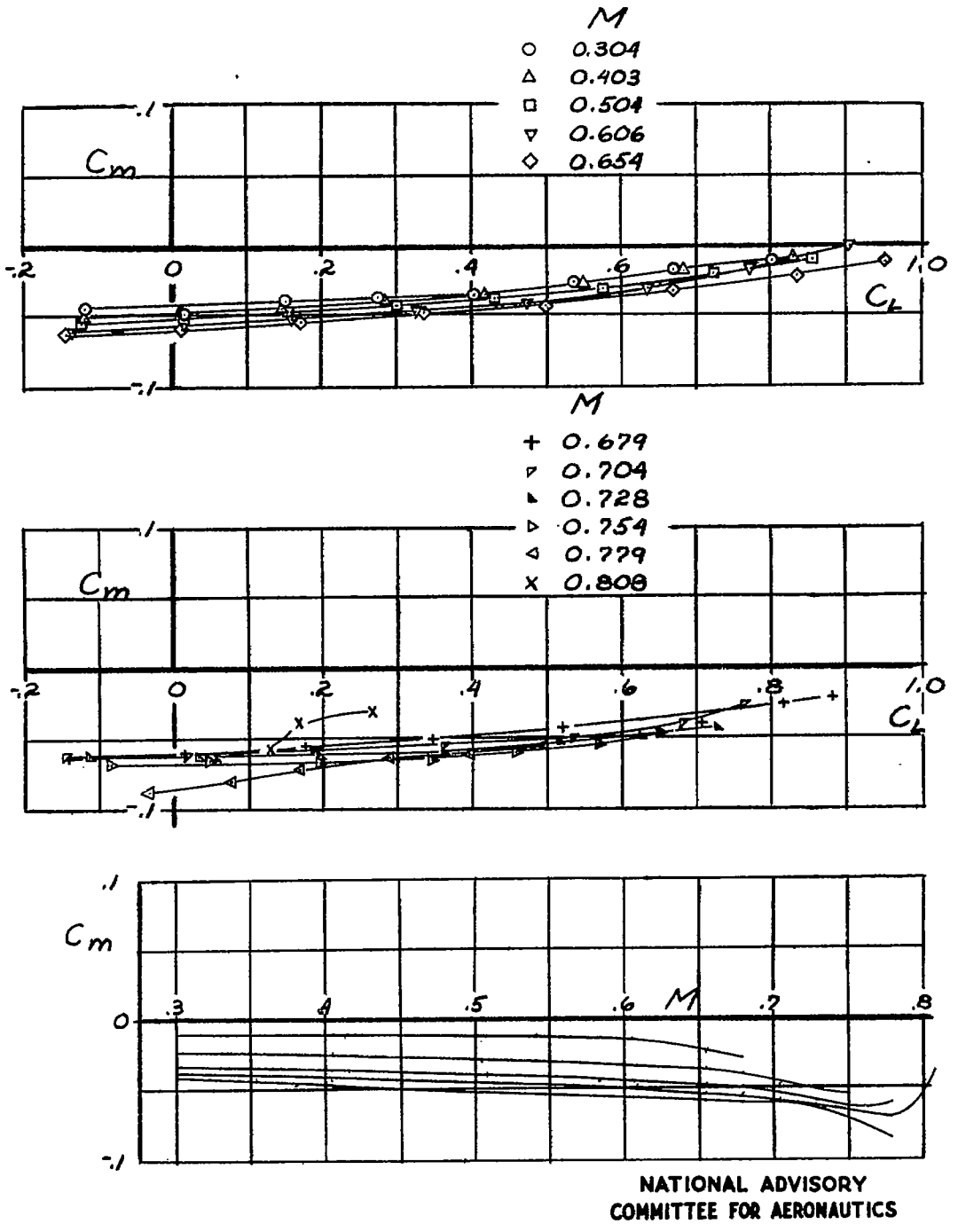

Figure 13.- The pitching-moment coefficient of the model with the empennage and cooling duct removed.

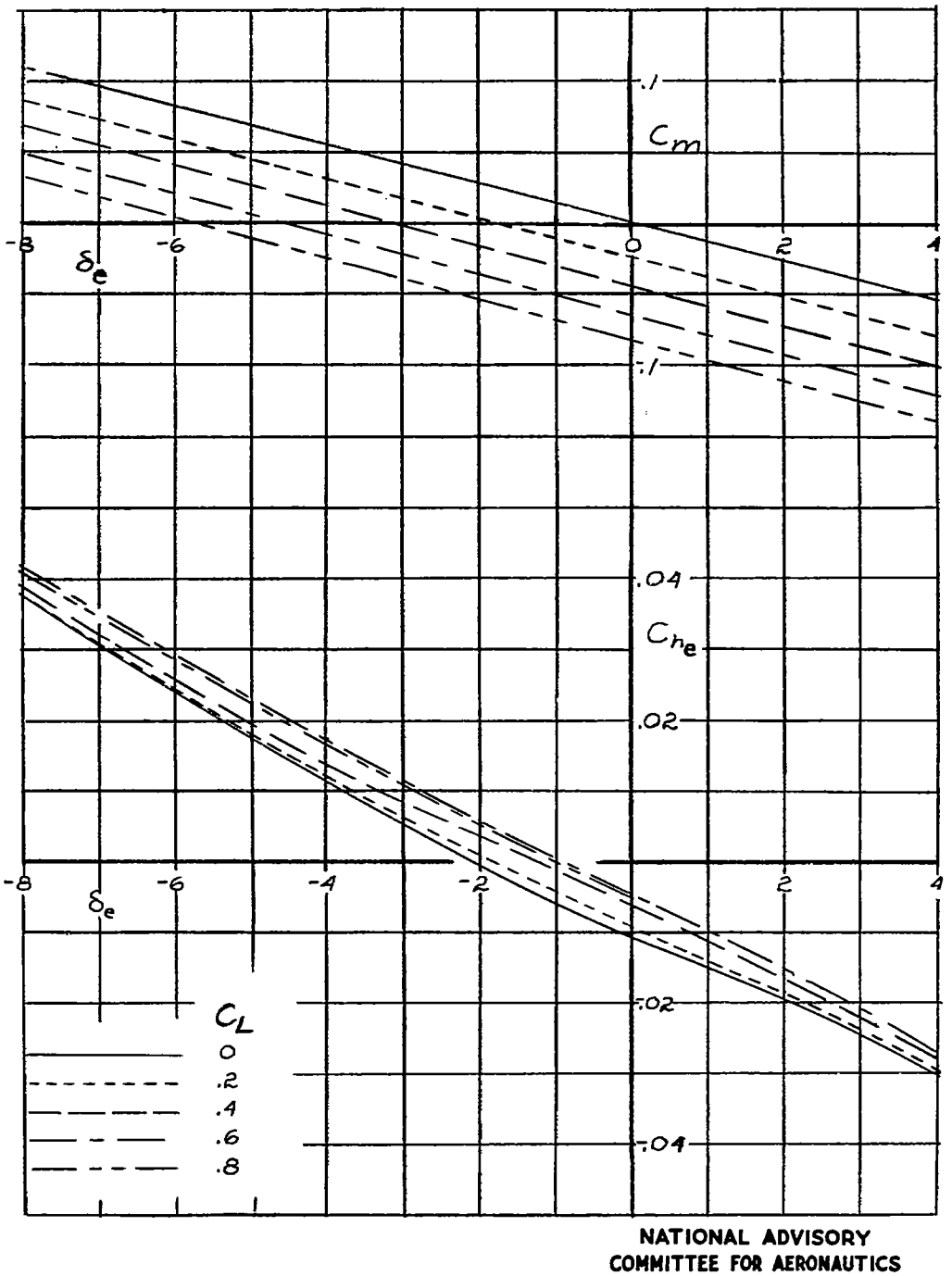

(a) 0.304 Mach number.

Figure 14.-The pitching-moment and elevator hinge-moment coefficients of the model with the H tail Cooling duct removed.

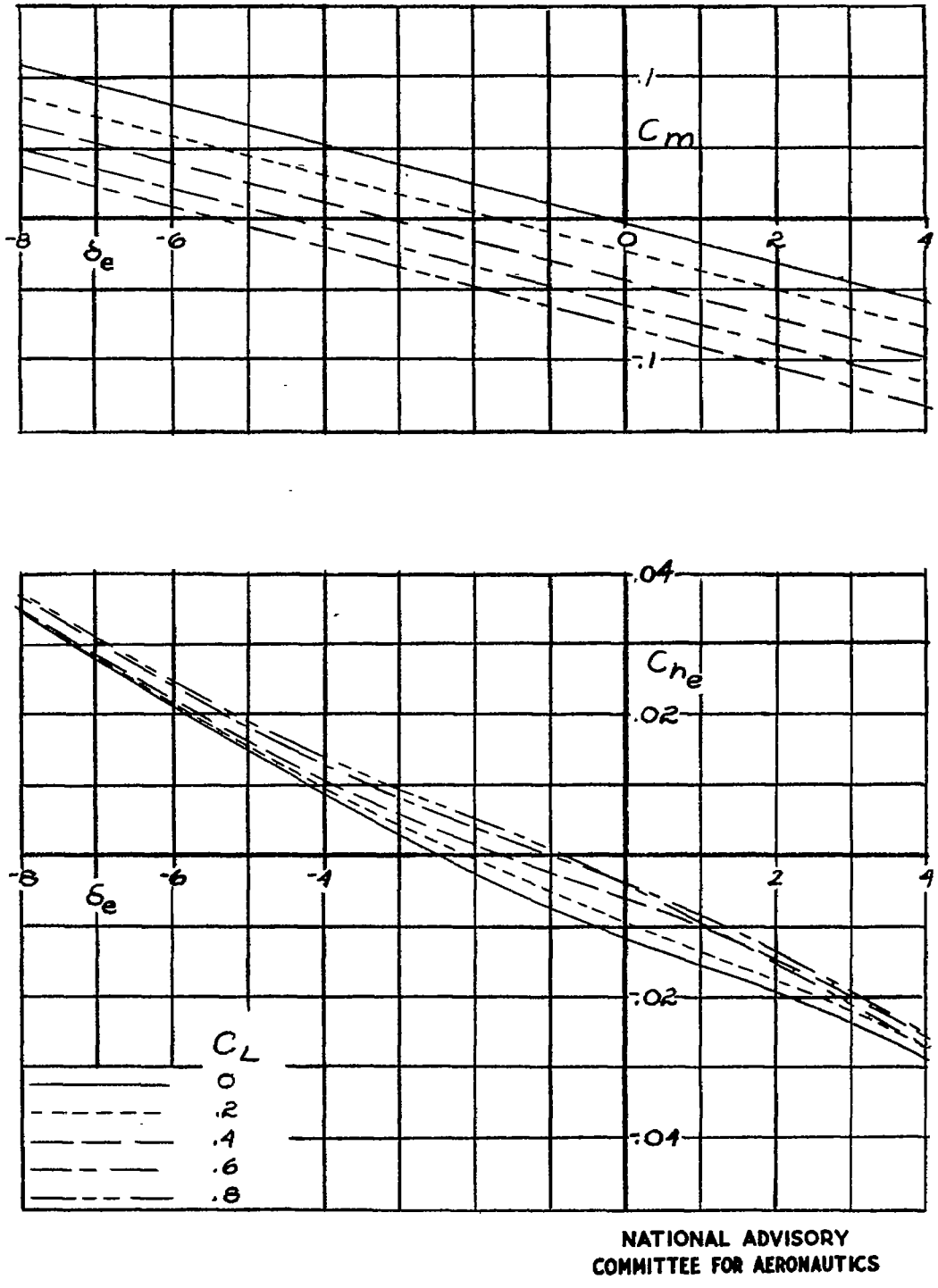

(b) 0.403 Mach number.

Figure 14.-Continued.

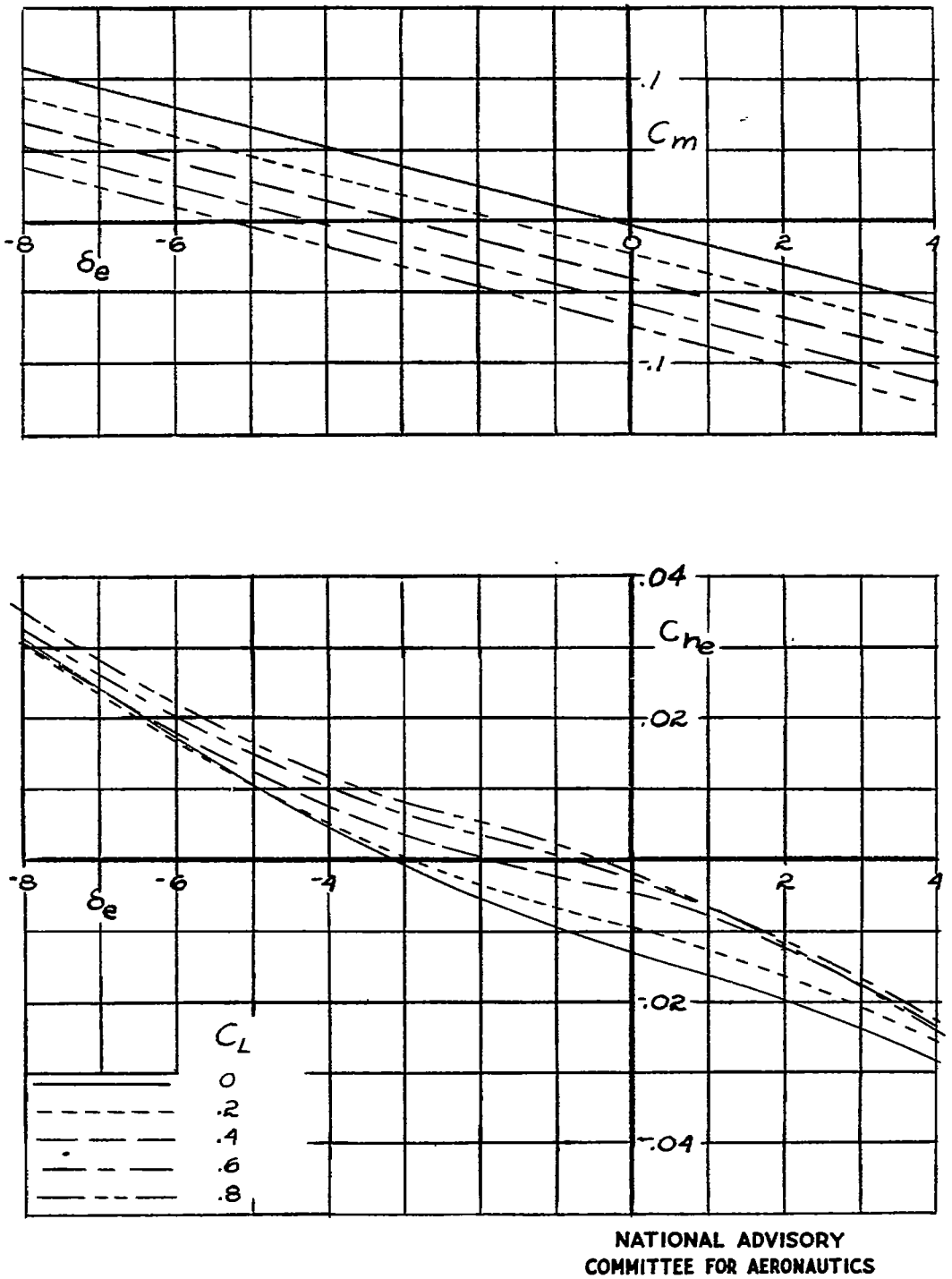

(c) 0.504 Mach number.

Figure 14.-Continued.

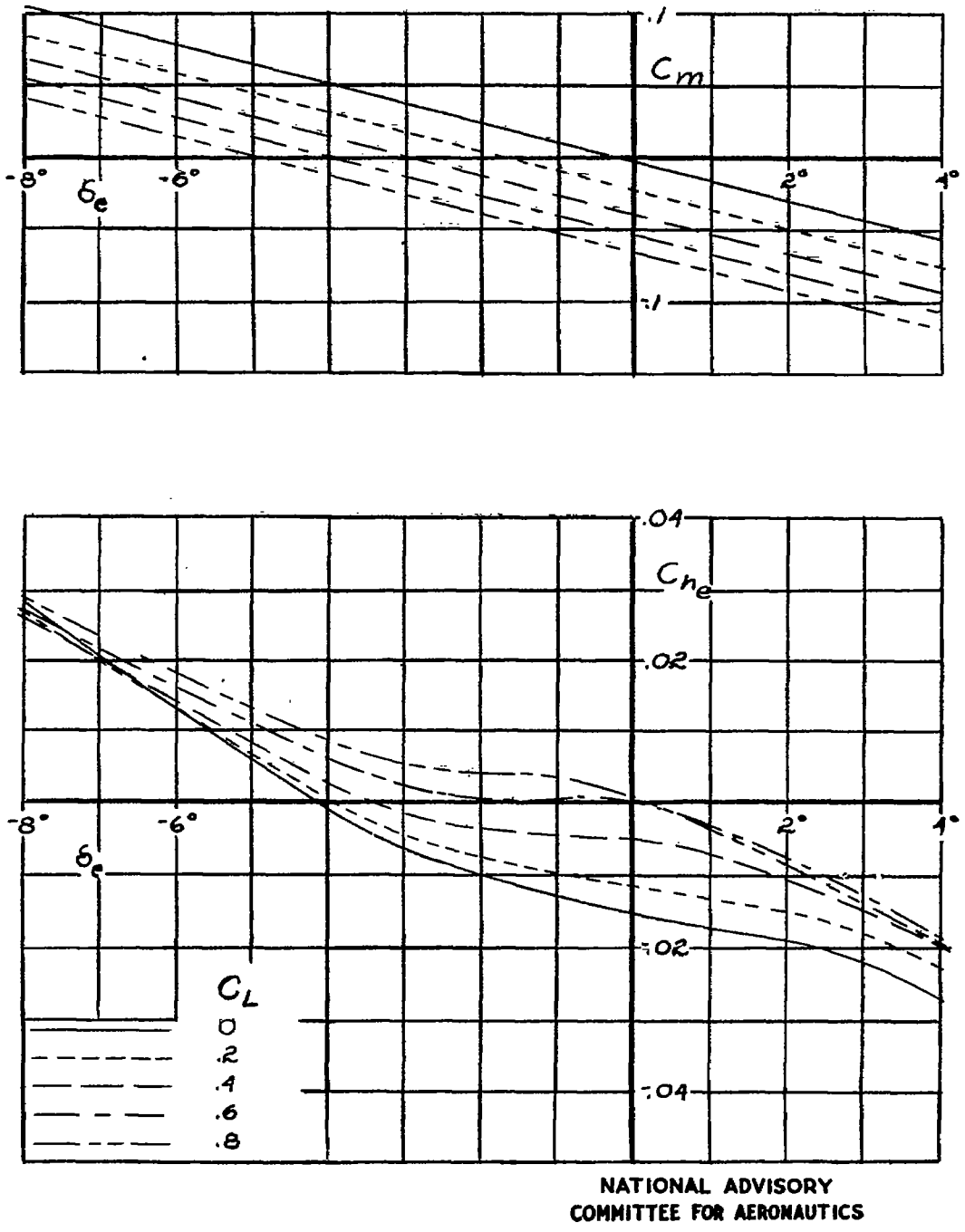

(d) 0.606 Mach number.

Figure 14.-Continued.

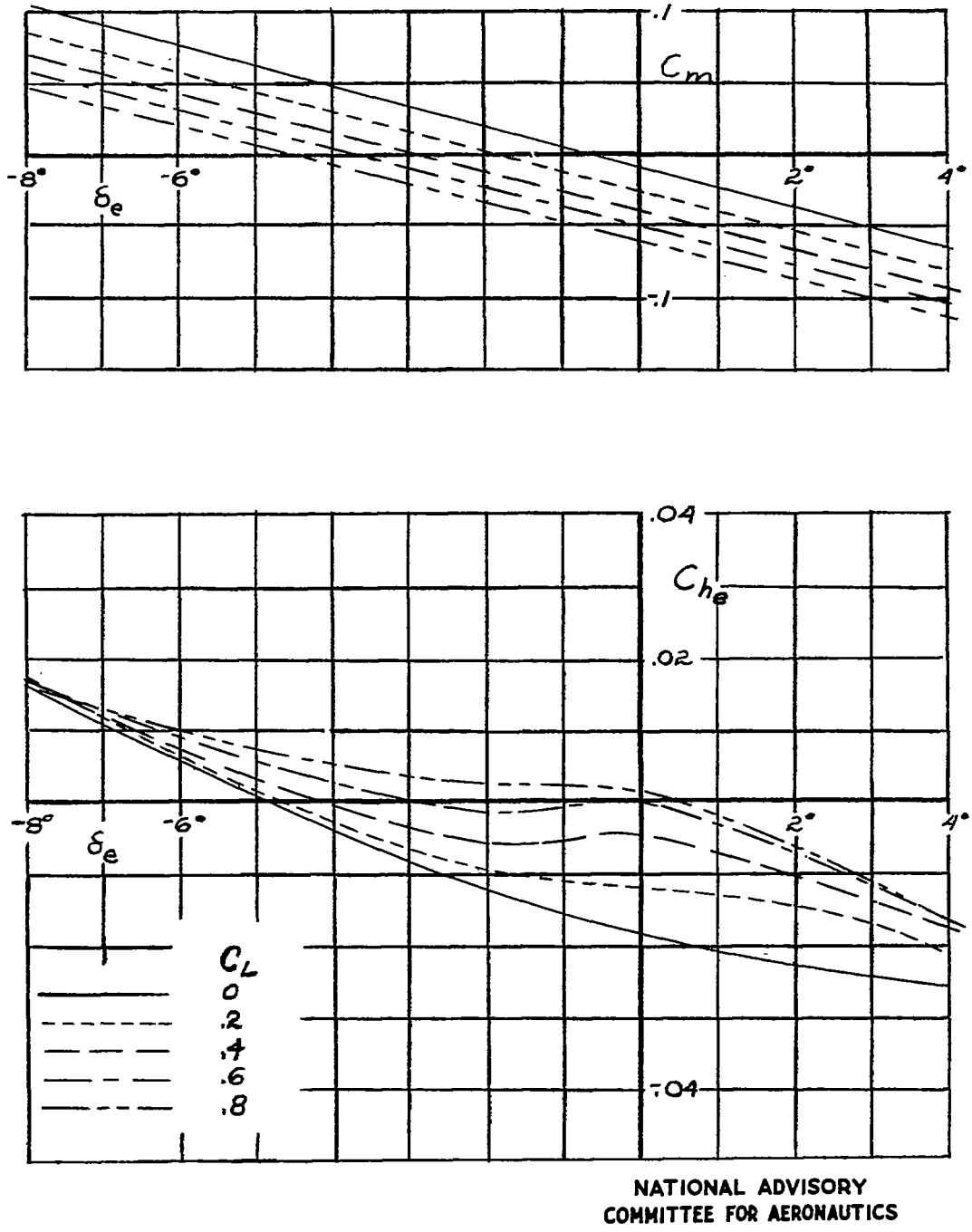

(e) 0.654 Mach number.

Figure 14.- Continued.

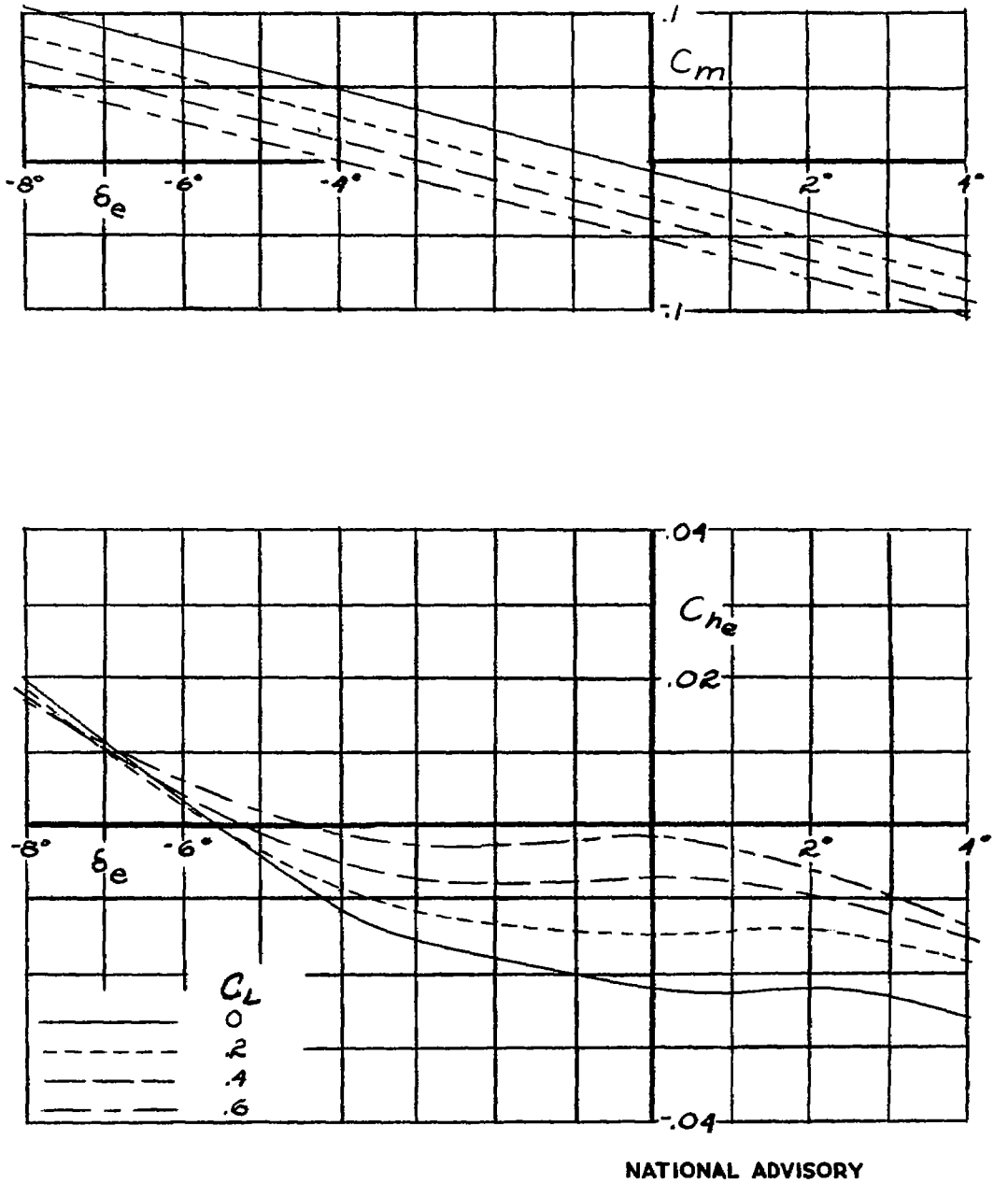

(f) 0.704 Mach number.

Figure 14.- Continued.

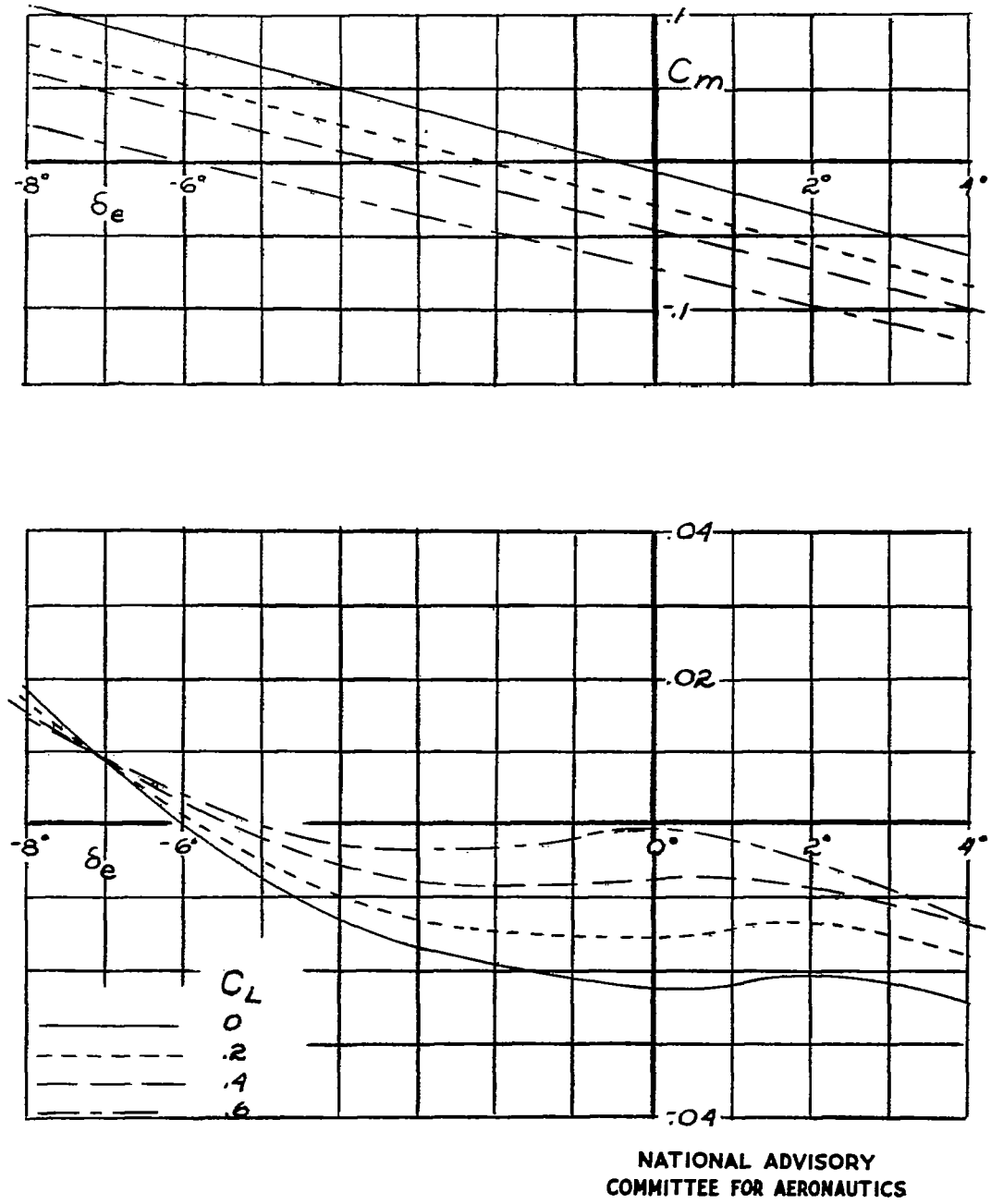

(g) 0.728 Mach number.

Figure 14.- Continued.

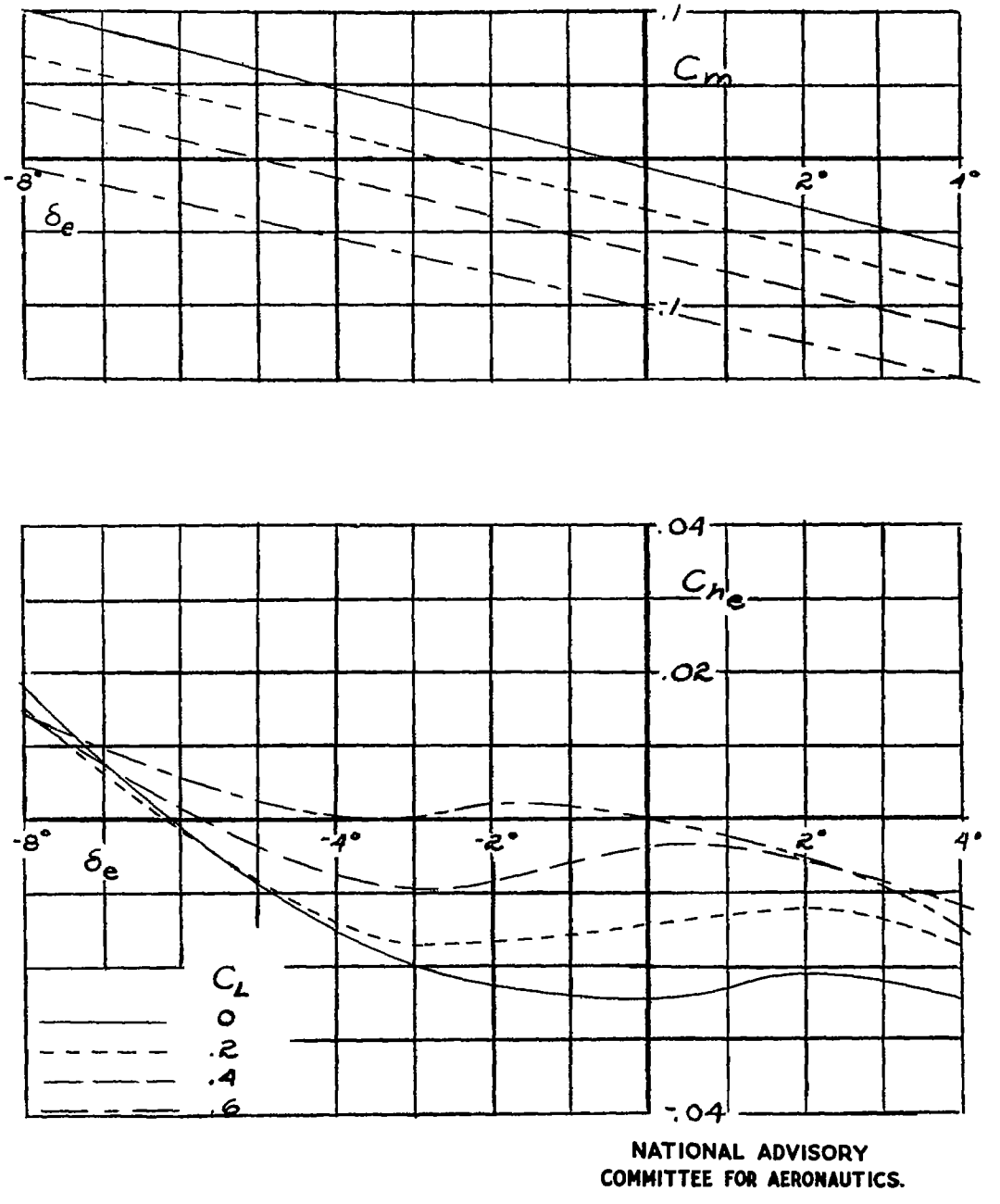

(h) 0.754 Mach number.

Figure 14.- Continued.

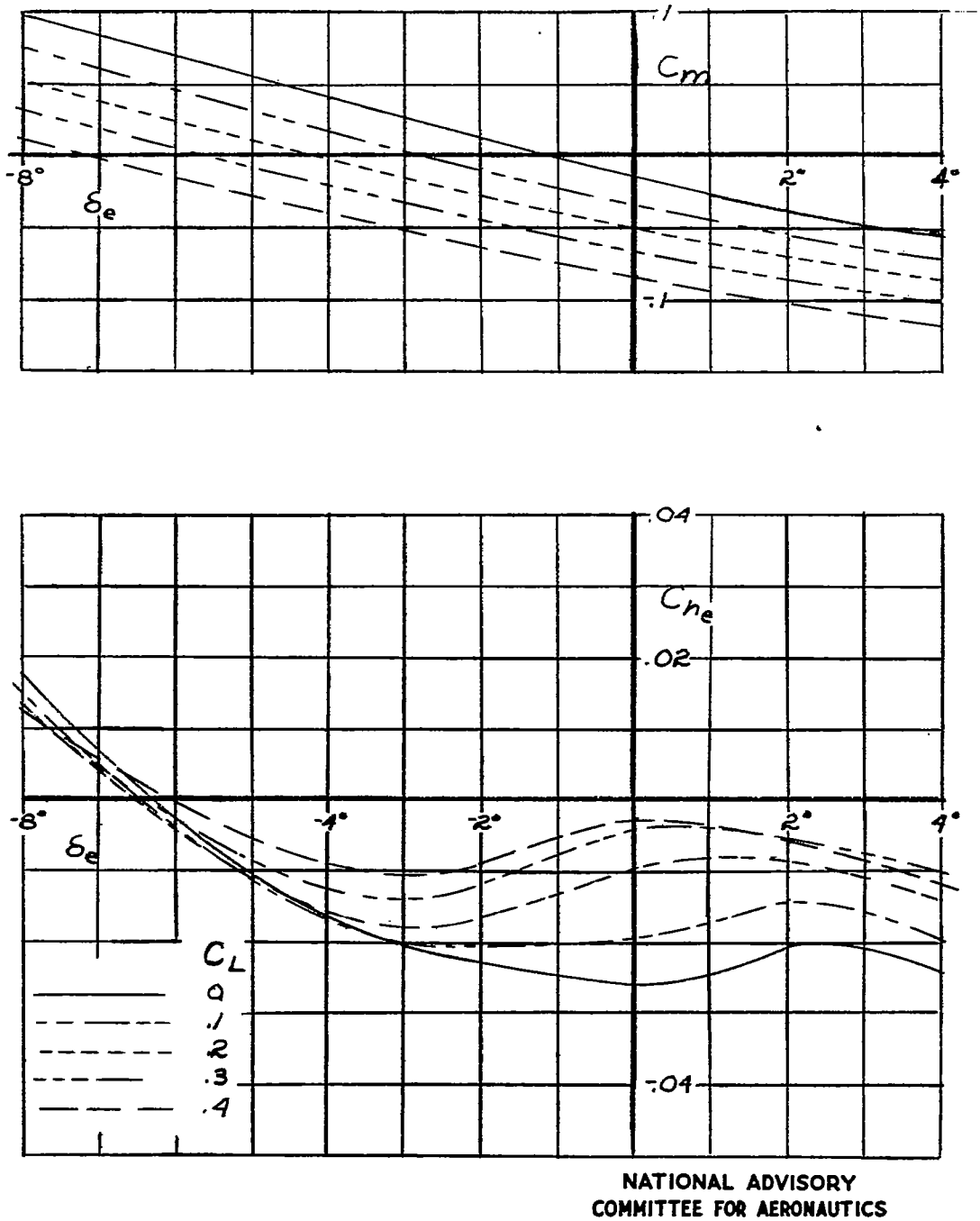

(i) 0.779 Mach number.

Figure 14.- Continued.

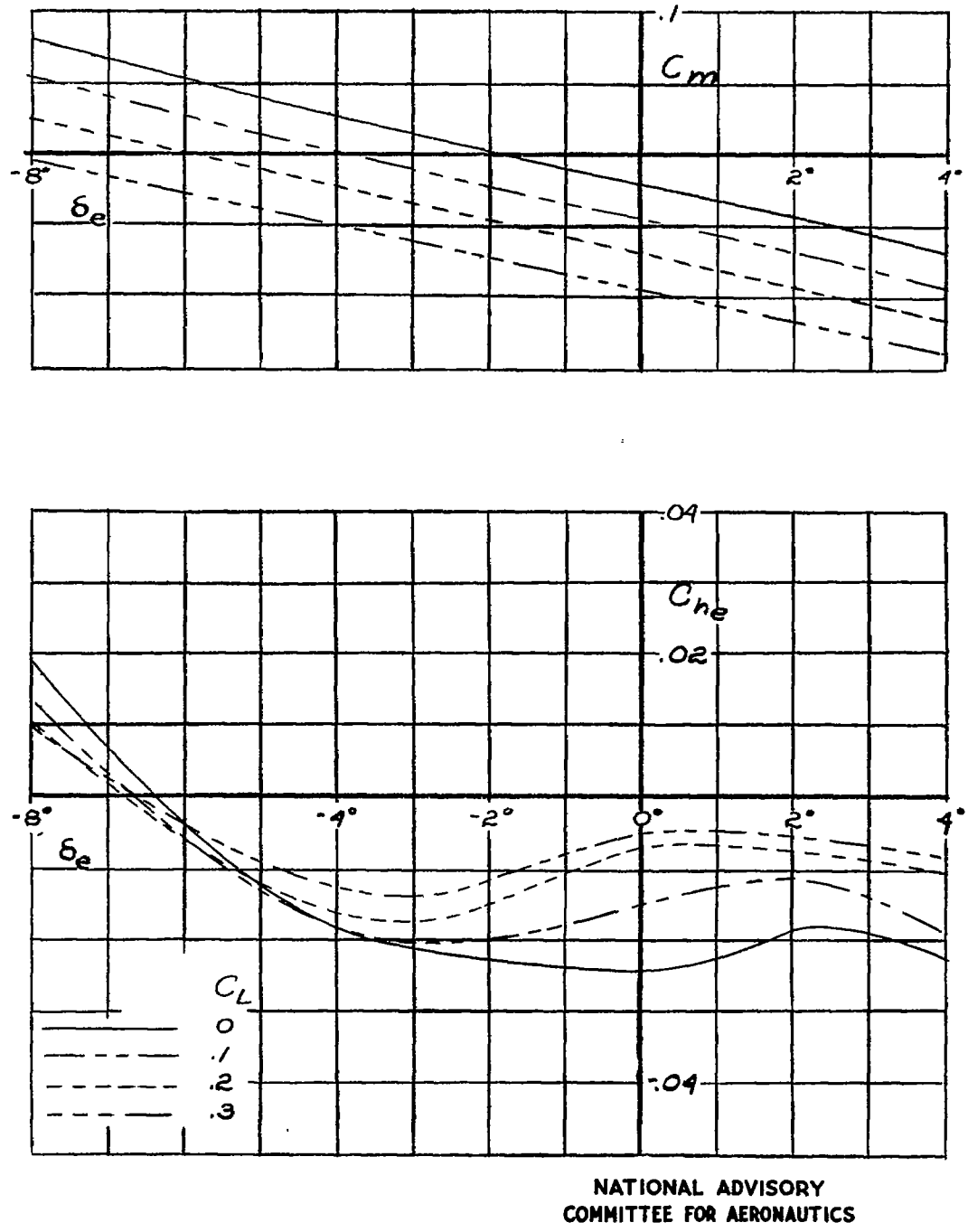

(j) 0.80 Mach number.

Figure 14.- Concluded.

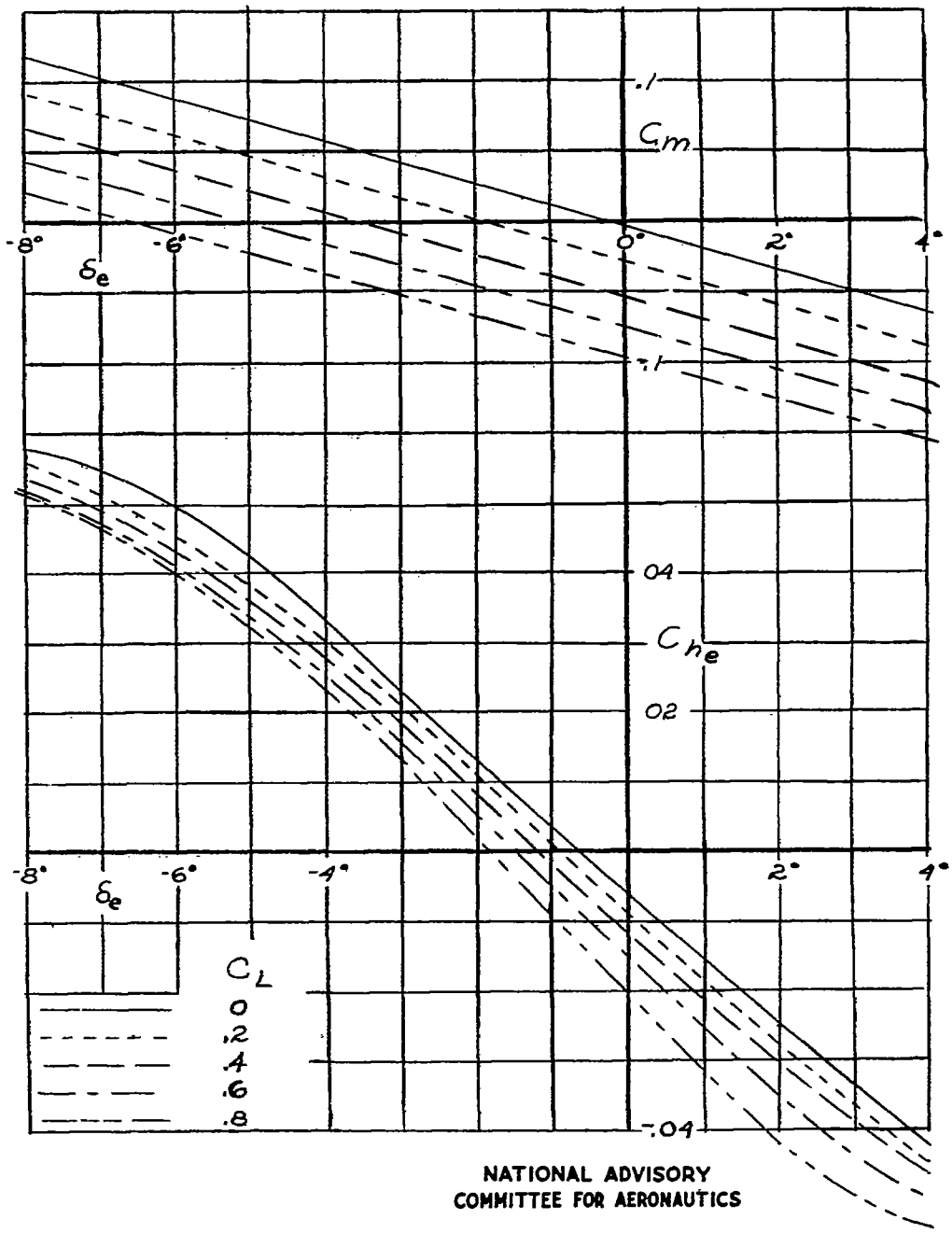

(a) 0.304 Mach number.

Figure 15.- The pitching-moment and elevator hinge-moment coefficients of the model with the H_o tail. Cooling duct removed.

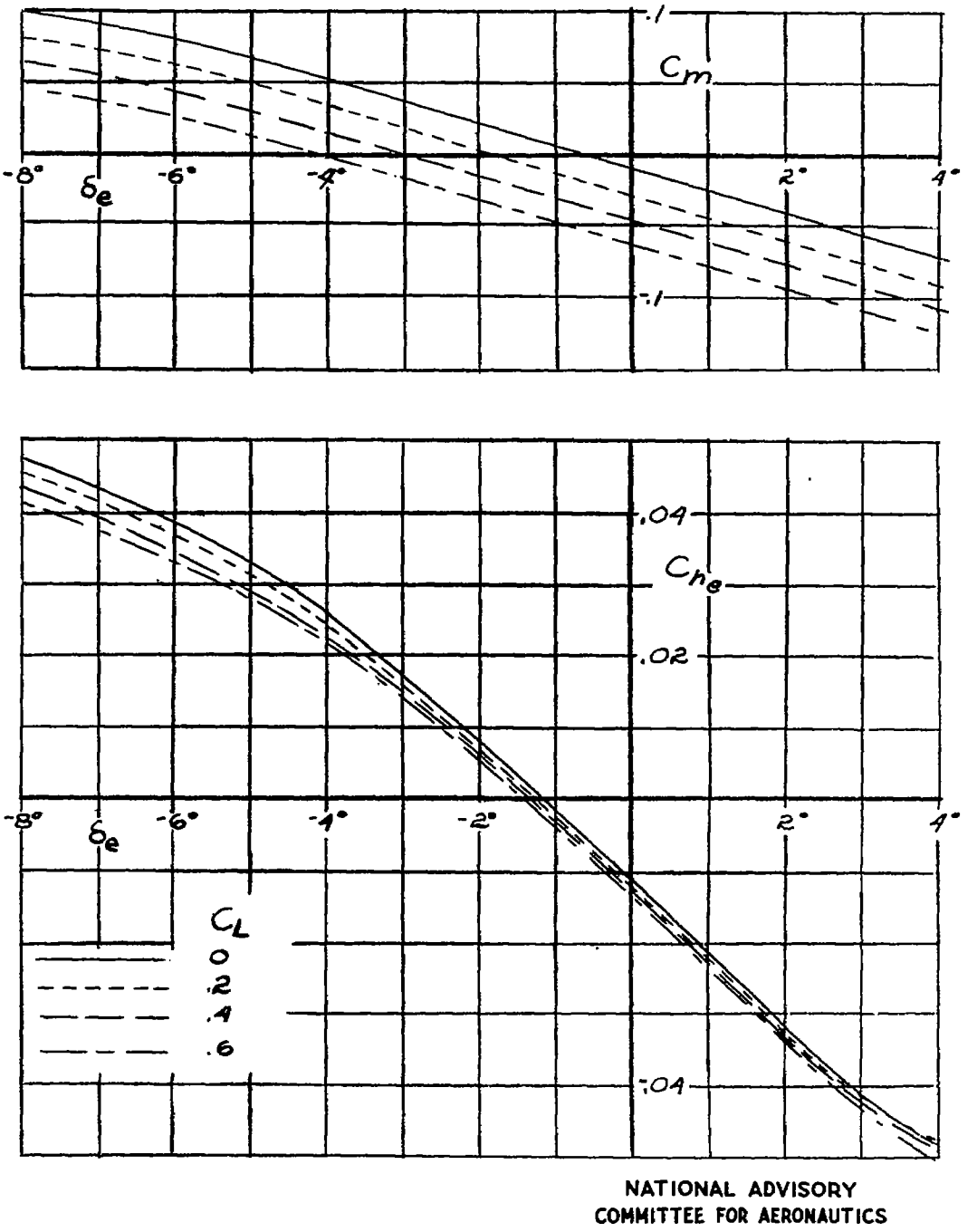

(b) 0.704 Mach number.

Figure 15.- Continued.

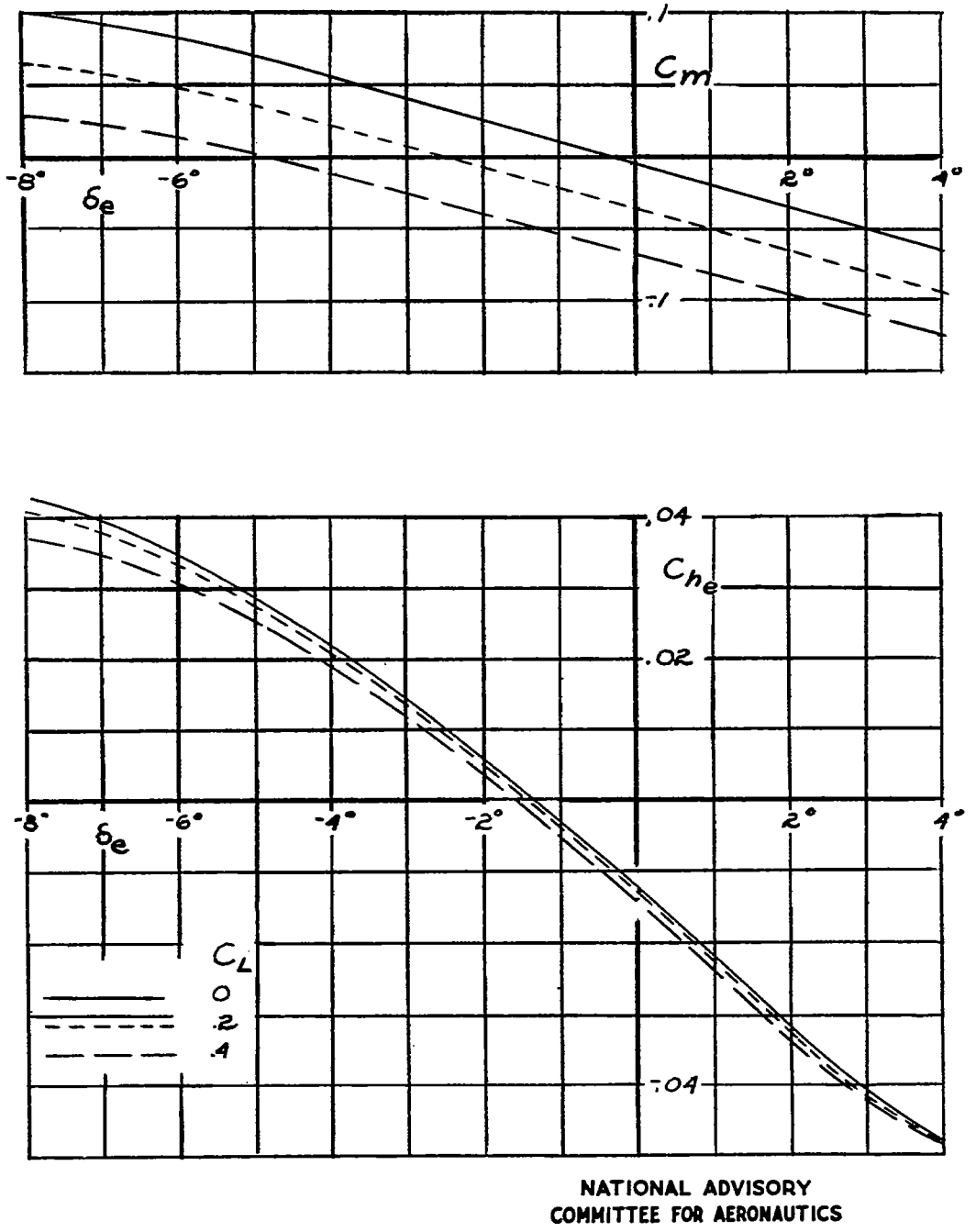

(c) 0.754 Mach number.

Figure 15.- Continued.

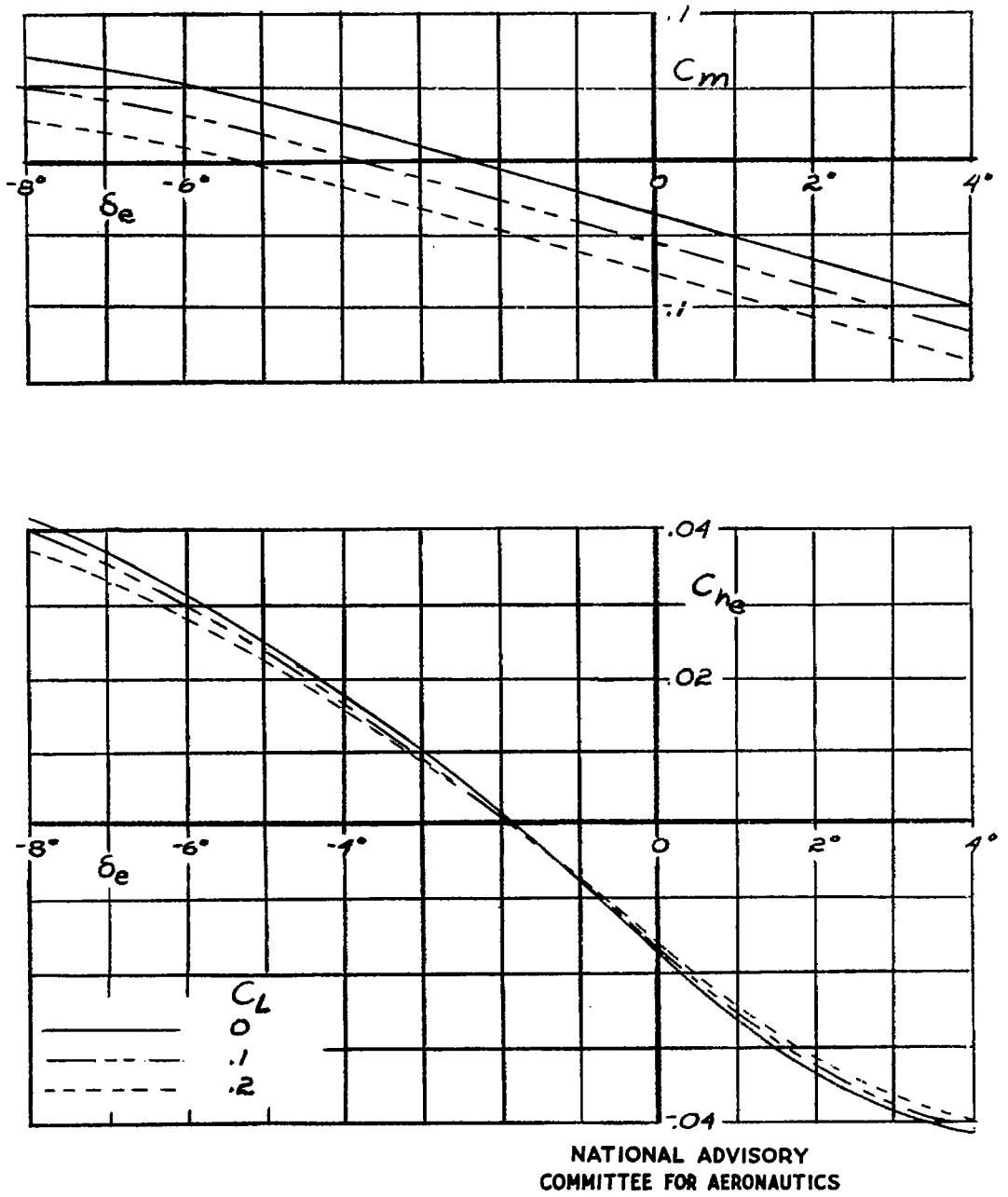

(d) 0.80 Mach number.

Figure 15.- Concluded.

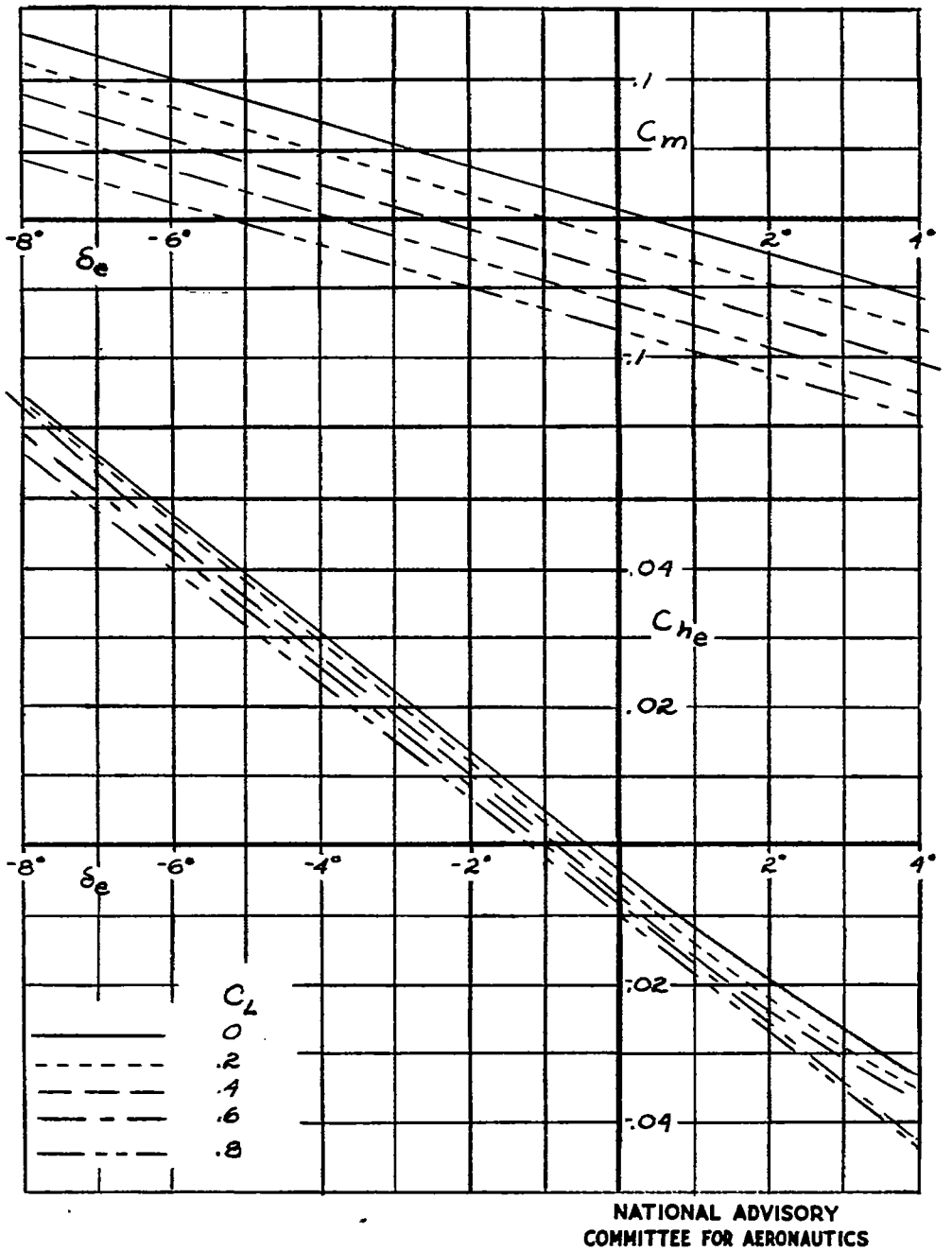

(a) 0.304 Mach number.

Figure 16.- The pitching-moment and elevator hinge-moment coefficients of the model with the H, tail.

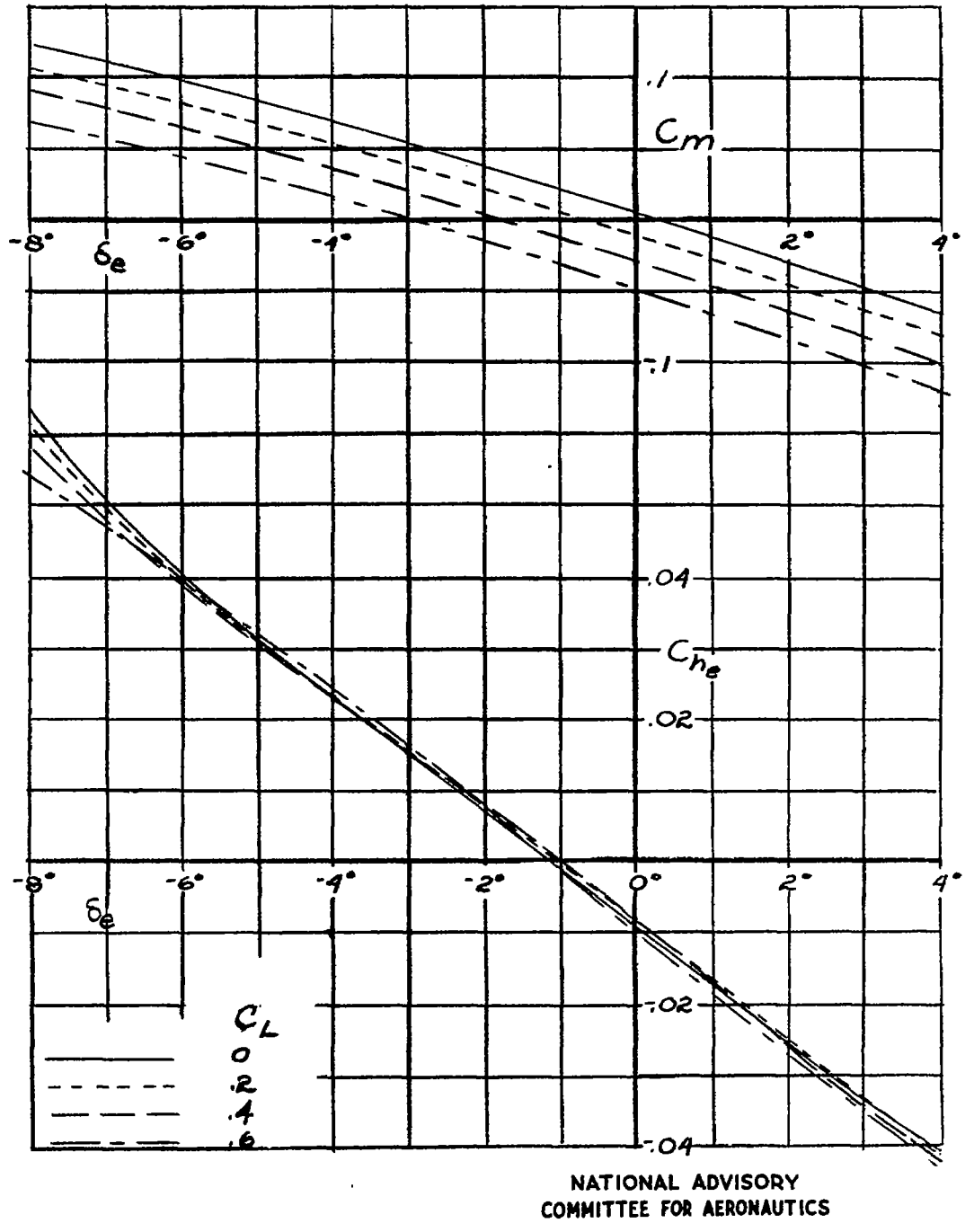

(b) 0.704 Mach number.

Figure 16.- Continued.

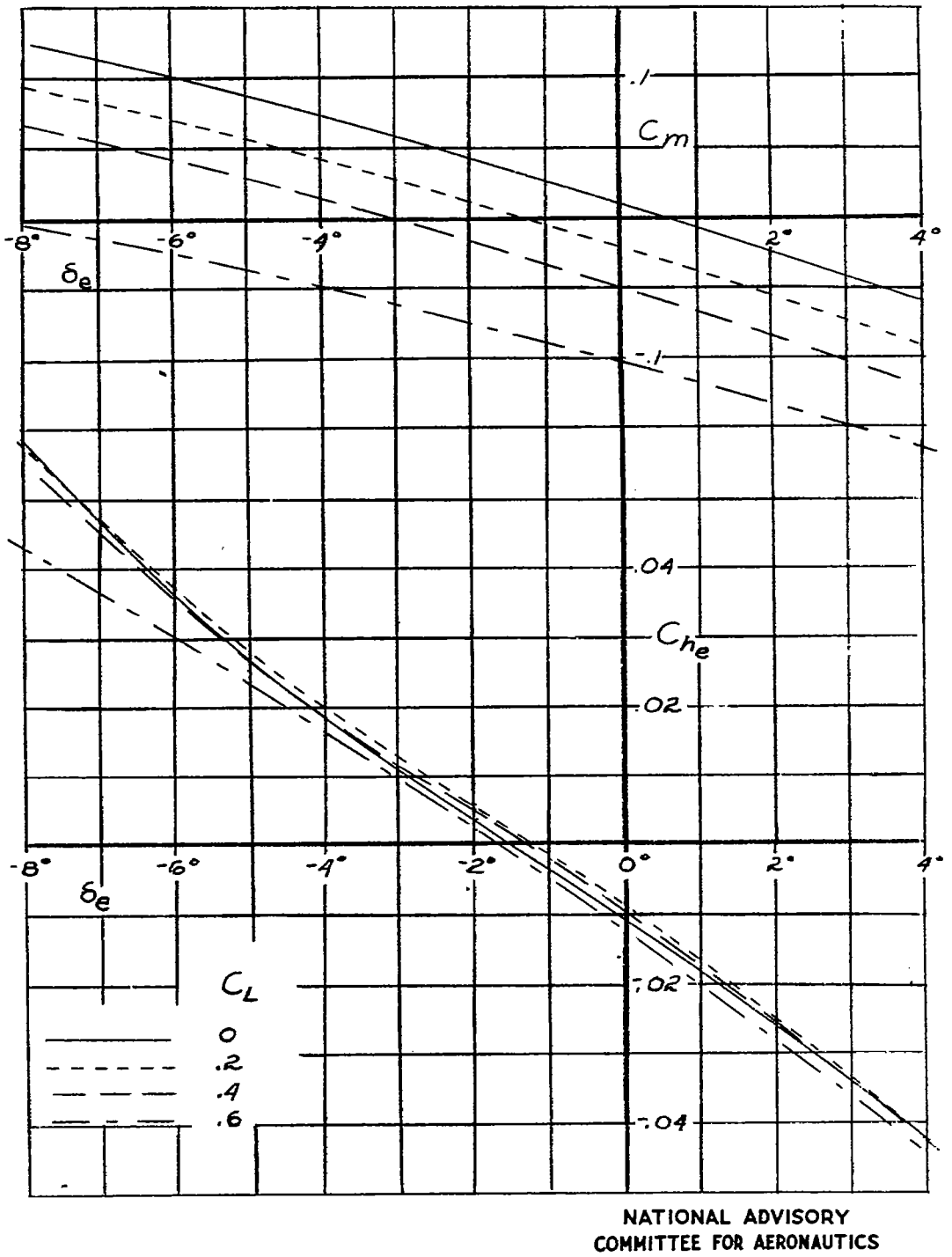

(c) 0.754 Mach number.

Figure 16.- Continued.

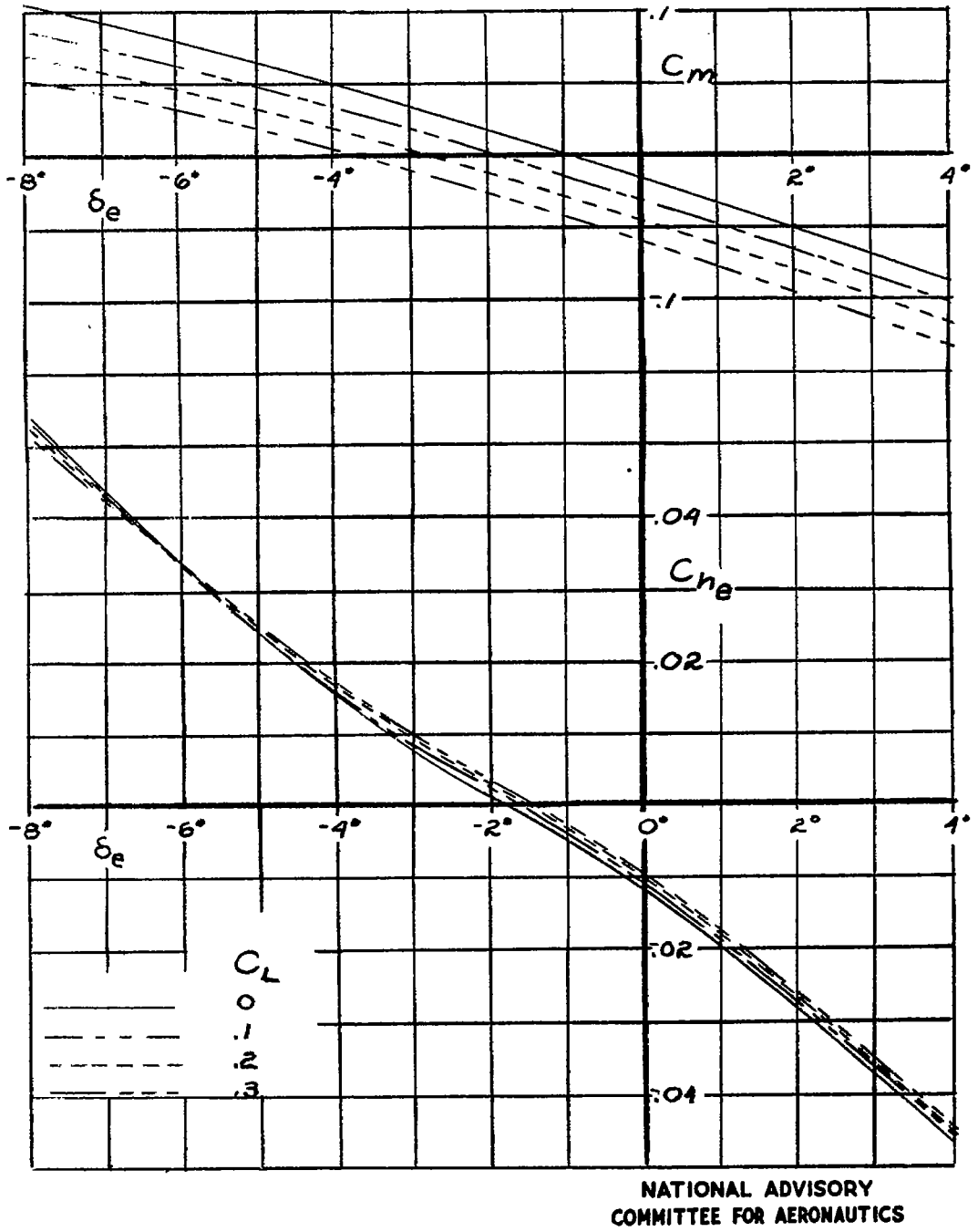

(d) 0.80 Mach number.

Figure 16.- Concluded.

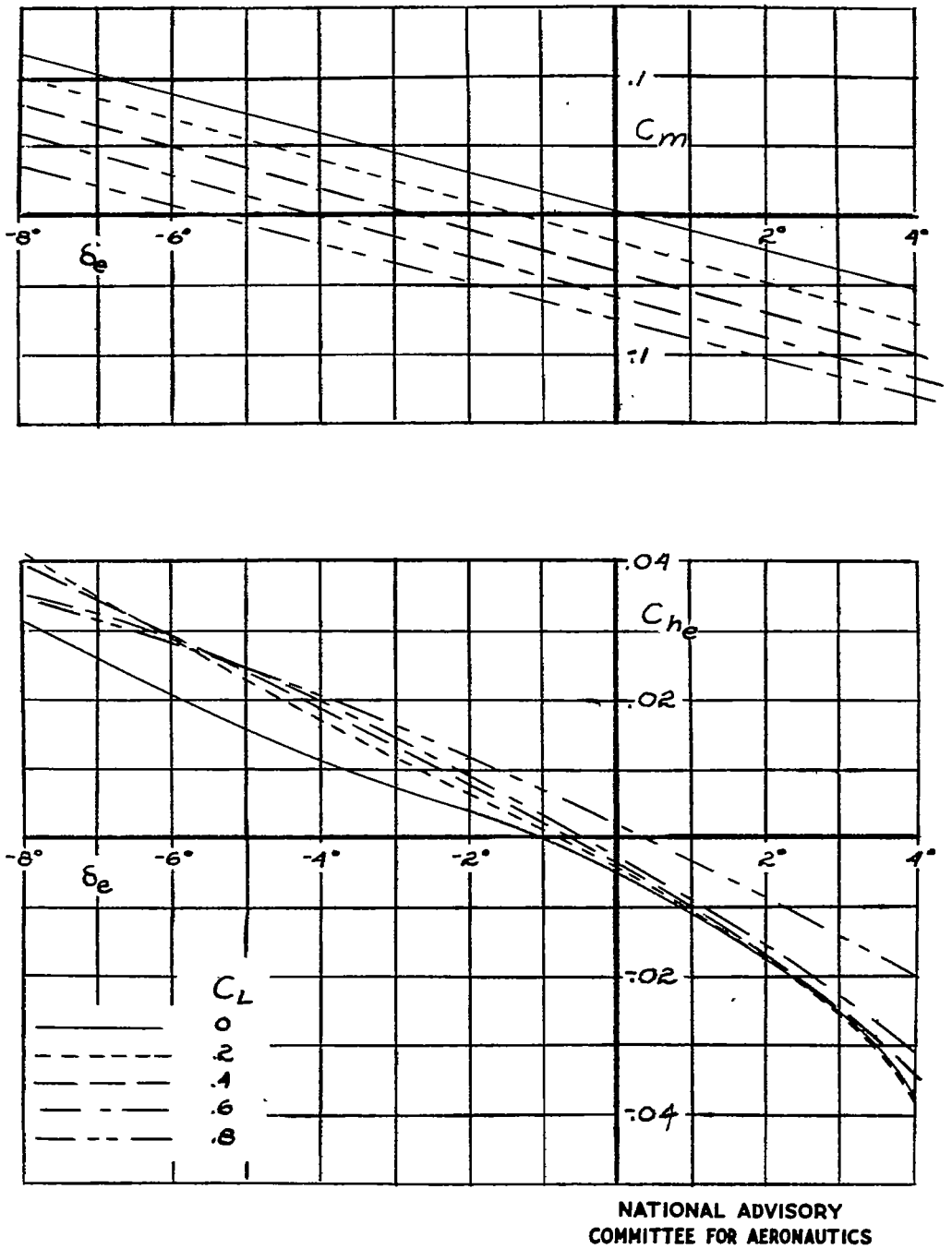

(a) 0.304 Mach number.

Figure 17.- The pitching-moment and elevator hinge-moment coefficients of the model with the H_2 tail.

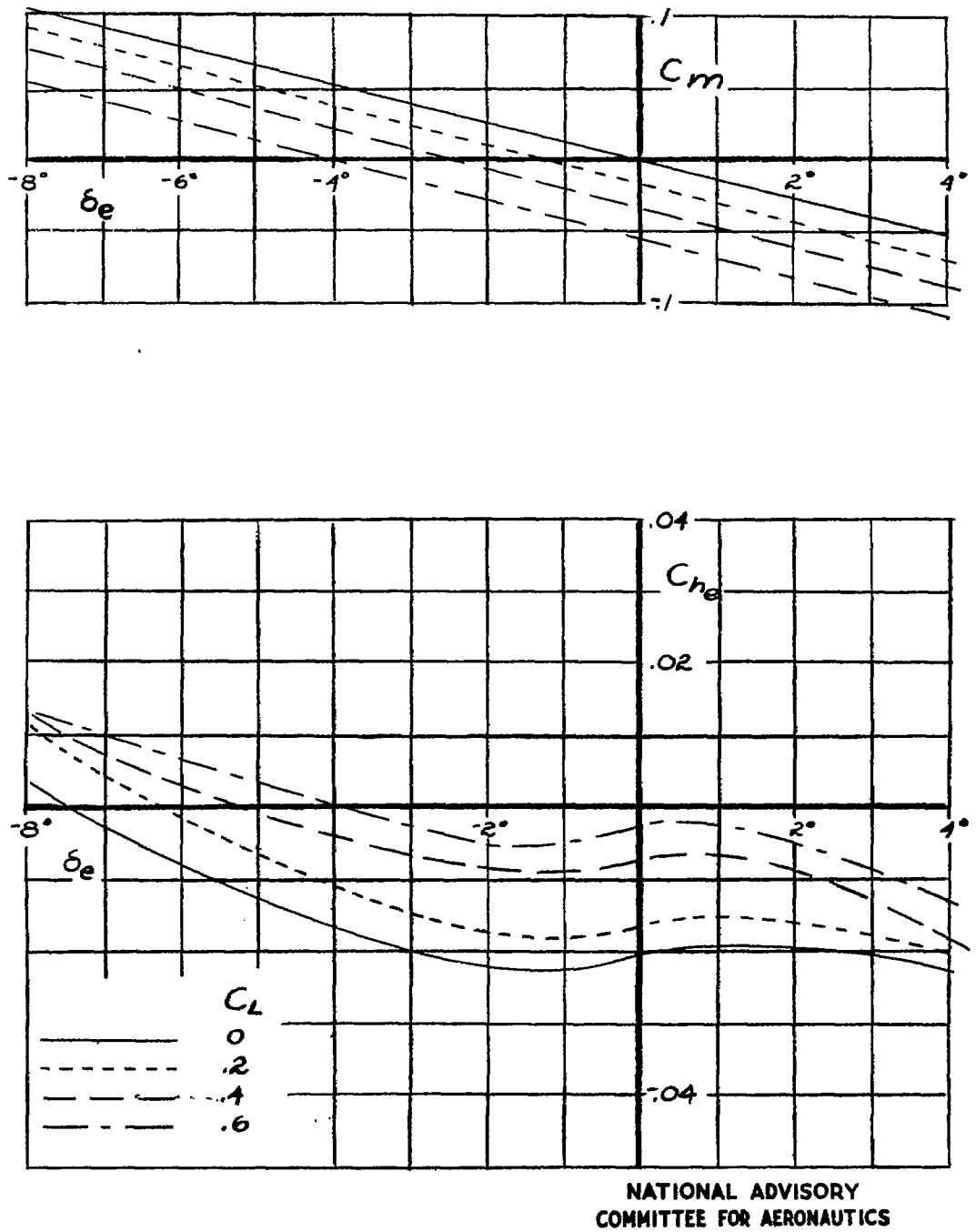

(b) 0.704 Mach number.

Figure 17.- Continued.

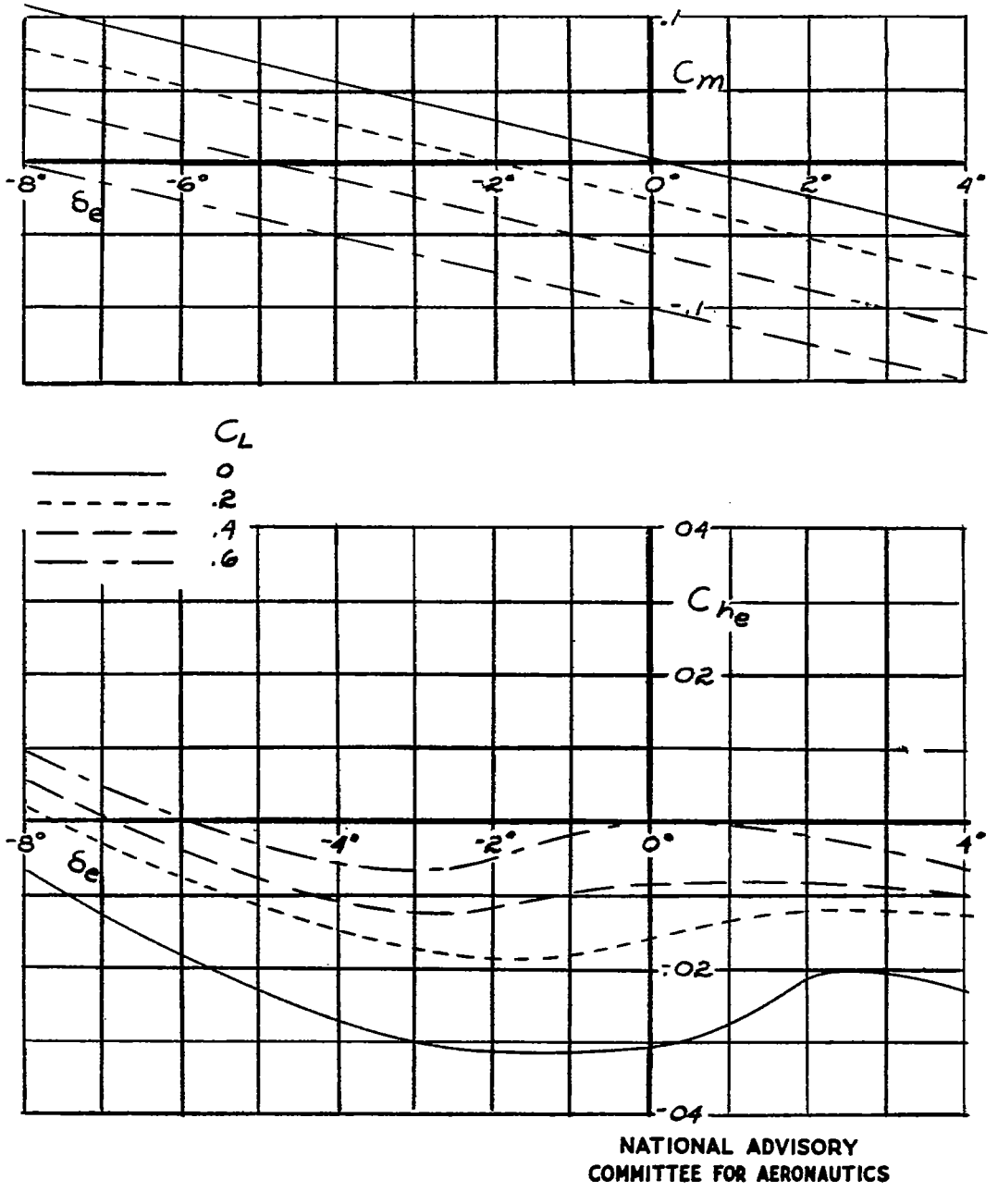

(c) 0.754 Mach number.

Figure 17.- Continued.

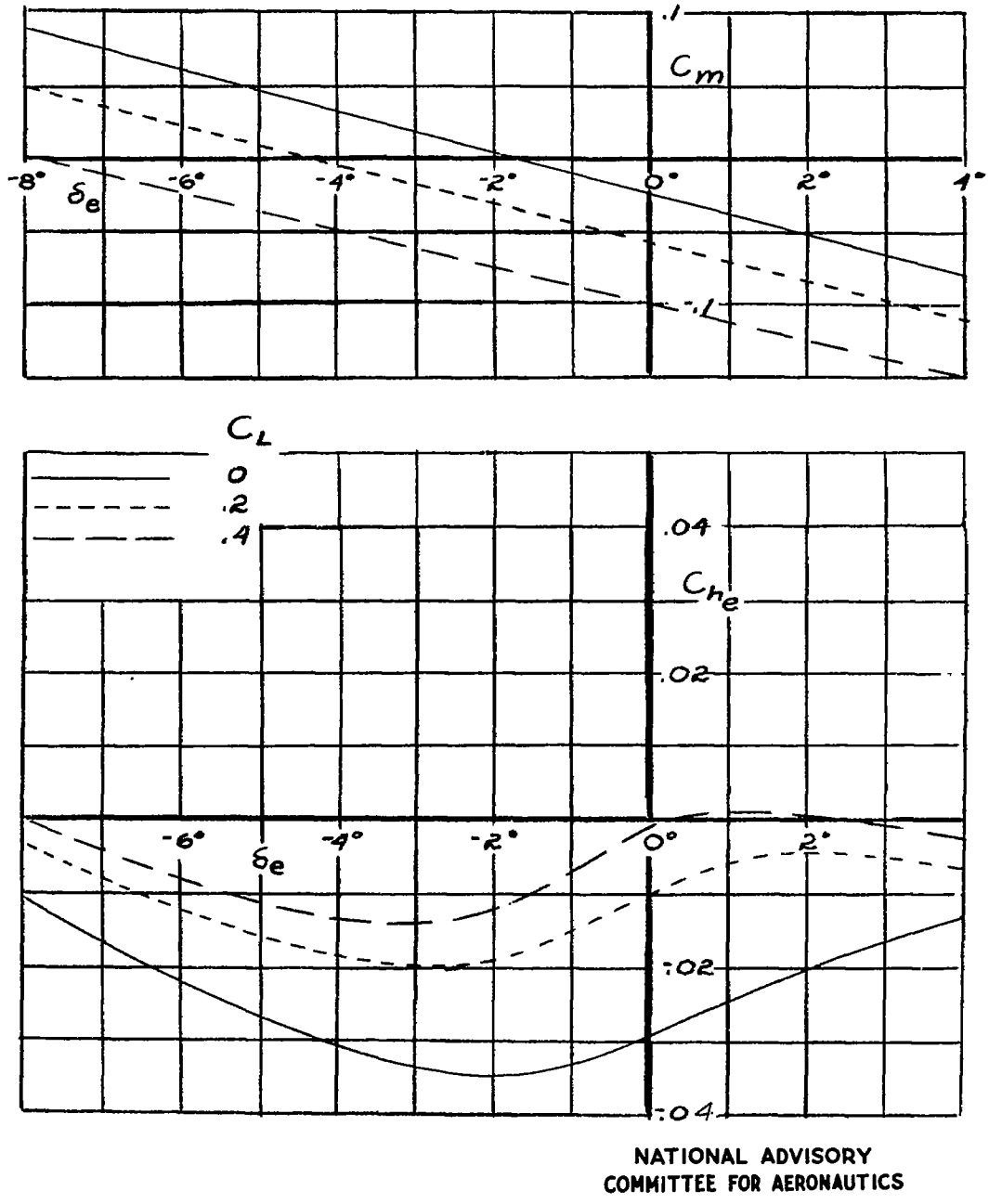

(d) 0.80 Mach number.

Figure 17.- Concluded.

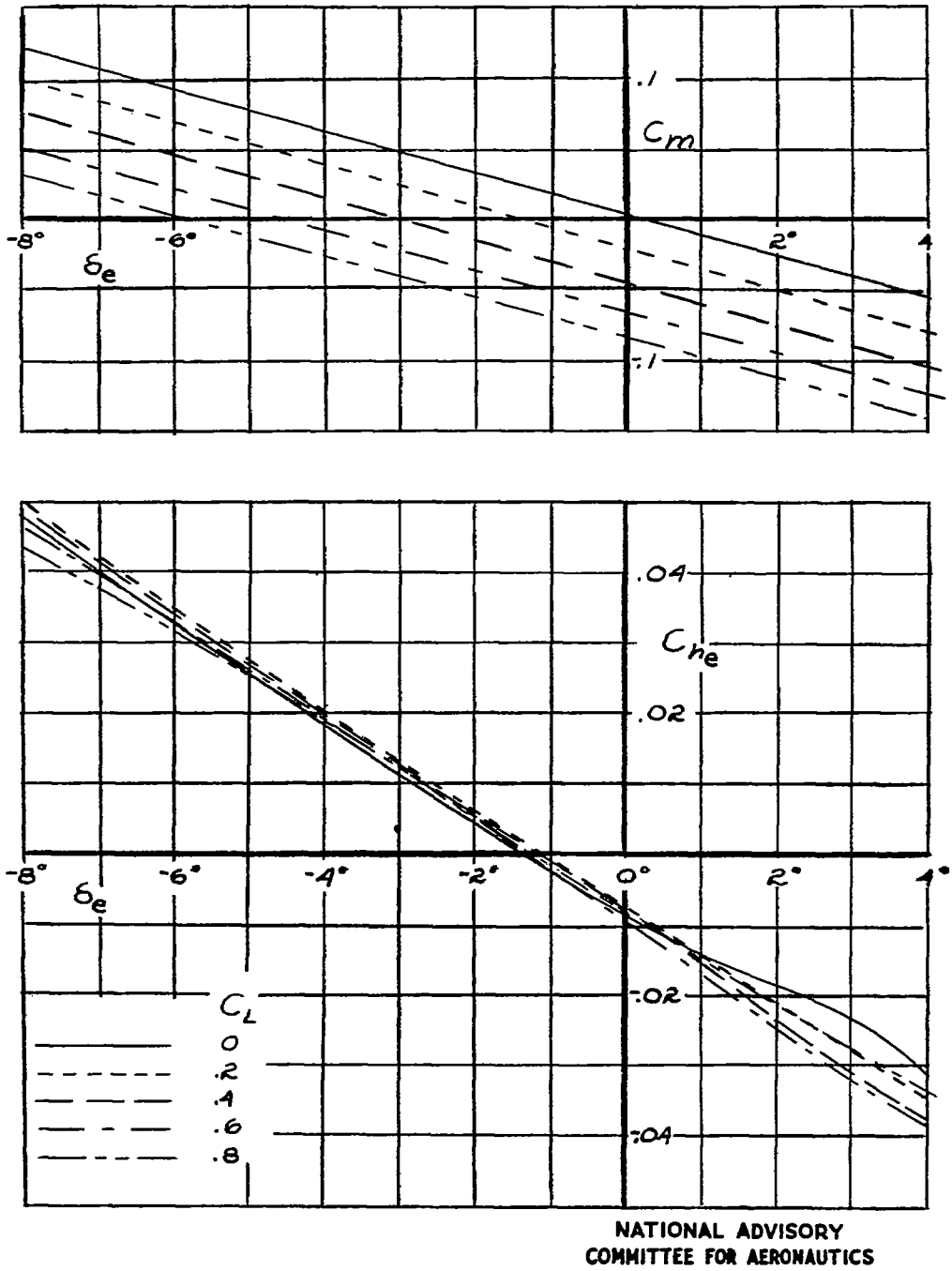

(a) 0.304 Mach number.

Figure 18. - The pitching-moment and elevator hinge-moment coefficients of the model with the H_3 tail.

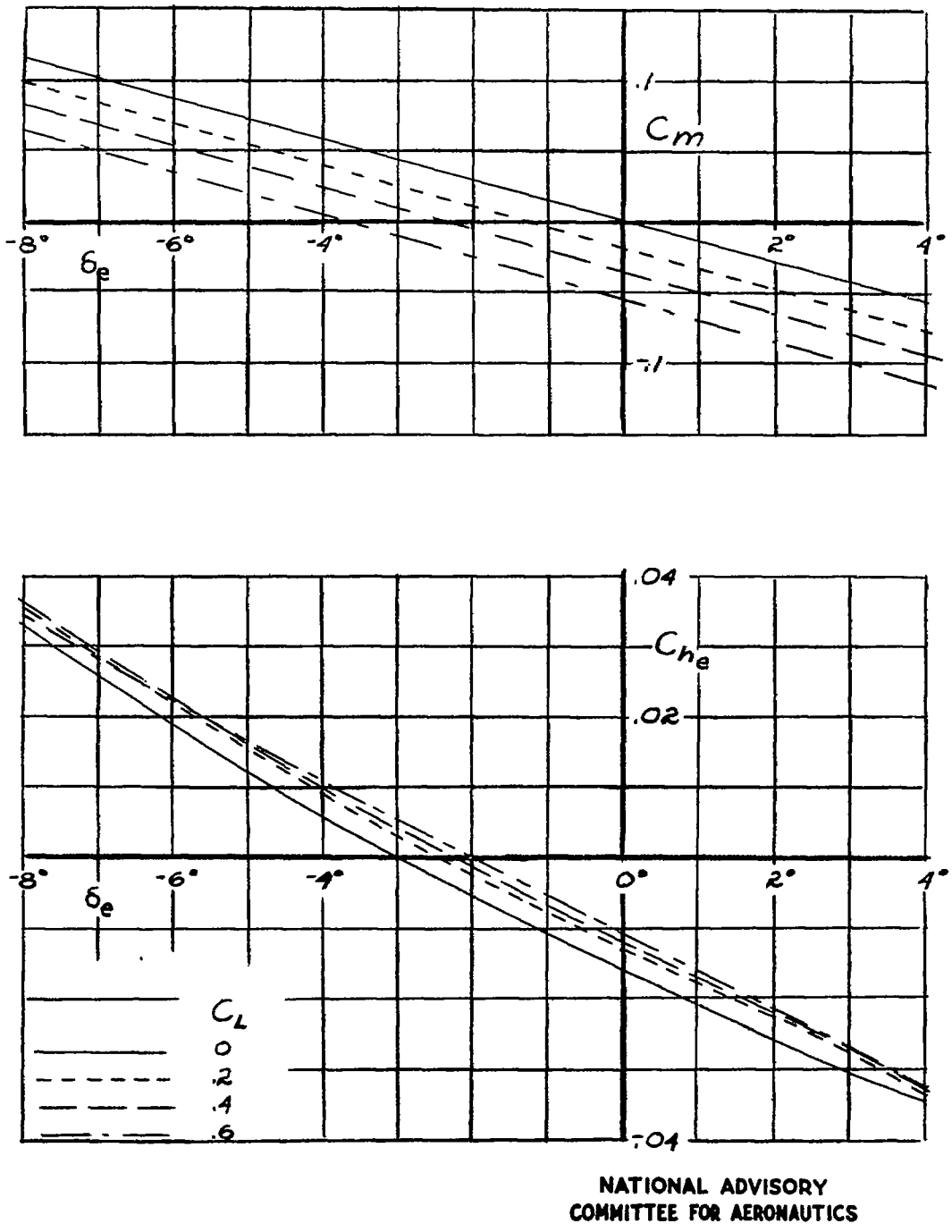

(b) 0.704 Mach number.

Figure 18.-Continued.

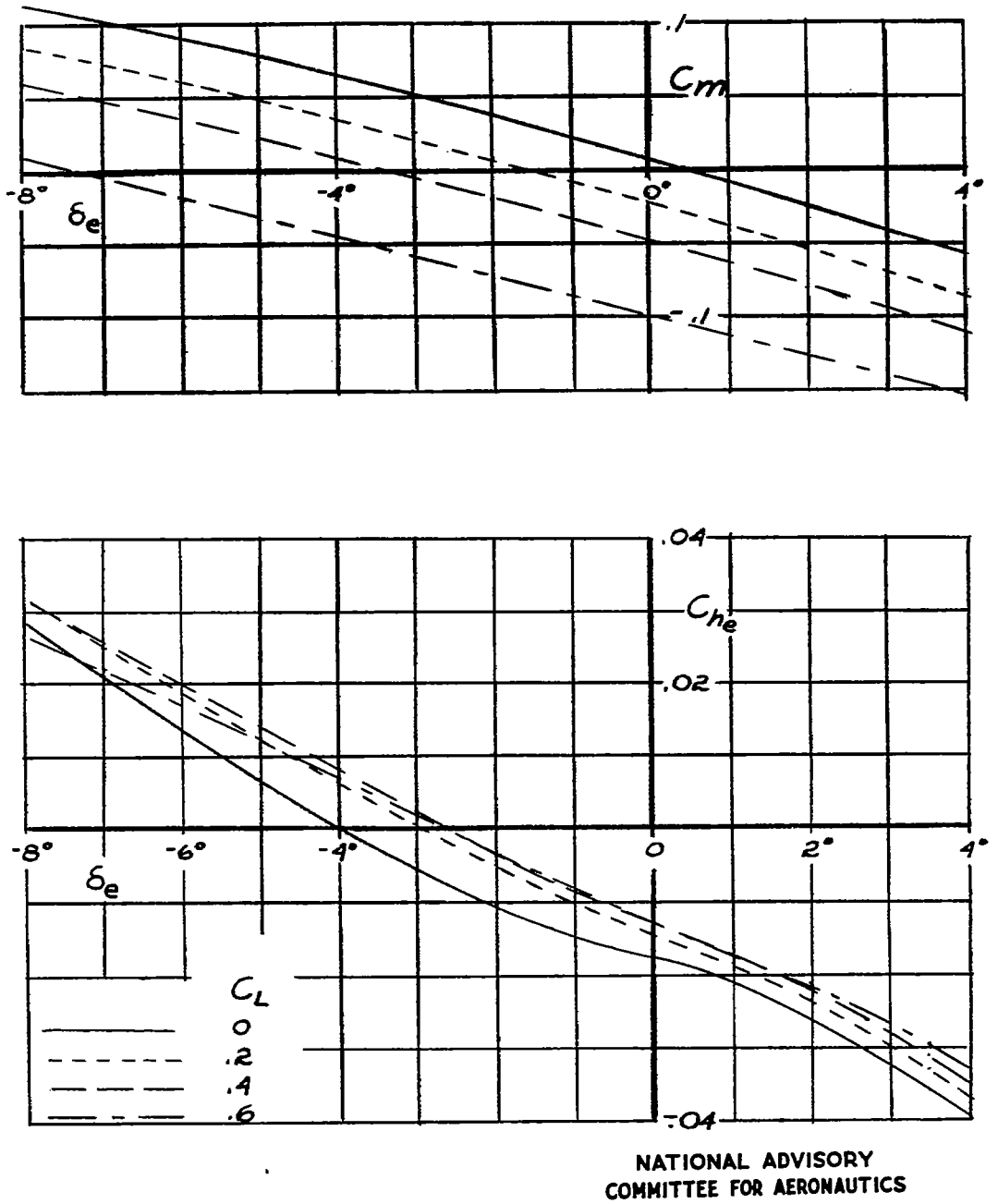

(c) 0.754 Mach number.

Figure 18. Continued.

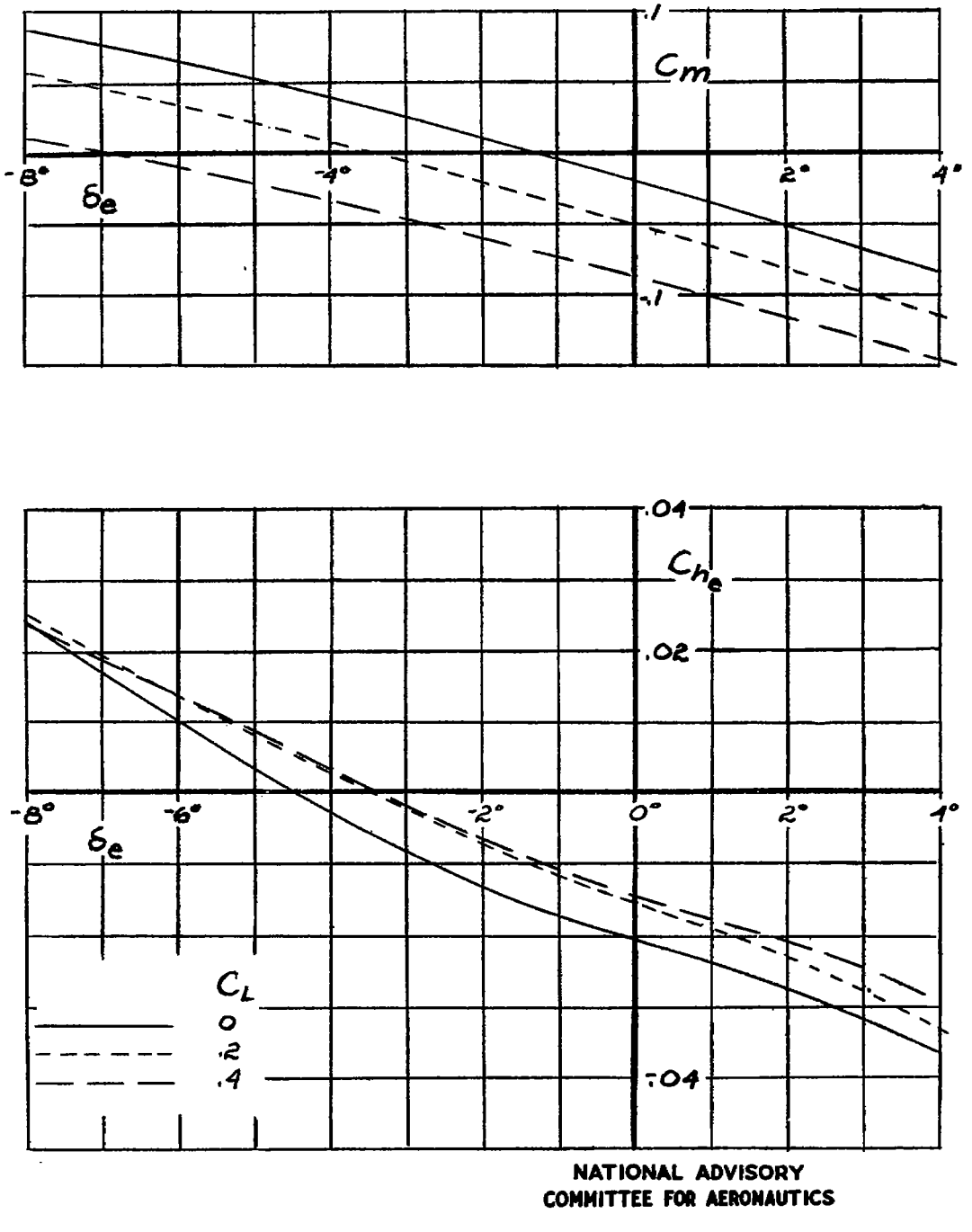

(d) 0.80 Mach number.

Figure 18.- Concluded.

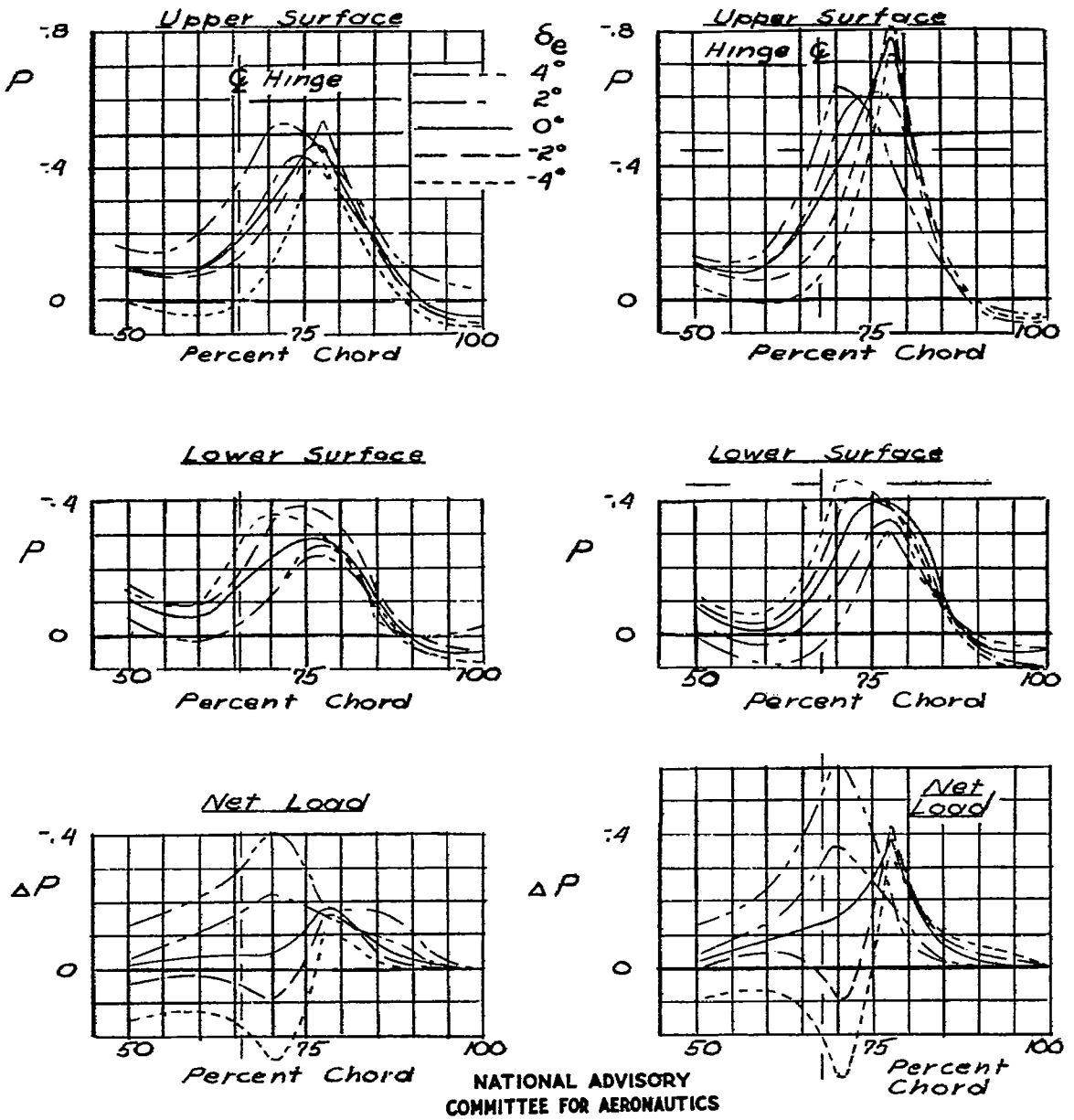

0.304 Mach number 0.808 Mach number

(a) H tail.

Figure 19.- Pressure distribution at horizontal-tail station 5.00. Angle of attack, $-\frac{1}{2}°$; 0.304 and 0.808 Mach number.

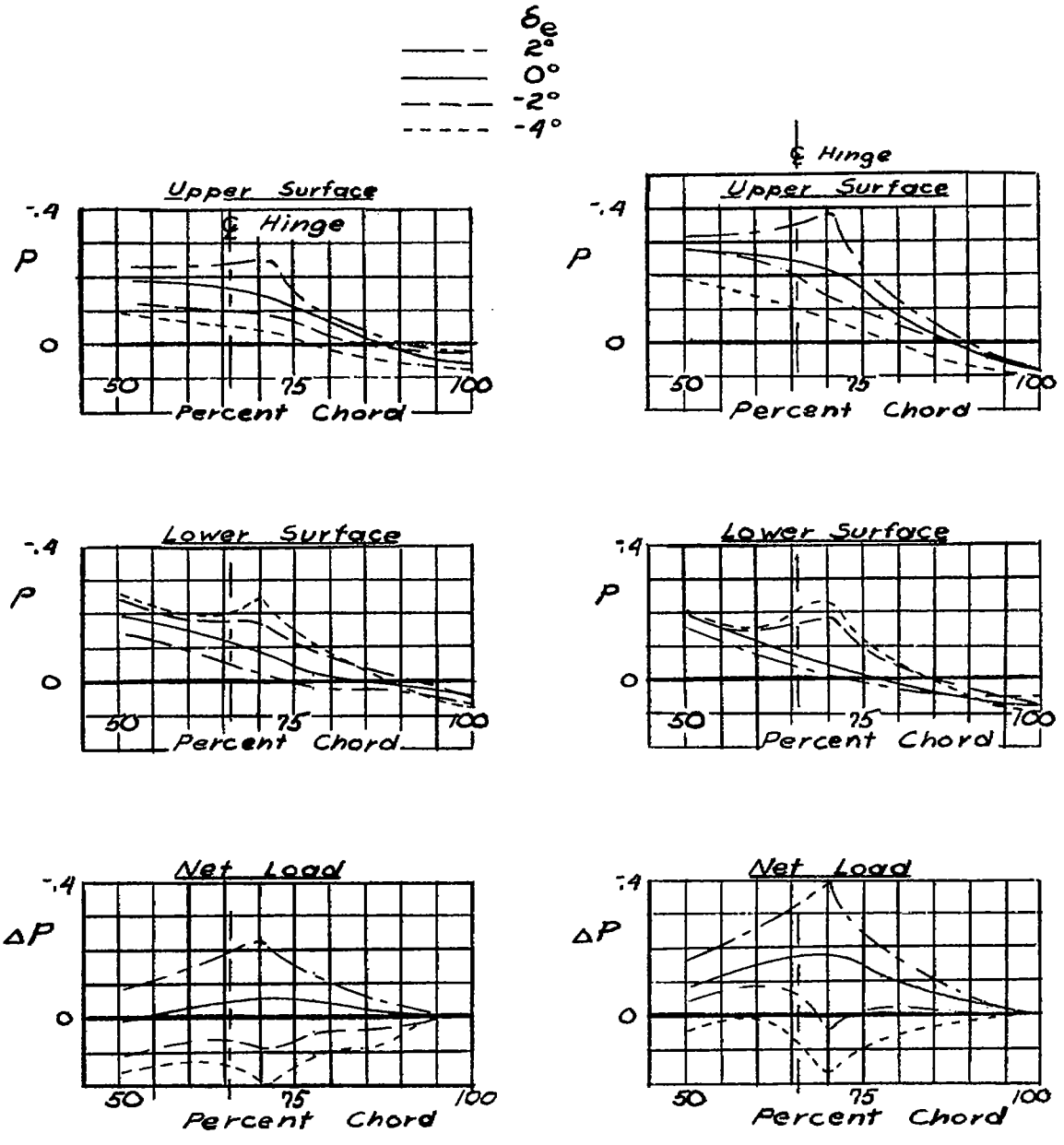

0.304 Mach number

0.808 Mach number

NATIONAL ADVISORY
COMMITTEE FOR AERONAUTICS

(b) H_o tail.

Figure 19.- Continued.

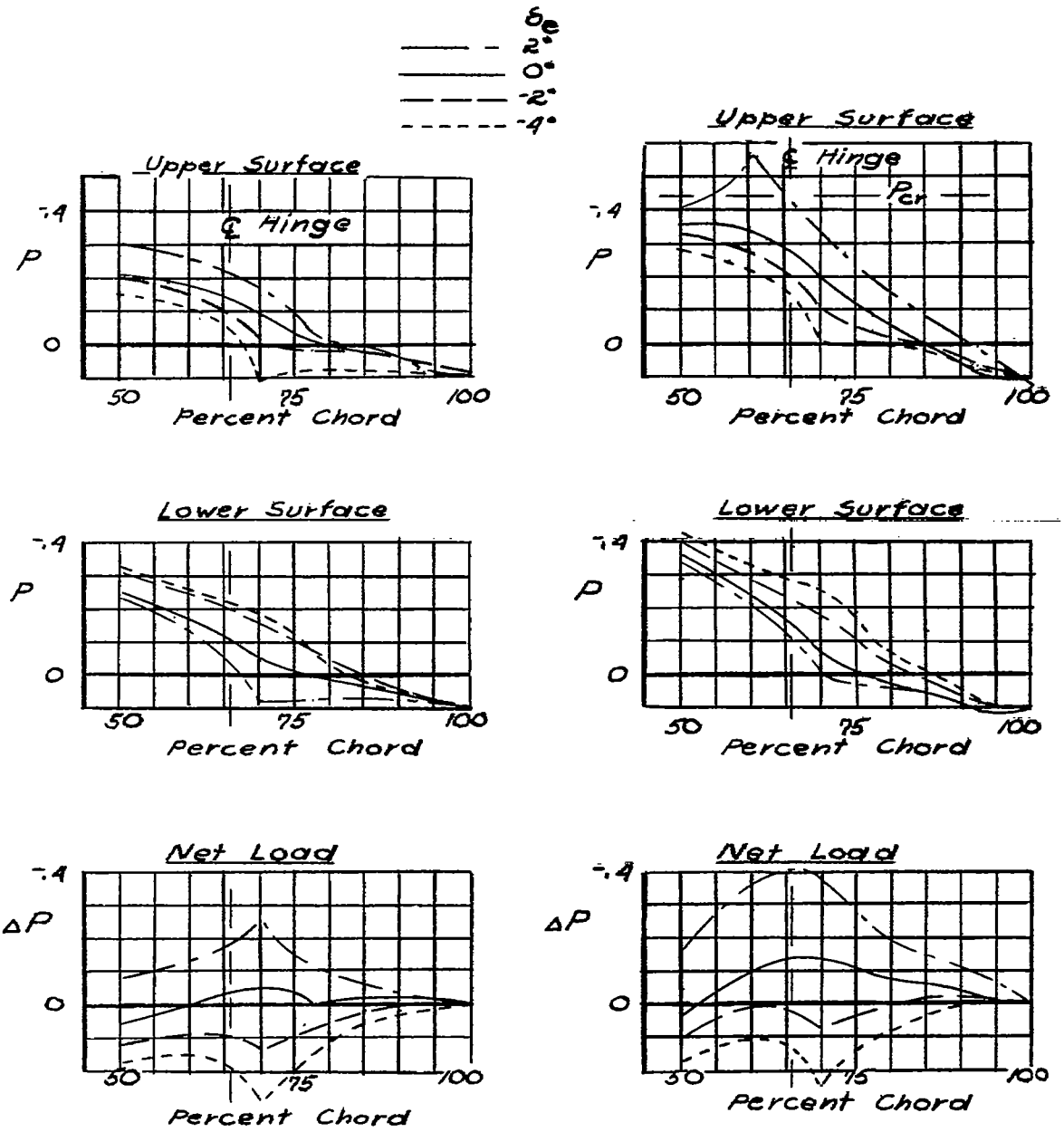

NATIONAL ADVISORY COMMITTEE FOR AERONAUTICS

(c) H_1 tail.

Figure 19.- Continued

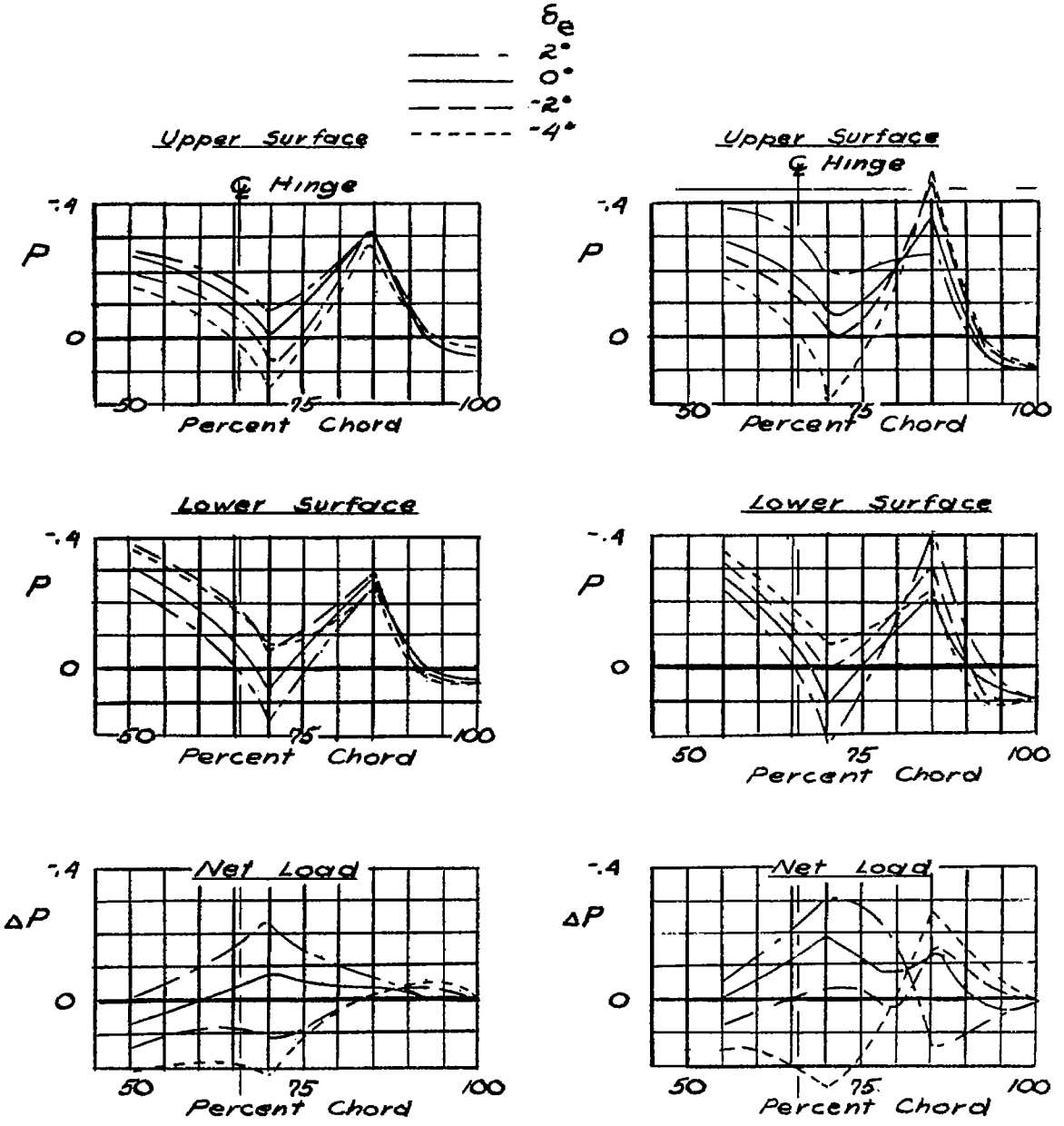

0.304 Mach number 0.808 Mach number

NATIONAL ADVISORY COMMITTEE FOR AERONAUTICS

(d) H_2 tail.

Figure 19.- Continued.

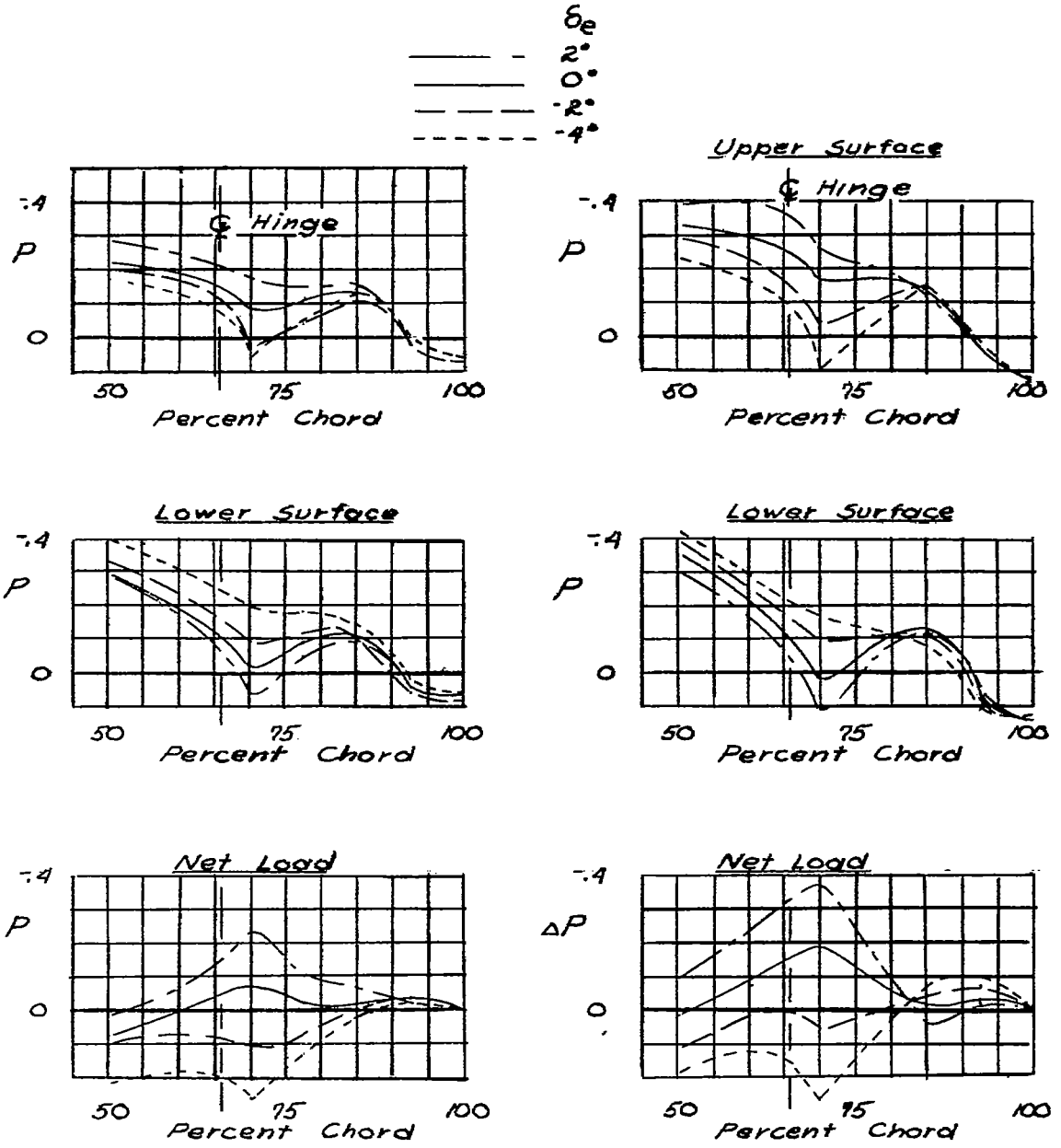

0.304 Mach number

0.808 Mach number

NATIONAL ADVISORY
COMMITTEE FOR AERONAUTICS

(e) H_3 tail

Figure 19.- Concluded.

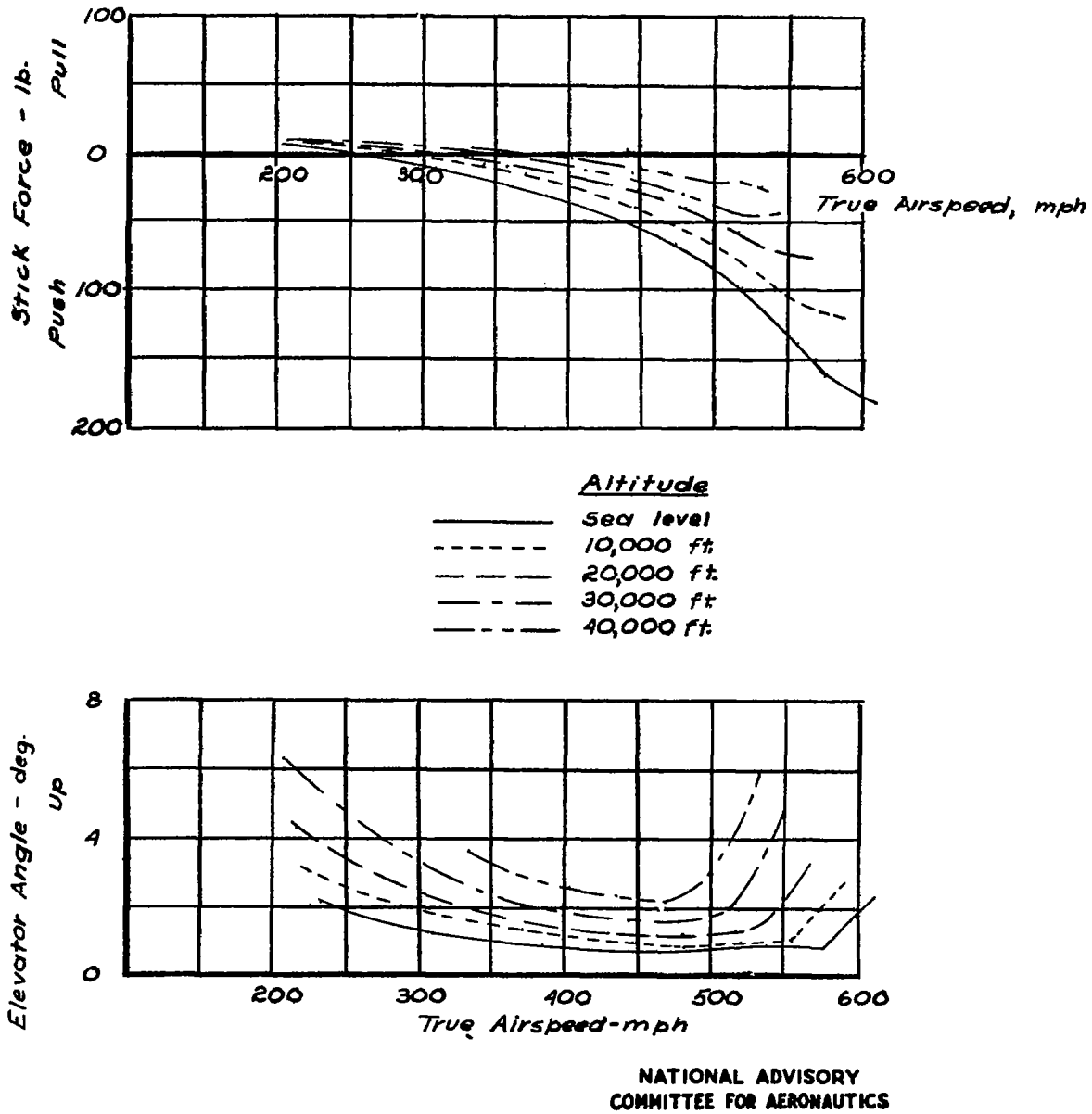

Figure 20.-Predicted stick force and elevator angle of the airplane in level flight at several altitudes. H tail.

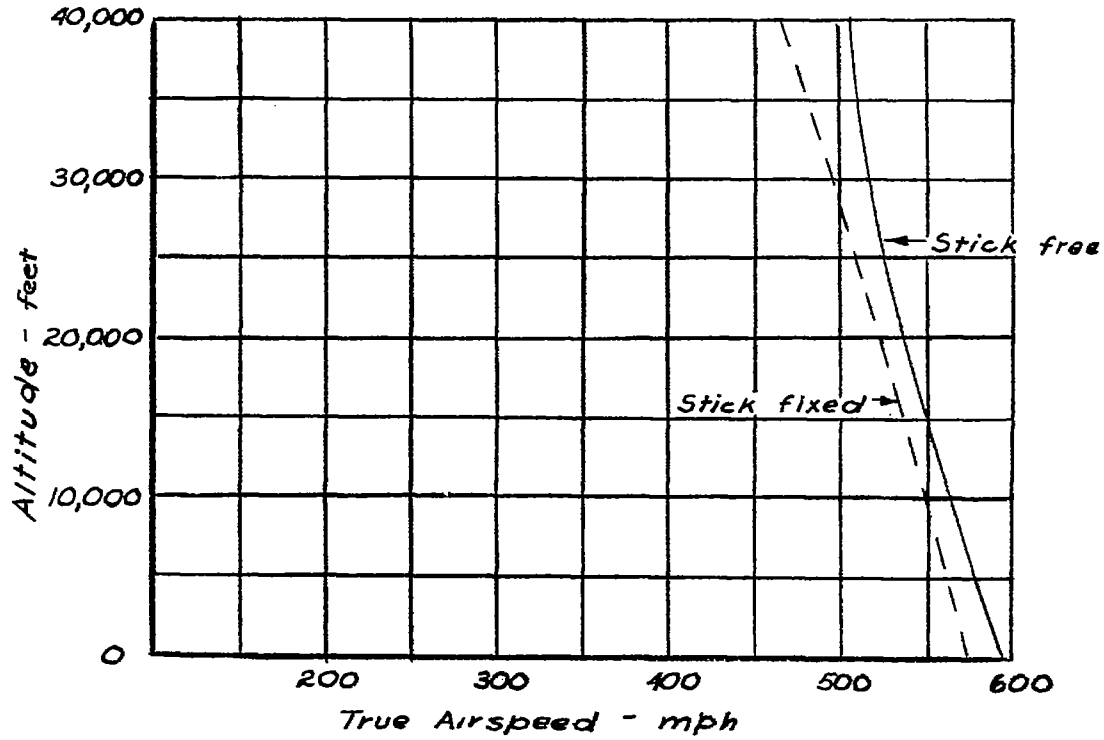

NATIONAL ADVISORY
COMMITTEE FOR AERONAUTICS

Figure 21.-Predicted velocities above which the airplane is unstable stick fixed and stick free in level flight. H tail.

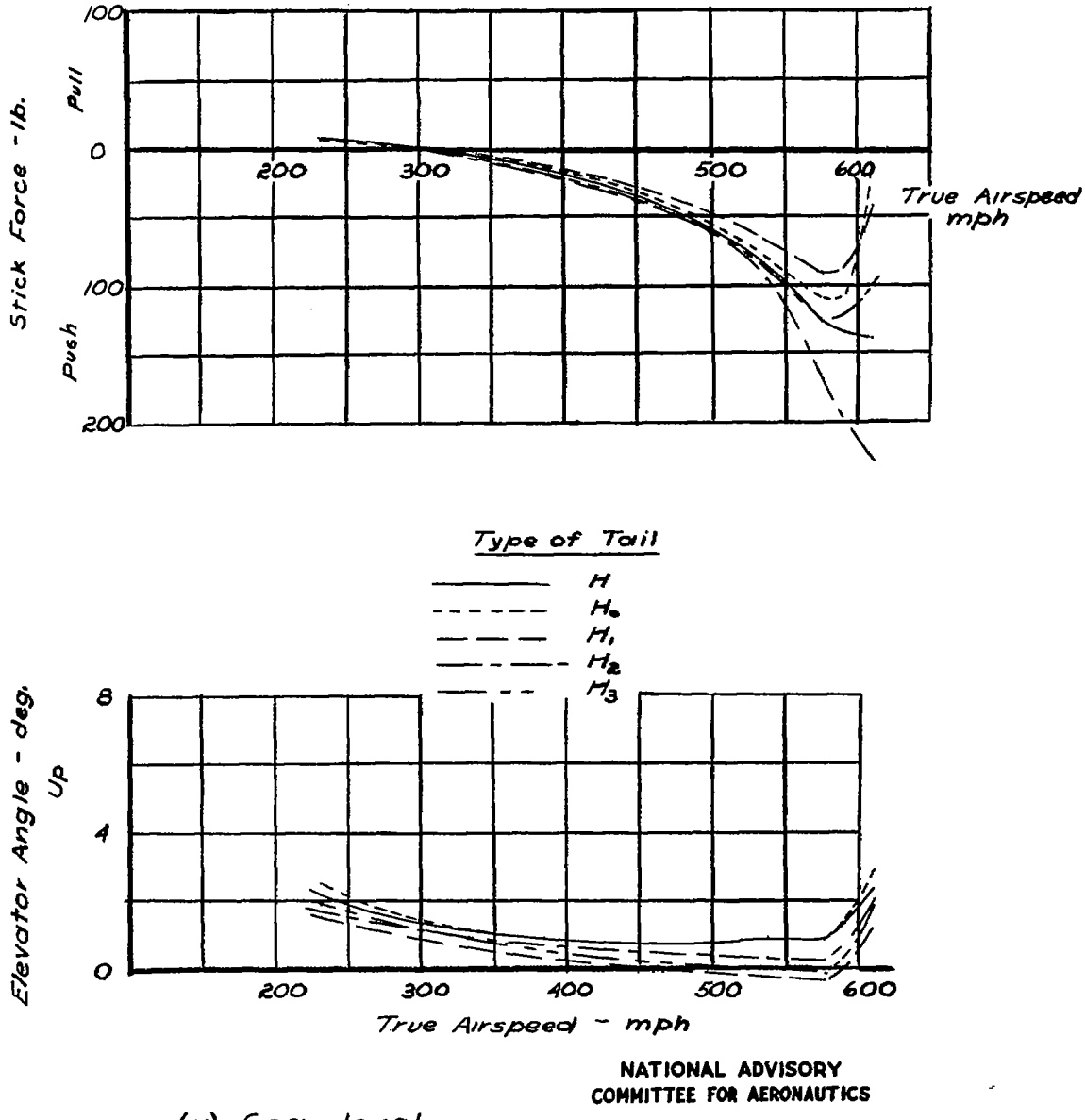

(a) Sea level.

Figure 22.-Predicted stick force and elevator angle of the airplane in level flight with several types of horizontal tail.

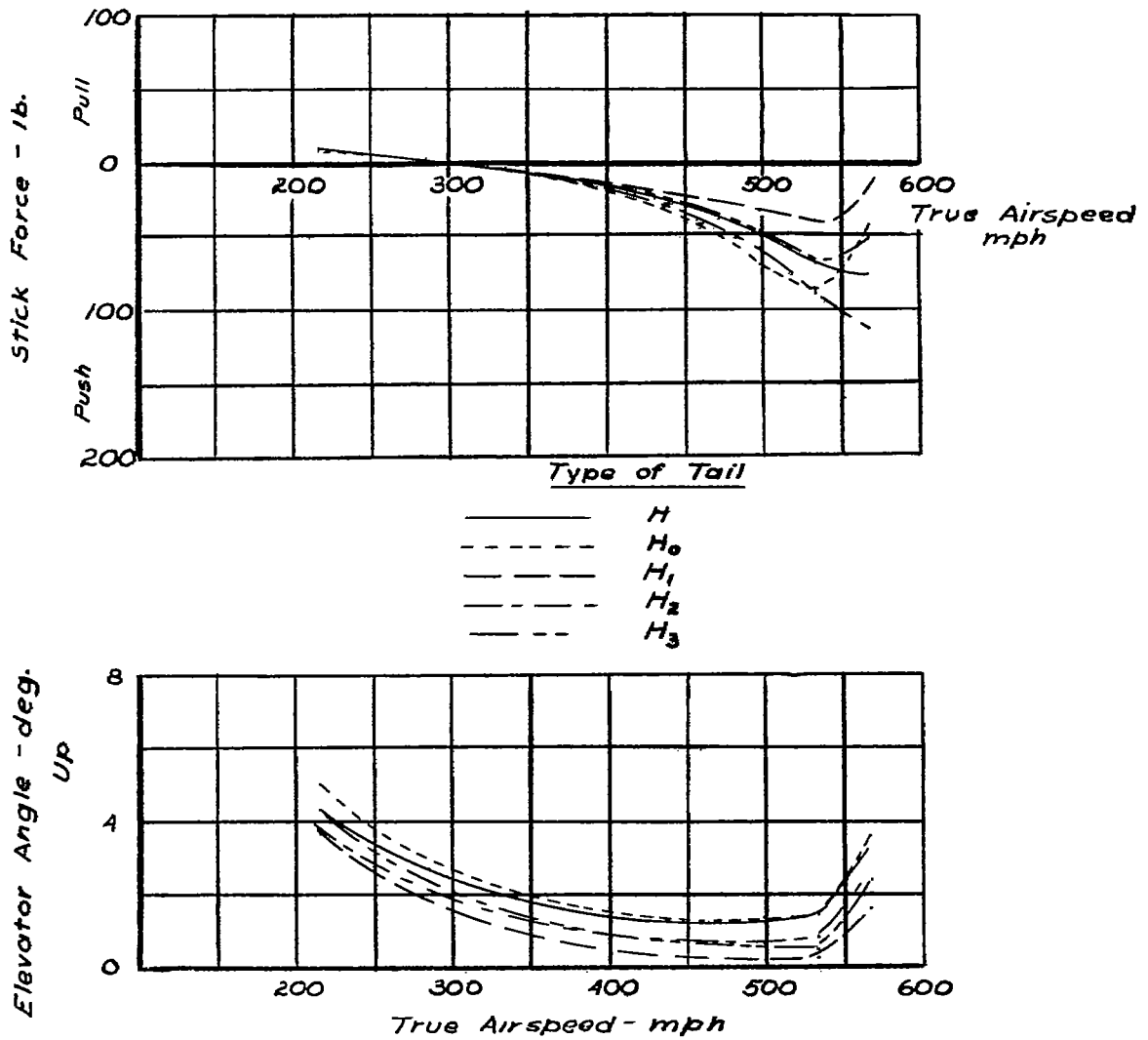

(b) 20,000 feet altitude

Figure 22.- Concluded.

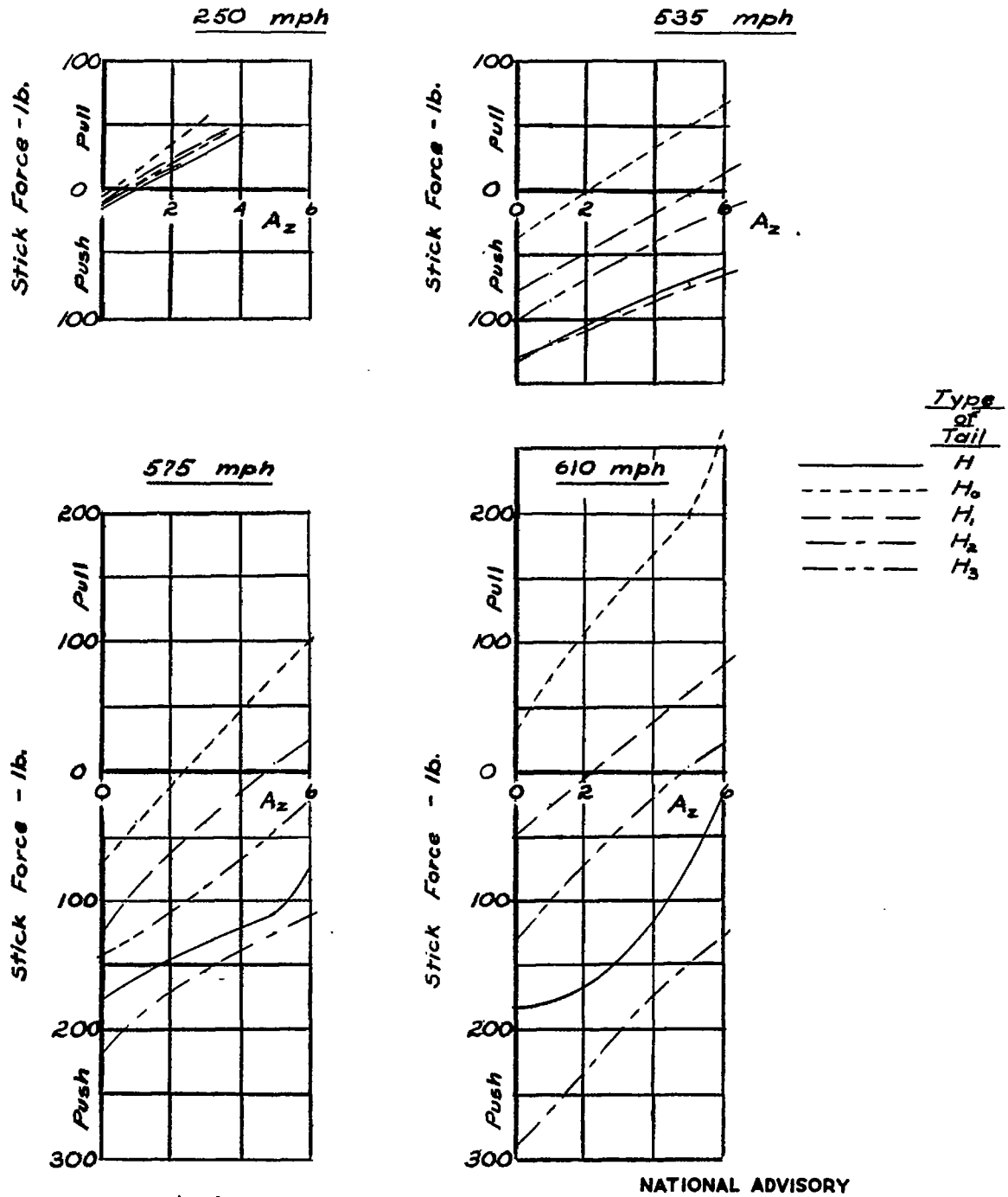

(a) Sea level.

Figure 23.- Predicted stick forces for the airplane with several types of horizontal tail.

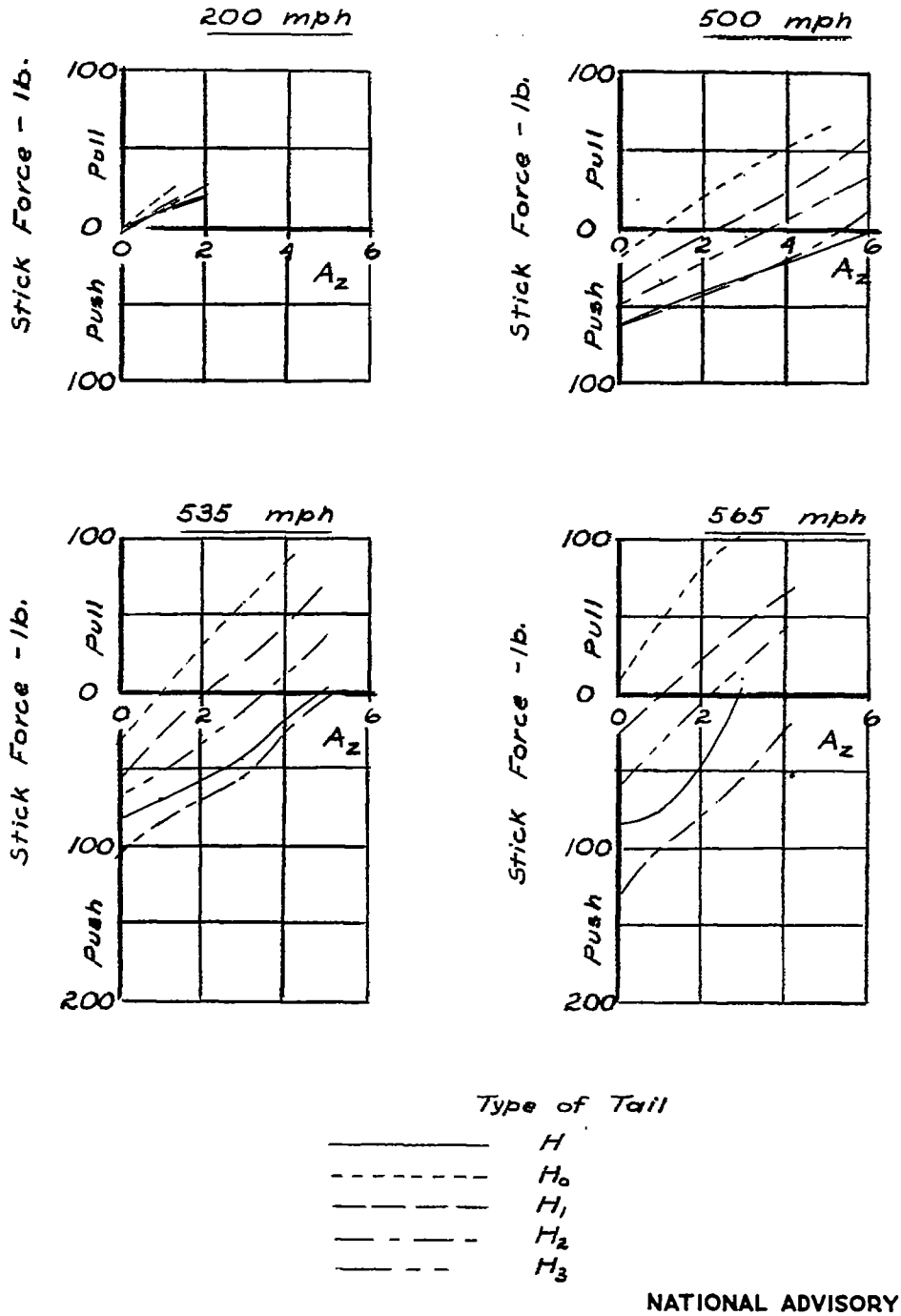

(b) 20,000 feet altitude

Figure 23.- Concluded.

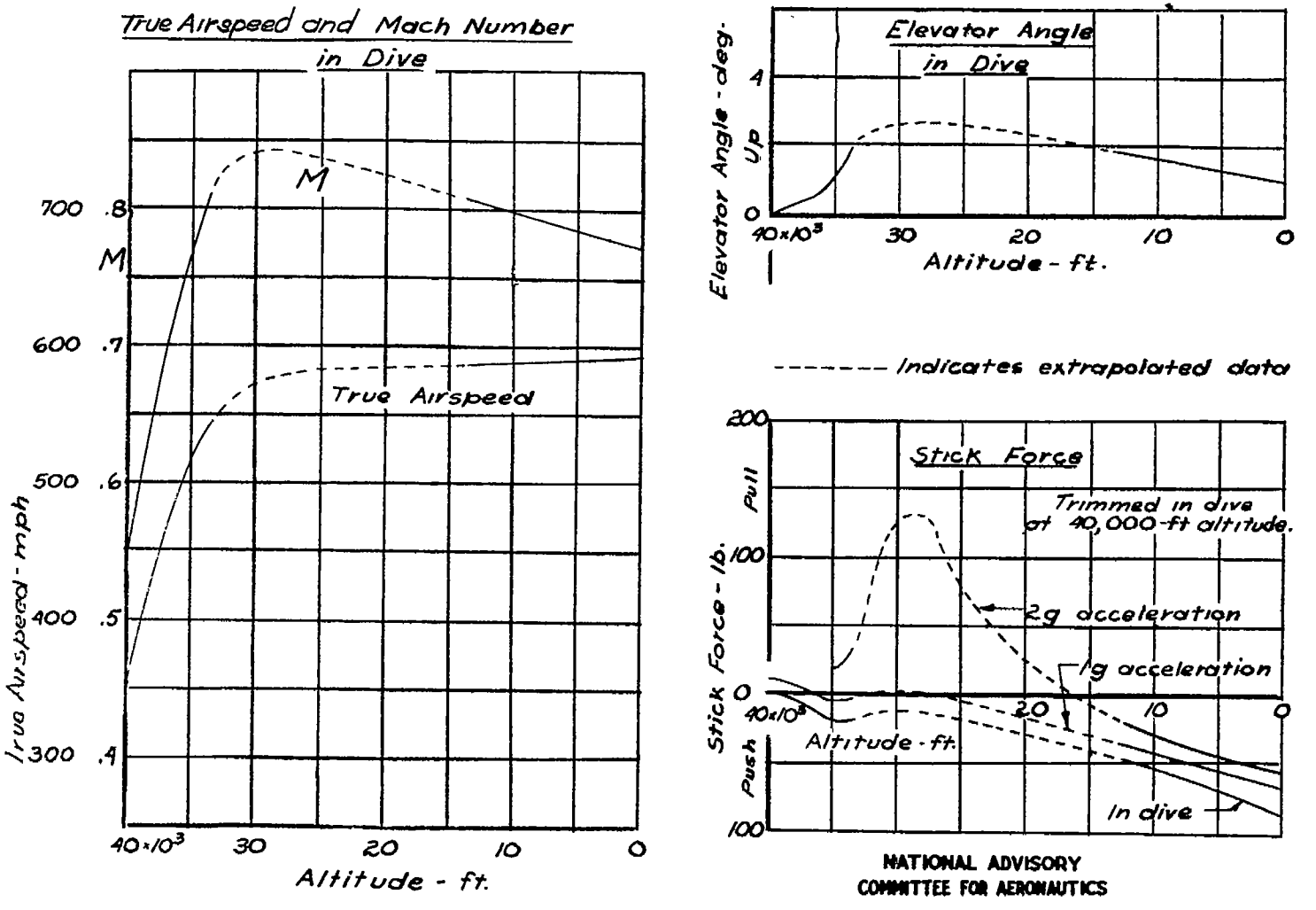

Figure 24.- Predicted characteristics of the airplane in a vertical dive with zero propeller thrust.

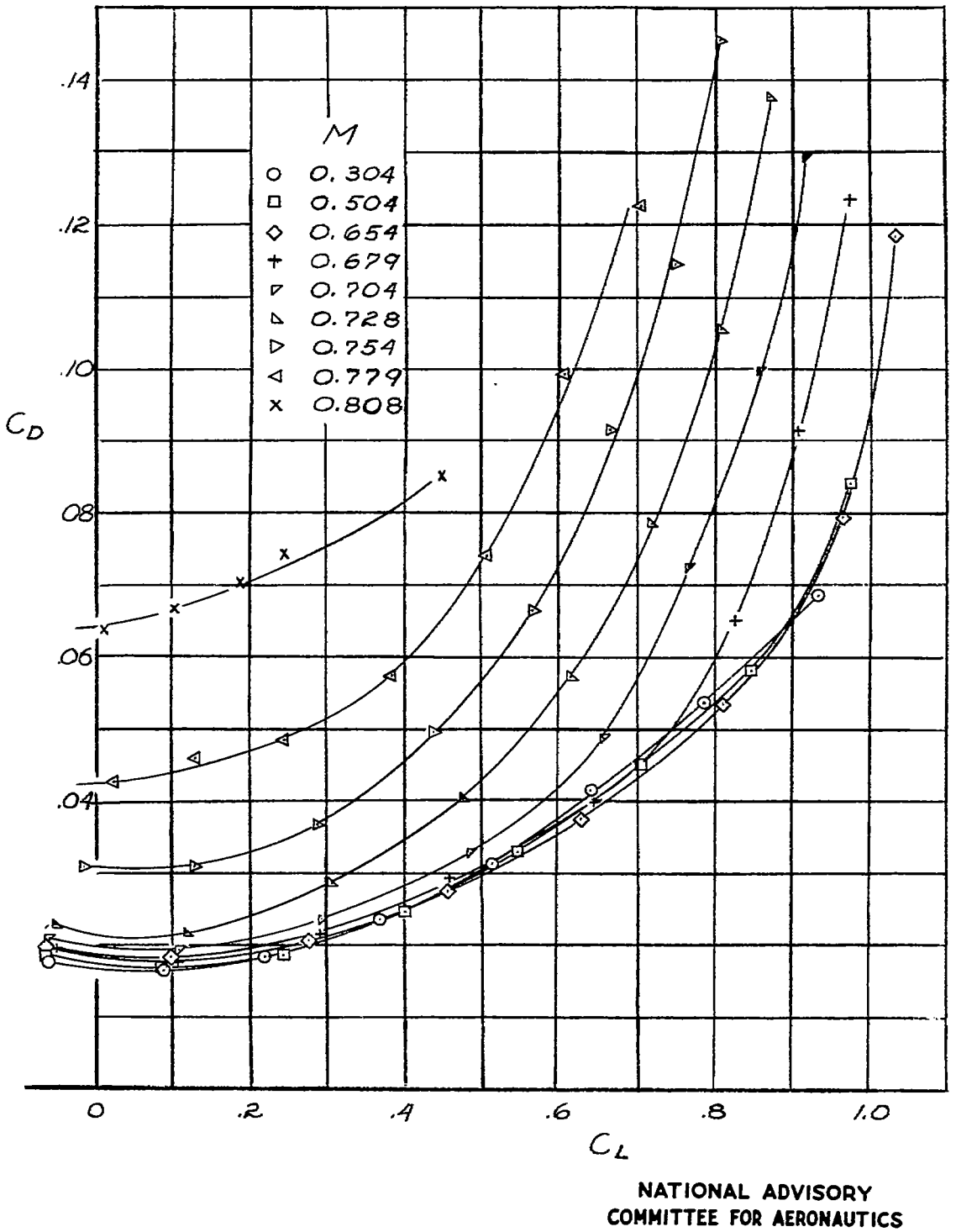

(a) In relation to lift coefficient.

Figure 25.- The drag coefficient.

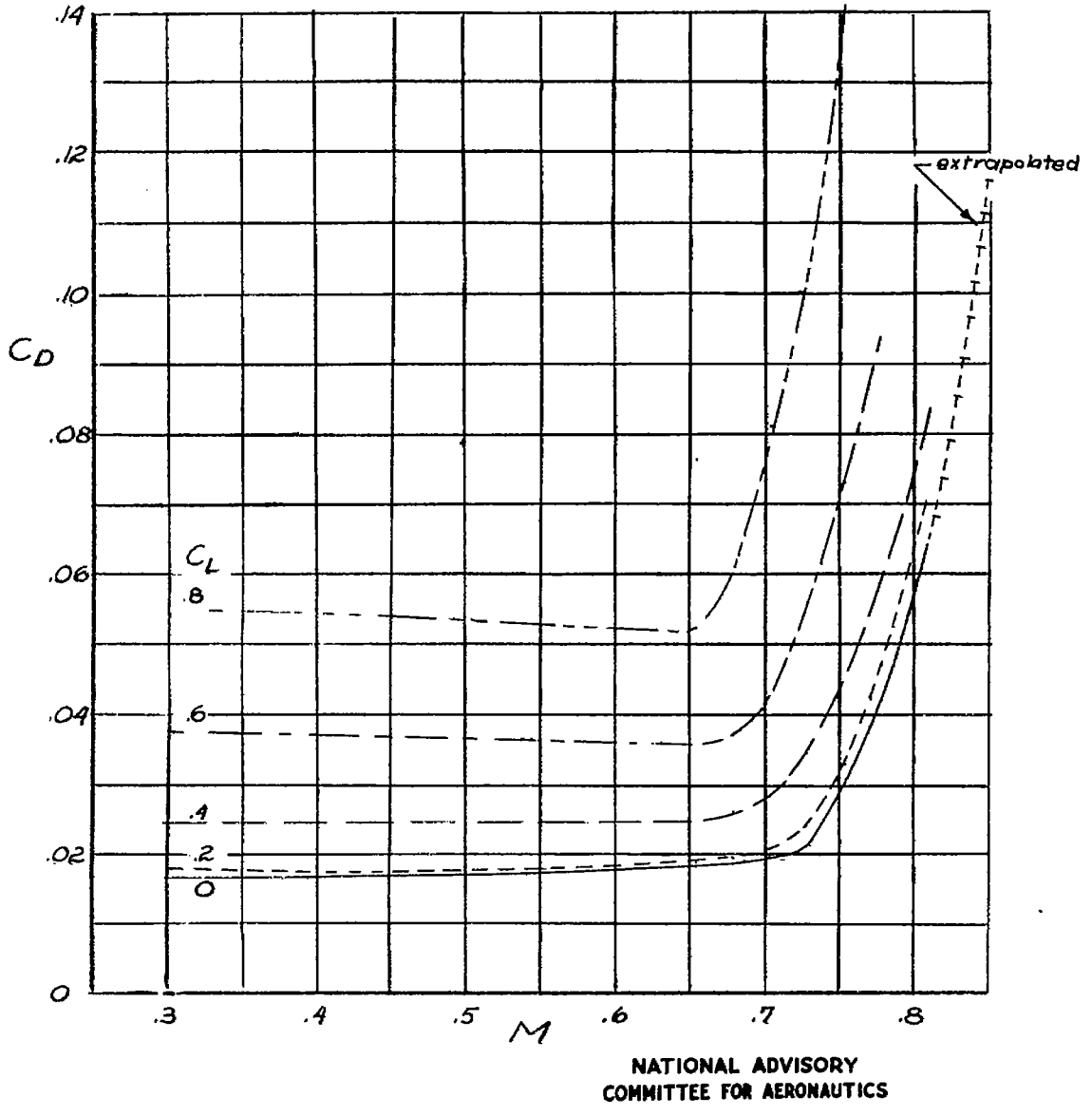

(b) In relation to Mach number.

Figure 25.- Concluded.